

ACCELEROMETER - ENHANCED SPEED ESTIMATION FOR LINEAR - DRIVE MACHINE TOOL AXES

THÈSE N° 1575 (1996)

PRÉSENTÉE AU DÉPARTEMENT D'INFORMATIQUE

ÉCOLE POLYTECHNIQUE FÉDÉRALE DE LAUSANNE

POUR L'OBTENTION DU GRADE DE DOCTEUR ÈS SCIENCES TECHNIQUES

PAR

Andrea GEES

Ingénieur électricien diplômé EPF
originaire de Scharans (GR)

acceptée sur proposition du jury:

Prof. J.-D. Nicoud, directeur de thèse
Dr S. Colombi, corapporteur
Prof. R. Longchamp, corapporteur
Dr J. Moerschell, corapporteur
M. H. Wild, corapporteur

Lausanne, EPFL
1996

Acknowledgements

This present dissertation is the result of three fruitful and interesting years that I spent at the Microcomputing Laboratory (LAMI) at the EPFL. I wish to express my gratitude to my thesis supervisor, Professor Jean-Daniel Nicoud, for his friendship and trust. I greatly profited from his effective guidance, invaluable comments, and his sense for innovative solutions.

I am also very grateful to Professor André Schiper for presiding the jury. I thank the other members of the jury, Dr Silvio Colombi, Professor Roland Longchamp, Dr Josephe Moerschell, and Harald Wild, for having accepted to take part in the committee.

Special thanks go to the project partners. I thank Dr Oliver Zirn from the Machine-Tool and Manufacturing Laboratory (IWF) of the ETH Zurich and Harald Wild and Guido Hayoz from the College of Engineering (ISBE) in Bern for the good collaboration and the fruitful discussions during the project. Furthermore, I wish to thank Dr Nicolas Wavre and Jean-Marc Vaucher from ETEL SA, Môtiers, for their advice and for putting a linear-drive axis at my disposal. I also thank the other project partners from industry, namely Almac SA, La Chaux-de-Fonds, Micron SA, Agno, and Num Güttinger AG, Teufen.

Many people contributed in one way or another to this dissertation. I especially want to thank Martin Dimmler for the fruitful discussions in a decisive phase of this dissertation. I thank Dr Silvio Colombi for the many discussions, his valuable advice and his insightful comments on earlier versions of this document. I am very grateful to Beat Liver for his careful reading and invaluable comments. I thank Irene Bircher for reading through parts of this dissertation and making many helpful suggestions and comments on the use of English.

The success of a research project depends to a high degree on the working conditions. I found at the LAMI a friendly and stimulating atmosphere. I want to thank all the staff from LAMI for the many discussions, the advice and technical support. Special thanks go to Christophe Marguerat for his advice and help with the signal processors. Furthermore, I want to thank our secretary, Marie-Jo Pellaud, for her friendliness and helpfulness.

Finally, I am very grateful to my wife Alice and my son Maurus, who provided good company and moral support while this dissertation was being written.

This dissertation is supported by the Swiss Commission for Technology and Innovation through the projects 2564.1 and 2868.3.

Abstract

Machine-tool axes for high-speed machining make great demands on the mechanical system, the actuators, and the numerical control. They require a high stiffness, a high bandwidth, and a precise motion at maximum speed. Linear motors as direct drives for machine-tool axes provide the basis to fulfil these requirements. They eliminate the gear-related problems of rotary drives with lead-screw transmission (from rotary to linear motion). In research and industrial projects, linear drives are already successfully implemented for machine-tool axes.

From the point of view of control, the accurate and low-noise estimation of the axis speed is a key issue. Due to the high bandwidths required, high sampling frequencies are employed. The estimation of the drive speed by differentiation of the measured position is sensitive to position quantisation at high sampling frequencies. All position-based speed estimation methods involve a trade-off between delay and quantisation noise on the estimated speed. Delay limits the achievable control bandwidth. Noise leads to audible control noise and might excite structural resonances. It limits the maximum values of the feedback gains and thus also limits the bandwidth. Given a certain position resolution, a substantial reduction of quantisation effects is only possible at the expense of a reduction of the stiffness. A further increase in position resolution limits the maximum axis speed with today's position encoders. This is not desired and other solutions have to be found.

A survey of different sensors for linear-axis control describes the state of the art. As a result, the use of acceleration measurement in addition to the position measurement for high-precision speed estimation is proposed. The commonly used aerospace methods of combining position with acceleration to obtain a high-precision speed estimate (complementary filters, Kalman filters) raise design and realisation problems for linear-axis applications. Therefore, we propose a novel method of accelerometer-enhanced speed estimation (AESE). This method lowers the demands on the position resolutions considerably. Generally speaking, the low frequency components are extracted from the position measurement and the high frequency components from the acceleration signal by observing the two measurements over a certain time period in the past. This solution is not sensitive to accelerometer measurement noise. Its design consists in the choice of one design parameter, the observation period length. The design is very easy, as the resulting speed quality is not very sensitive to this parameter. An analysis of the closed-loop system demonstrates that, by the use of accelerometer-enhanced speed estimation, the position quantisation influence on the speed feedback path is equalised to the one of the position feedback path. Therefore, high controller bandwidths and thus high sampling frequencies are possible without noise on the speed signal.

On-line identification algorithms for the accelerometer gain and offset parameter, which are proposed in this dissertation, simplify commissioning of the system with the additional accelerometers. They are based on the proposed AESE-method.

Low-cost inertial accelerometers are used for the experimental validation of the proposed algorithms on real linear-drive axes. They demonstrate that the AESE-algorithm provides an accurate, low-noise speed estimate with a delay in the range of the delay of the direct position differentiation over one sampling period.

Altogether, the proposed AESE-method is well-suited for an industrial application because of the high quality of the obtained speed signal, the simple design, the low cost, the low measurement-noise sensitivity, and the on-line parameter identification.

Résumé

Dans le domaine de l'usinage à grande vitesse, les machines-outils exigent des performances élevées du système mécanique, des actionneurs et du contrôle numérique. Une rigidité élevée, une grande bande passante et des mouvements précis à haute vitesse sont requis pour le contrôle de tels axes. Les moteurs linéaires sont bien appropriés pour entraîner des axes de machines-outils avec de telles spécifications. Ils éliminent les problèmes mécaniques dus aux vis à billes qui, dans les machines conventionnelles, transforment le mouvement rotatif en mouvement linéaire. Dans des projets de recherche et industriels, les moteurs linéaires ont déjà été utilisés avec succès dans des machines-outils.

Un des principaux problèmes de la commande des moteurs linéaires consiste en l'estimation de la vitesse de l'axe. A cause de la large bande passante, une fréquence d'échantillonnage élevée est nécessaire, mais l'estimation de la vitesse par différentiation de la position est très sensible au bruit de quantification pour des fréquences élevées. Toutes les méthodes d'estimation de la vitesse basées sur la position mènent à un compromis entre le bruit de quantification et un retard sur le signal de vitesse. Le bruit de quantification est audible et pourrait exciter des résonances de la structure mécanique. Des retards et constantes de temps limitent la bande passante de la boucle de réglage. Pour une résolution de position constante, une diminution de l'effet de quantification n'est possible qu'en diminuant la rigidité. Une augmentation de la résolution des encodeurs de position limite toujours la vitesse maximale de l'axe avec les encodeurs courants, et exige d'autres solutions.

Un aperçu des capteurs pour les axes de machines-outils décrit l'état de l'art. La mesure de l'accélération en plus de la position est proposée afin d'obtenir une estimation de vitesse de haute qualité. Les méthodes utilisées en aéronautique pour la fusion de la position et de l'accélération pour obtenir la vitesse (filtres complémentaires, filtres de Kalman) posent des problèmes de synthèse et de réalisation pour des axes linéaires. C'est pourquoi une nouvelle méthode pour estimer la vitesse à partir de la position et de l'accélération est proposée dans cette thèse. Cette méthode diminue les exigences sur la résolution du capteur de position. Elle extrait par filtrage les basses fréquences du signal de position et les hautes fréquences du signal d'accélération en observant les mesures dans une fenêtre fixe dans le passé. La solution proposée n'est pas sensible au bruit de mesure de l'accélération. Sa synthèse consiste à ne choisir qu'un seul paramètre et est simplifiée par le fait que la qualité du signal de vitesse n'est pas sensible à ce paramètre.

Des algorithmes pour l'identification du gain et de l'offset de l'accéléromètre en temps réel sont proposés. Ils sont basés sur l'algorithme d'estimation de vitesse. La mise en service d'accéléromètres supplémentaires est simplifiée par cette méthode d'identification.

Pour la validation expérimentale de la méthode proposée, des accéléromètres bon marché ont été utilisés sur des axes linéaires. Le résultat de ces expériences est une estimation de vitesse avec très peu de bruit et avec un retard qui est dans le domaine de celui de la différentiation directe.

L'étude du système en boucle fermée démontre qu'avec la solution proposée l'influence de la quantification sur le signal de retour de vitesse est du même ordre de grandeur que celle sur

le signal de retour de position. Il est donc possible de disposer d'une bande passante élevée en maintenant un faible bruit sur l'estimation de vitesse.

La nouvelle méthode d'estimation de vitesse proposée dans cette thèse se prête bien à l'utilisation dans une application industrielle, à cause de la bonne qualité du signal obtenu, la synthèse simple, la faible sensibilité au bruit de mesure et l'identification automatique des paramètres de l'accéléromètre.

Contents

Acknowledgements	iii
Abstract	v
Résumé	vii
1 Introduction	1
1.1 Motivation and Problem	1
1.2 State of the Art	3
1.3 Contributions	4
1.4 Structure of this Dissertation	5
References	6
2 Basic Notions	7
2.1 Linear Machine-Tool Axes	7
2.2 Basic Notions of Axis-Control	9
2.2.1 Motion Control Definitions	9
2.2.2 Digital Control of Dynamic Systems	10
2.2.3 Controller Structure	12
2.2.4 Performance Requirements and Measures	12
2.3 Components of Linear-Drive Axis	13
2.3.1 Current Controller and Power Electronics	13
2.3.2 Permanent-Magnet Linear Motor	15
2.3.3 Disturbances Acting on the Controlled System	17
2.3.4 System State Acquisition	17
2.3.5 Model of the Controlled System	17
2.4 Problems due to Position Quantisation	18
2.5 Experimental Environment for Validation	20
2.5.1 Digital Controller	20
2.5.2 Linear-Drive Axes	21
2.6 Conclusion	21
References	22

3	Sensors for Linear Axis Control	23
3.1	Introduction	23
3.2	Quality of Measured Signals	24
3.3	Linear Position Measurement	25
3.3.1	Magnetic and Optical Position Measurement	25
3.3.2	Laser Interferometers for Linear Position Measurement	30
3.4	Acceleration Measurement	31
3.4.1	Mechanical Characteristics of Accelerometers	31
3.4.2	Detection Methods	32
3.5	Other Measured Variables	37
3.5.1	Axis Speed	37
3.5.2	External Force	38
3.6	Summary and Conclusions	38
	References	39
4	High-Precision Speed Estimation	41
4.1	Introduction	41
4.2	Position-Based Solutions	42
4.2.1	Introduction	42
4.2.2	Survey of Position Differentiation Algorithms	43
4.2.3	State Observers	46
4.2.4	Oversampling	48
4.3	Accelerometer-Enhanced Speed Estimation	53
4.3.1	Related Work	54
4.3.2	Fusion of Position and Acceleration	56
4.3.3	Analysis of Algorithm in Frequency Domain	63
4.3.4	Accelerometer Parameter Identification	66
4.3.5	Design Guidelines	72
4.3.6	Sensor Failure Detection	75
4.3.7	Experimental Results	76
4.3.8	Concluding Remarks on Accelerometer-Enhanced Speed Estimation	81
4.4	Conclusions	83
	References	85
5	Axis Control with Acceleration Measurement	87
5.1	Influence of Speed Estimation on Closed-Loop Control	87
5.1.1	Cascade Controller Structure	88
5.1.2	Control Loop and Parameters	88
5.1.3	Quantisation Effects	92
5.1.4	Design Example from Practice	94
5.2	Acceleration Feedback	96

5.3	Conclusion	97
	References	98
6	Conclusions	101
6.1	Contributions	101
6.2	Future Research Topics	102
A	Mathematical Derivations	103
A.1	Summary of Stochastic Signals	103
	A.1.1 Basic Definitions	103
	A.1.2 Quantisation-Noise Modelling and Analysis	104
A.2	Variances of Position-Only Speed-Estimation Algorithms	105
	References	106
B	Sensor Data Specification	107
B.1	Interpolation of Optical Position Encoders	107
B.2	Laser Interferometer	108
B.3	Accelerometers	108
	References	109
C	Experimental Environment	111
C.1	Brushless Linear Drives	111
	C.1.1 Air-Cushion 75N Drive Axis	111
	C.1.2 2200N Machine-Tool Drive Axis	112
C.2	DSP-Based Numerical Controller Environment	113
	C.2.1 Schematic and Elements of the Environment	113
	C.2.2 Programming and User-Interface	114
	References	114
	List of Symbols	115
	Abbreviations	117

List of Figures

- 1.1 Schematic components of a closed control loop. 2
- 2.1 Rotary motor driven machine-tool axis. 8
- 2.2 Permanent-magnet linear-motor machine tool axis. 8
- 2.3 General structure of motion control device. 10
- 2.4 Basic discrete (z-domain) transfer function. 11
- 2.5 Control loop composed of discrete controller and analog system. 11
- 2.6 Cascade controller structure with speed and position feedback loop. 12
- 2.7 Components of open linear axis control loop. 13
- 2.8 Block diagram of power electronics with current controller. 14
- 2.9 (a) Converter from DC-voltage to motor phase currents; (b) Example of phase voltage and current. 14
- 2.10 Transfer function of current controller and power electronics model. 15
- 2.11 Schematic of permanent-magnet (a) rotary and (b) linear synchronous motor. . . 15
- 2.12 Linear model of synchronous motor phase in vector notation. 16
- 2.13 Complete model of power electronics and linear drive. 18
- 2.14 Cascade controller structure with quantisation and position differentiation ($\frac{z-1}{Tz}$). 18
- 3.1 Definition of accuracy and repeatability. 24
- 3.2 General setup of optical encoder. 26
- 3.3 Placing of interpolation electronics. 29
- 3.4 Digital output modes of interpolation units. 29
- 3.5 Principle setup of laser interferometer. 30
- 3.6 Schematic of piezoresistive accelerometer. 33
- 3.7 Schematic of capacitive accelerometer. 35
- 3.8 Linear velocity transducer (LVT). 38
- 4.1 Elements of differentiation algorithm. 45
- 4.2 Total speed transfer function of different differentiation methods. 46
- 4.3 State observer structure. 47
- 4.4 Setup of position oversampling. 49
- 4.5 Position oversampling in burst mode. 49

4.6	Probability to have a certain absolute error for different oversampling burst lengths.	51
4.7	Experimental results with oversampling for constant axis speeds and for different oversampling ratios N: (a) $0.35 \frac{m}{s}$; (b) $0.7 \frac{m}{s}$	52
4.8	Complementary filter implementation.	54
4.9	Example of axis movement.	57
4.10	(a) Backward rectangular and (b) trapezoidal discrete integration method.	60
4.11	Block diagram of proposed speed estimation algorithm.	63
4.12	Total transfer function of (a) acceleration and (b) position component.	64
4.13	Total transfer gain of position and acceleration component.	65
4.14	Influence of observation period (N_i) on acceleration component.	65
4.15	Total speed transfer function of the algorithm for different integration methods.	66
4.16	Position and acceleration measurement setup.	68
4.17	Magnitudes of transfer functions from position (P) and acceleration (A) measurement to the respective speed component (observation period: 2s).	73
4.18	Combination of transfer functions to final transfer function $\frac{v_k}{v_{real,k}}$	74
4.19	Position-to-speed transfer function of position-only methods with $T_{sampl} = 100\mu s$	75
4.20	Speed response on a force impulse with (a) $\Delta t_i = 5ms$ and (b) $\Delta t_i = 2.5ms$	77
4.21	Speed signal at a frequency of about 110Hz.	78
4.22	Distribution of normalised estimated accelerometer gain K	79
4.23	Speed estimation at (a) 260Hz and at (b) 375Hz.	80
4.24	Distribution of estimated accelerometer gains.	81
4.25	Transfer functions from acceleration to speed component: (a) proposed method; (b) complementary filter method.	83
4.26	Delay/quantisation-noise characteristics of different speed estimation methods.	84
5.1	Cascade controller structure.	88
5.2	Motor transfer function for pseudo-continuous modelling.	89
5.3	Pseudo-continuous model of controller and axis.	90
5.4	Model of simplified speed loop.	91
5.5	Model of position feedback loop.	91
5.6	Subsystem with acceleration feedback.	97
A.1	Digital filter model.	105
C.1	75N prototype linear-drive axis.	112
C.2	Block diagram of the numerical controller environment.	113

List of Tables

2.1	Equations of permanent-magnet synchronous linear motor.	16
2.2	Variance σ^2 of v_{ref} as a function of sampling period and necessary increase in position resolution to compensate the increased variance.	19
3.1	Available signal period and maximum deviation within one period.	26
3.2	Comparison of piezoresistive, capacitive, and piezoelectric accelerometers.	36
4.1	Comparison of variance and delay of position-only speed estimation methods.	44
4.2	Characteristics of 75N experimental drive.	51
4.3	Summary of the different components of the proposed speed estimation algorithm.	61
4.4	Recipe for recursive implementation of double integration.	62
4.5	Characteristics of position and acceleration component for typical observation periods.	75
5.1	Quantisation error factors n_{diff} of different speed estimation methods.	93
5.2	Variances on controller output for different speed estimation algorithms.	94
5.3	Technical data of 2200N linear-drive axis.	94
5.4	Effect of delay: feedback gains K_{px} , K_{pv} , and closed-loop bandwidths f_x and f_v	95
5.5	Effect of position quantisation: worst case error on a_{ref} ($a_{max} = 22\frac{m}{s^2}$).	96
B.1	Specification of HEIDENHAIN interpolation boxes.	107
B.2	Technical data of CSO HC250 interferometer.	108
B.3	Performance specifications for ICSensors piezoresistive accelerometers.	109
C.1	Technical data of 75N prototype linear-drive axis.	111
C.2	Technical data of 2200N linear-drive axis.	112

Chapter 1

Introduction

To increase the productivity of machine-tool axes, their speed has to be raised while maintaining their accuracy. In addition, a high stiffness is required to minimise the influence of external disturbances. Linear motors as direct drives for machine-tool axes provide the basis for the desired precise high-bandwidth and high-velocity motion. So far, mainly rotary drives with lead-screw transmission (from rotary to linear motion) have been employed for machine-tool axes. Compared to these drives, linear-drive axes eliminate gear-related problems. In recent research projects, linear drives have been successfully implemented on machine-tool axes [Phi92, Alt94, Zir96]. They are now mature to be employed on standard machine-tool axes [PFST95]. However, to take full advantage of the increased performance of linear drives, all components interacting in the control loop have to be adapted.

This dissertation argues that controller, actuator, and mechanical system of linear-drive machine-tool axis control have made substantial progress in recent years. It is now the system-state estimation, which is purely based on position measurement, which constitutes the limiting factor of the achievable control performance. The thesis which we defend is that the additional use of low-cost acceleration measurement provides the necessary motion information for high-performance motion control.

This chapter provides the motivation for this work. It describes the addressed problems and the state of the art. It further summarises the contributions of this dissertation and gives an overview of this document.

1.1 Motivation and Problem

Compared to rotary drives with mechanical lead-screw transmission, linear-drive machine-tool axes have a number of advantages. They simplify the mechanical structure and thus reduce the order of the system model. Non-linearity due to the gear (e.g. backlash, additional friction, and structural flexibility) is removed and the lifetime of the drive increased. Problems related to the spindle, such as a limited spindle velocity and spindle warm-up, are eliminated. According to [PFST95], electrical direct drives are more and more frequently employed for commercial machine tools and production equipment today. This trend is mainly due to progress in signal processing, power electronics, and motor development. A typical field of their application is high-speed machining. Direct drives are well adapted to this application due to their high

maximum velocities, high accelerations, low masses and high control dynamics. They provide at least the same precision as lead-screw drives at higher velocities.

On the other hand, the linear-drive solution also has two major drawbacks. First, external disturbances from machining and friction act directly on the drive, because they are not attenuated by the gear reduction. The same problem arises, moreover, for high-speed spindles which are used for high-speed machining. Because of their low reduction ratio, external disturbances are almost not attenuated by the gear. Second, the windings of linear drives have to be placed on the axes and might warm up the machine structure. Often, active cooling of the windings is necessary. Furthermore, direct drives are not well adapted if high forces are required and the space is limited [PFST95].

One of the main requirements of linear-axis control is a high stiffness. The term *stiffness* denotes the relationship between an external force acting on the system and the caused positioning error. A high stiffness ensures accuracy in the presence of external disturbances. For linear-drive axes, the same stiffness requirements apply as for lead-screw axes. To give an idea of the requirements on axis control, the specifications for a typical machine-tool application [Wav94] will now be summarised:

- The *dynamic stiffness* is between 300 and 700 $N/\mu m$.
- The *closed-loop bandwidth* of the position control loop is around 150Hz. Eigen-frequencies of the mechanical modes of the drive must be higher.
- The *position resolution* is in the range of $0.1\mu m$.
- *Maximum axis velocities* of $1-3\frac{m}{s}$ are required.

The main elements of a control loop are illustrated in Figure 1.1. By using linear motors instead of rotary drives with lead screws, the *mechanical system* becomes simpler. The axis is mainly modelled as an ideal double integrator with friction. The *actuator*, comprising power electronics, current control loop, and the motor itself, has the maximum force as its main limitation. A small time constant in the order of a hundred microseconds results from the current control loop. High-performance *digital controllers* based on digital signal processors (DSP) easily achieve the necessary sampling frequencies of some kilohertz, even if being programmed in high-level programming languages. Commercial numerical controllers work at lower sampling rates. But more powerful controllers based on DSPs are under development and will soon be available.

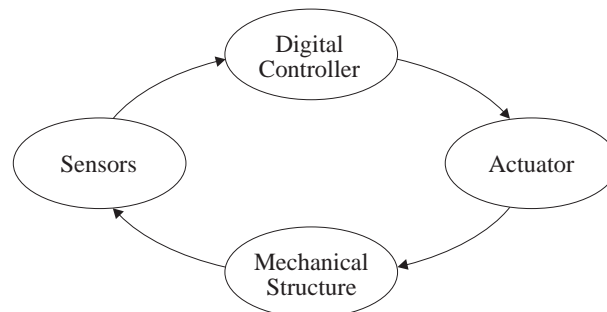


Figure 1.1: Schematic components of a closed control loop.

In the following, our thesis that the *sensors* constitute the main limitation for achieving high-performance control action is further substantiated. It is based on the assumption that

optimised, state-of-the-art components are used for all control-loop components. Usually, a cascaded controller structure is employed for the control of machine-tool axes. For linear-drive axes, only the axis position is measured, in contrast to lead-screw drives, where the position of the rotary drive is also measured. Problems arise for the accurate estimation of the axis speed, which is estimated on the basis of the differentiation of the measured position. This differentiation operation is sensitive to position quantisation for high sampling rates. Observer solutions to the determination of the axis speed are not well adapted to linear-drive axis control. Conventional observers cause problems due to the increased influence of external disturbances on the motion. Disturbance observers do not provide the necessary bandwidth.

According to [Phi92], the general limitations of the control of direct-drive machine-tool axes are the current control loop bandwidth, the controller sampling frequency, the controller calculation delay, quantisation, and the quality of the measured position. The current loop is usually implemented as analog control loop and provides high bandwidth. The problems of controller delay and sampling frequency are solved by using DSPs. The problem which persists is the quality of the measured position, or more generally speaking, the accuracy of the system state measurement. The solutions presented in [Phi92, Zir96] do not provide a low-noise speed estimation with a high bandwidth. Therefore, this dissertation focuses on high-accuracy speed estimation.

1.2 State of the Art

The state of the art of the use of electrical linear drives for machine-tool axes is presented in [PFST95]. For linear-axis motion control, cascade controller structures consisting of a current, a speed, and a position control loop are usually employed. System state estimation (position, speed) is purely based on axis position measurement. The mechanical structure of an axis determines axis precision and dynamics to a high degree. Low sampling periods ($< 500\mu s$) and a high position resolution ($< 0.1\mu m$) are required to meet the requirements of axis control.

Direct-drive actuators pose controller-design problems which are quite different from the ones of lead-screw drives. These motors have no inherent static stiffness so that all external disturbances have to be actively compensated for. Therefore, high maximum motor forces are required to achieve the desired control performance. On the other hand, dynamic error compensation and active vibration suppression is possible due to the increased dynamics of linear drive axes [Alt94].

Philipp in [Phi92] investigates different controllers (state space controllers of 2nd and 3rd order with different observers, cascade controllers), which are purely based on position measurement. He concludes that approximately the same power dissipation results for a desired stiffness, independently of the controller structure. Philipp determines the following general relationships, which are almost independent of the used controller structure. First, the dynamic stiffness increases with the square of the sampling frequency and proportional to the slider mass. Second, the power dissipation due to position quantisation significantly increases for higher sampling frequencies and higher position-quantisation step-size. Philipp states that, given a certain position resolution, a substantial reduction of quantisation effects is only possible at the expense of a reduction of the stiffness. For future research, he proposes the development of robust measurement systems for high velocities and high resolutions.

Zirn in [Zir96] investigates the influence of position resolution on linear-drive machine-tool axis control. He derives a criterion to determine the presence of stationary limit cycles as a

function of speed amplification and the friction force. The criterion is based on the harmonic balance [SL91]. In practice, quantisation noise effects are also audible with feedback factors below the limit of stationary limit cycles. He states that excitation of mechanical resonances due to position quantisation might be possible. He discusses the use of low-pass filtering of signals obtained by direct position differentiation and states that this leads to a reduced maximum speed amplification.

Alter in [Alt94] investigates linear-drive control aspects of a single-axis machine tool by the example of a feed-drive of a turning machine. He especially considers dynamic stiffness, disturbance rejection and servo tracking. He concludes that H_∞ controller design [DFT92] leads to significant stiffness improvements over PD control. Tool force feedback enhances the dynamic stiffness when using H_∞ theory for design. His experimental results show the potential of linear motors for driving machine-tool axes. The controllers presented in this reference are optimised for turning non-circular shapes. Nevertheless, he states that experimental necessity of the H_∞ method in force-feedback control design has not been shown. Less complicated methods might provide similar (experimental) results. For future research, Alter proposes the use of measured acceleration feedback instead of force feedback to enhance servo loop stiffness.

In [Phi92] a trade-off between axis stiffness and noise power for a given resolution has been identified. In [Phi92] and [Zir96], it is stated that the design of state observers for speed determination results in a trade-off between noise reduction and observer bandwidth. Quantisation noise leads to audible noise in such cases. Noise reduction with a given position resolution limits the closed-loop controller bandwidth. One possibility to achieve the performance is to increase position encoder resolution. However, in practice, this limits the maximum axis speed. Therefore, it is understandable that researchers in the field of direct-drive axis propose the use of additional sensors. Alter in [Alt94] uses tool-force measurement for a high-performance feed drive of a turning machine.

From the above-cited references, it can be concluded that position quantisation poses a problem for high-performance axis control. Standard solutions for purely position-based speed estimation always end up in a trade-off between control chatter and achievable controller bandwidth. As external disturbances are often not deterministic, they have to be measured. Therefore, more sophisticated approaches (extended observer structures) based on the system model do not promise better results. Two solutions are possible. First, the position resolution can be increased. Second, additional sensors can be used.

When using additional sensors, the notion of *smart sensors* [Ise96] is of major importance. Isermann observes a development from a classical measurement to a smart sensor component. The concept of smart sensors comprises functionalities added to the simple measurement function of a sensor. Among these functionalities are bus connections, supervision, fault detection and calibration. This concept is of importance in our context as it provides the facilities to simplify the commissioning of systems with additional sensors.

1.3 Contributions

Based on the restrictions which are imposed by the position quantisation, the use of improved or additional sensors for linear-drive axis control is investigated in this work. *The thesis which we defend is that the use of additional low-cost acceleration measurement provides the required axis-motion information for high-performance, high-stiffness axis control.* The main contributions of this thesis are as follows:

- The influence of the quality of speed estimation on the closed control loop performance is determined and the need for an accurate speed estimation is demonstrated. The limitations of purely position-based speed estimation methods are pointed out.
- Based on a survey of commercially available sensors, additional acceleration measurement is proposed to the position measurement. A novel method of accelerometer-enhanced speed estimation is developed. Improvements on conventional observer-based fusion methods for acceleration and position are determined.
- Practical aspects of the use of acceleration measurement are addressed. First, algorithms for the on-line estimation of the accelerometer parameters are derived. Second, a recursive implementation of the fusion algorithm is developed in order to reduce the requirements on the digital controller.
- Design guidelines for the proposed algorithms are given. They simplify the implementation of the algorithms.
- Experimental results demonstrate that acceleration measurement for machine-tool axes is feasible and that low-cost accelerometers provide high-quality acceleration information. They further prove that the proposed algorithms can be implemented on real axes and that they give the expected results.

1.4 Structure of this Dissertation

The main matter of this document consists of six chapters.

Chapter 1 provides the motivation for this work, describes the state of the art, and summarises the contributions which are achieved.

Chapter 2 introduces the main elements of the linear-drive axis control loop as well as the necessary theoretical notions. Performance requirements and measures which are used in the field of linear-axis control are defined. Thereafter, the importance of an accurate speed estimation, as the motivation for this dissertation, is demonstrated. Finally, the experimental environment used for the validation of the proposed solutions is briefly presented.

Chapter 3 surveys possible sensors for linear-axis control. Their physical basics are briefly explained. Focusing on commercially available products, the different sensors are explained with respect to their resolution, precision, inaccuracies, and cost. The use of a combination of position and acceleration measurement, as proposed in this work, is motivated.

Chapter 4 is dedicated to high-precision speed estimation. Different methods of speed estimation, which are purely based on position measurement, are introduced and compared. Thereafter, the fusion of position and acceleration measurement to a highly accurate speed estimation is discussed. First, a review of related work is given. Then, a novel algorithm for this fusion including accelerometer gain and offset identification is presented. The mathematical equations are derived and analysed, focusing on quality of the obtained speed, practical aspects, and design issues. Accuracy and feasibility of the proposed solutions are validated by experiments.

Chapter 5 discusses the benefits of the acceleration measurement for closed-loop control. First, the influence of the accelerometer-enhanced speed estimation on controller bandwidth and noise is analysed for the cascade controller structure. Then, the use of acceleration feedback

is briefly reviewed. Furthermore, possible limits of the combined use of both approaches are outlined.

Chapter 6 summarises and assesses the achieved results, and identifies future work.

Appendix A describes the mathematical basics of the employed statistics and contains some mathematical derivations from Chapter 4. Appendix B gives the specification of the employed position and acceleration measurement sensors. Appendix C explains the experimental environment which is used for the experimental validation of the results. This environment consists of a DSP-based numerical controller and two different linear-drive axes.

References

- [Alt94] D.M. Alter. *Control of Linear Motors for Machine Tool Feed Drives*. PhD thesis, University of Illinois at Urbana-Champaign, 1994.
- [DFT92] J.C. Doyle, B.A. Francis, and A.R. Tannenbaum. *Feedback Control Theory*. Macmillan Publishing Co, New York, 1992.
- [Ise96] Rolf Isermann. On the design and control of mechatronic systems — a survey. *IEEE Transactions on Industrial Electronics*, 43(1):4–15, February 1996.
- [PFST95] G. Pritschow, C. Fahrbach, and W. Scholich-Tessmann. Elektrische Direktantriebe im Werkzeugmaschinenbau. *Antriebstechnik*, 137(3/4):76–79, March/April 1995.
- [Phi92] W. Philipp. *Regelung mechanisch steifer Direktantriebe für Werkzeugmaschinen*. Springer Verlag, Berlin, 1992.
- [SL91] Jean-Jacques E. Slotine and Weiping Li. *Applied Nonlinear Control*. Prentice Hall, Englewood Cliffs, N.J., 1991.
- [Wav94] Nicolas Wavre. Hochdynamische elektrische Linearantriebe. ISW Lageregelseminar, Stuttgart, 1994.
- [Zir96] Oliver Zirn. *Beitrag zum Entwurf von Vorschubantrieben für die Hochgeschwindigkeitsbearbeitung*. PhD thesis, ETH Zürich, 1996.

Chapter 2

Basic Notions

This chapter provides the basic notions and definitions of linear-drive axis control. The main differences between rotary drives with lead-screw rotary-to-linear motion conversion and the here used linear motors are outlined in Section 2.1. The basic notions of axis control are reviewed in Section 2.2. The definitions of motion control are given and performance requirements for the axis control problem are defined. The components of the linear-drive control-loop are discussed in Section 2.3. In particular, the model of the controlled system is defined. Section 2.4 outlines the problems of controller design and motivates the solution approach taken in this dissertation. Section 2.5 describes finally the experimental environment which is used in this work.

2.1 Linear Machine-Tool Axes

Machine tools are composed of axes with different kinds of movements. For example, milling machines have at least three degrees of freedom for linear motion between workpiece and tool. In addition, there are often different axes to turn tool and workpiece in different directions to obtain special shapes on the final workpiece. Grinding machines perform quite similar movements than milling machines. Turning machines need two linear tool axes in two directions in addition to the basic rotating axis on which the workpiece is mounted. Precise and fast linear motion is often required in the field of machine tools.

Usually, these linear axes are driven by rotary motors. The employed basic setup is schematically illustrated in Figure 2.1 for the example of a linear milling-machine axis. A rotary motor mounted on the base of the axis drives a spindle. The rotary motion is converted into a linear slider motion by a lead-screw gearing. The slider is mounted on the axis with bearings of different types, e.g. roller, hydrostatic, and rarely air cushion bearings. This slider moves with reference to the tool axis which remains immobile in direction of the axis. The lead-screw structure has certainly the advantage that it provides a high inherent mechanical stiffness against external disturbances. On the other hand, gear inevitably causes backlash and additional friction. Due to the reduction factor from rotary to linear motion, the effective motor inertia is increased. This leads to a high total inertia of the axis.

Linear-drive machine-tool axes [WV94] have the advantage of a simpler mechanical structure, as illustrated in Figure 2.2. Despite their higher speeds, they provide the same precisions as lead-screw axes. One part of the linear motor, usually the part which is equivalent to the stator of the rotary motor, is mounted on the slider of the axis. Therefore, the power cables

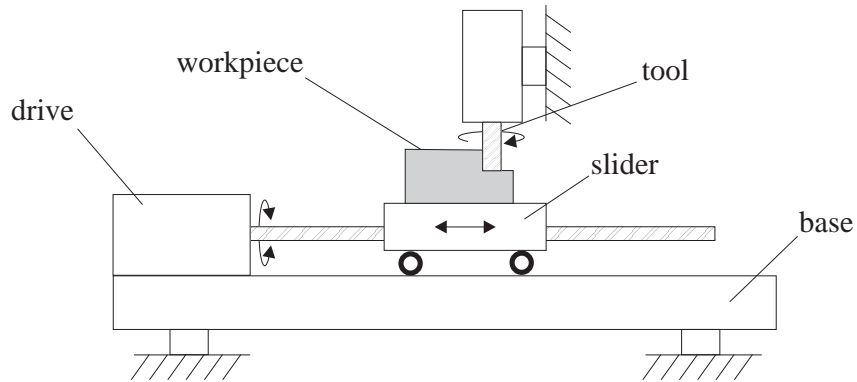


Figure 2.1: Rotary motor driven machine-tool axis.

have to be connected to the mobile slider part. It contains the windings of the linear motor. The second part of the linear motor, equivalent to the rotor of a rotary motor, is mounted on the base. In our case of a permanent-magnet linear motor, it consists of permanent magnets of rare earth type. Induction linear motors are also successfully used for machine-tool axis drives [Phi92]. Replacing the gear structure of the lead-screw drives by linear direct drives eliminates the problems of hysteresis, reduces friction, and reduces the elasticity of the removed mechanical parts. Maintenance is considerably reduced by the simplified mechanical structure. The controlled system bandwidth can be increased by a factor of 5 to 10 [WV94]. Stiffness of linear-drive axes has to be actively obtained by compensating external disturbance forces by equivalent drive forces. Besides machine-tool axes, linear drives can also be used for a variety of different applications, such as wire bonding machines, PCB drilling, chip manufacturing machines, and forming machines [WV94].

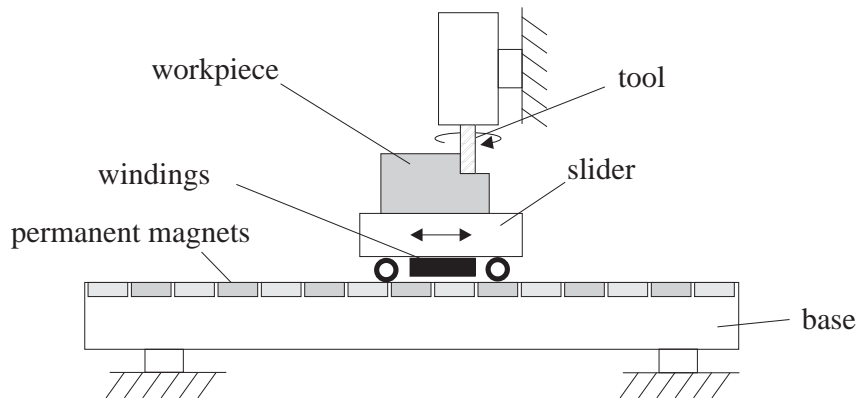


Figure 2.2: Permanent-magnet linear-motor machine tool axis.

The presented differences between the lead-screw setup and the linear-drive setup are not as important any more in the case of high-speed spindles, i.e. spindles with a steep slope and thus a low reduction factor: similar control problems arise for high-speed spindle drives and for linear drives. A comparison of linear-drives with high-speed spindle drives is given in [Zir96]. The author concludes there that linear drives are especially advantageous in the case of small and medium slider masses, high motion ranges, small and medium required stiffness, high life expectancy, and required compactness.

2.2 Basic Notions of Axis-Control

This section summarises the basic definitions of motion control, of digital control, and the cascade structure employed in this work. Furthermore, it introduces the performance requirements and measures of machine-tool axis control.

2.2.1 Motion Control Definitions

According to [DC93], motion control has emerged as a separate field within control systems theory. It deals with design and implementation of controlled mechanical systems. Its importance is mainly due to a request from industry to have advanced technologies to increase productivity and to save energy consumption. High performance is desired for control of mechanical systems and design. General implementation guidelines are looked for. A motion control system is composed of the following components:

- *Sensors* measure some of the mechanical variables (e.g. position, velocity, acceleration, tool force).
- *Transducers* measure electrical variables (e.g. phase currents and voltages).
- *Force generators* (i.e. controlled converter-motor units) accelerate the mechanical system.
- *Controllers* implement the control strategy for the converter-motor units.

Two main tasks are separated in motion control, namely, disturbance rejection and trajectory following. The *disturbance rejection* indicates by what degree external disturbances influence the system's behaviour. A high stiffness signifies a good disturbance rejection. The term *disturbance* is defined as all causes which modify the desired value of the controlled variable. In control, the term *noise* is used to summarise all uncertainties of sensors and transducers. The *trajectory following* characteristics are related to the precision to follow a given trajectory in closed-loop control. Three types of tracking errors are differentiated [See94]:

- *Positioning errors* are related to the repeatability and accuracy. They indicate the precision to move repeatedly to the same position and the closeness to the desired real value. Positioning errors are mainly caused by frictional forces and measurement errors.
- *Stationary tracking errors* are persistent deviations from a given trajectory. This type of error occurs for example for ramp trajectories if proportional position error feedback is employed.
- *Dynamic tracking errors* are in contrast to stationary tracking errors only of short duration. They may be caused by distortions in the transfer function of motion control systems (e.g. actuator saturation). They typically occur if sharp edges are machined at high speed and the drive bandwidth is not sufficient.

The structure of a motion control loop is shown in Figure 2.3. The shown loop constitutes the lowest level in the axis control hierarchy. External control components are numerical controllers for trajectory generation based on CAD (computer aided design) data as well as controllers for coordinating different axes with spline interpolation to generate reference trajectories. Usually,

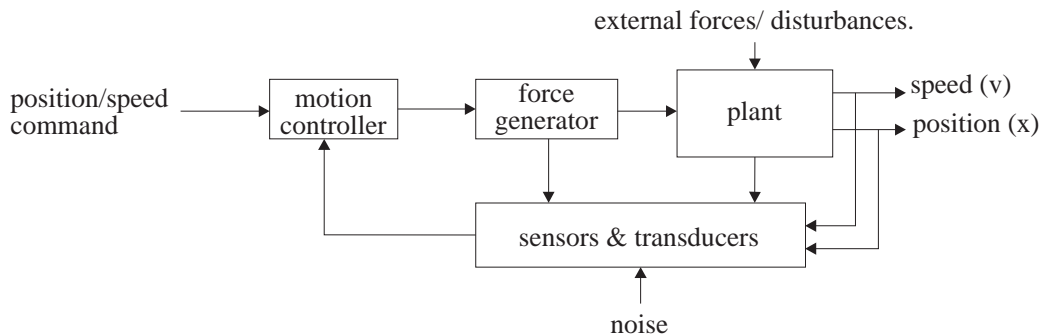


Figure 2.3: General structure of motion control device [DC93].

position and speed are the controlled variables in this low level loop. Sometimes, additional variables, such as acceleration and tool force, are fed back to increase stiffness. The load, denoted by external forces/disturbances in Figure 2.3, is composed of friction, machining, and inertial forces. Additional external forces representing the energy transferred to other mechanisms are usually not present in the case of linear-drive axes, because these drives provide only positioning action and no explicit machining action. For slow dynamics, the inertial force is less important than all other torques. However, for very rapid dynamics, the inertial force becomes dominant compared to all other forces interacting.

De Carli states in [DC93] that conventional control strategies optimise trajectory following and disturbance rejection at the same time. According to him, this is well adapted to slow or very slow dynamics. Dynamics improvements are obtained with feed-forward control and direct disturbance compensation in case of directly measured disturbance values. Innovative controller structures completely separate between disturbance rejection and trajectory following. The disturbance rejection controller is based on the measured system variables and the control variable from the feed-forward controller. It estimates the total of all disturbance forces and directly compensates them. The on-line estimation of disturbance torque is used to improve accuracy and dynamics of the controlled system. In case of insufficient knowledge of the system state for disturbance estimation, additional sensors (e.g. accelerometers) might be used to directly measure them.

In this work, the low-level position control loop and especially an accurate estimation of the drive speed are of major interest. We do not consider the trajectory following problem here. For disturbance rejection, an accurate estimation of the system state variables (position, speed) is necessary.

2.2.2 Digital Control of Dynamic Systems

In this work, digital control with a fixed sampling frequency f_{sampl} is exclusively employed. The input values are read at equally spaced points in time. The output of the controller is, in our case, an analog value, as the employed power electronics only provides an analog interface. The analog output is kept constant from one sampling to the next. This relationship is modelled by a so called *zero order hold* element (ZOH).

In the following, some characteristics of discrete control systems which are of major importance for understanding aspects of this dissertation are briefly reviewed. In depth discussions of

methods for design and analysis of such discrete systems in z -domain are found in the literature, e.g. [ÅW84, Lon95].

Discrete transfer functions are defined in a similar way as continuous transfer functions. For discrete cascaded blocks, feedback blocks, and so on, the same basic operations as for continuous blocks apply in general. The basic discrete transfer function $G(z) = \frac{Y(z)}{U(z)}$ is illustrated in Figure 2.4. Numerator and denominator of $G(z)$ are composed of polynomials in z^{-1} . The transfer

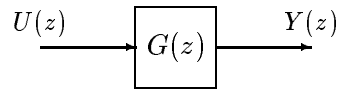


Figure 2.4: Basic discrete (z -domain) transfer function.

function z^{-1} corresponds to a delay of one sampling period. The following equations exemplify the relationship between the discrete input-output equation on the left and the corresponding discrete transfer function on the right.

$$y(k) = u(k) - 2u(k-1) + 5u(k-2) \quad G(z) = \frac{Y(z)}{U(z)} = 1 - 2z^{-1} + 5z^{-2}$$

Most digital control systems consist of a discrete controller part and a continuous system part. Such a system can be completely transformed into z -domain and analysed by means of the theory from discrete control and digital signal processing. The closed-loop system is divided into a discrete controller part $K(z)$ and an analog system part $G(s)$. These two parts are linked by A/D and D/A converters, as shown in Figure 2.5. The transfer function between

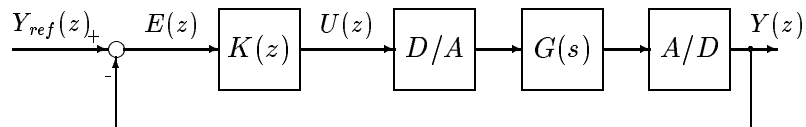


Figure 2.5: Control loop composed of discrete controller and analog system.

the command variable $U(z)$ and the controlled variable $Y(z)$ can be characterised by a discrete transfer function $H(z)$. The transfer function of this block composed of a D/A converter, the continuous system $G(s)$, and the A/D converter (with ZOH) is obtained with the following equation [Lon95]:

$$H(z) = \frac{Y(z)}{U(z)} = \frac{z-1}{z} \mathcal{Z} \left\{ \mathcal{L}^{-1} \left[\frac{G(s)}{s} \right] \right\} \quad (2.1)$$

The operator \mathcal{L}^{-1} denotes the inverse Laplace-transform [Unb89], the operator \mathcal{Z} the z -transform.

2.2.3 Controller Structure

The cascade controller structure of Figure 2.6 has some practical advantage compared to a global controller. Beginning with the innermost feedback loop, each loop is independently designed and commissioned. Therefore, this controller setup is commonly used for machine-tool axis control. In this work, exclusively the cascade controller structure with proportional feedback gains is employed. First, this structure enables one to analyse the inner loop independently from the outer one. Second, with this structure, limitations (e.g. limited speed and limited maximum force) of the controlled system are easily taken into consideration. However, with the design in cascaded loops, the obtained control loop is in general slower than with a global controller design. It should be noted that in practice PI-feedback for the inner loop and PD-feedback for the outer loop are employed. By PD/PI feedback, higher bandwidths are possible than by proportional feedback. For the analysis of the influence of measurement errors on the closed-loop system, however, we restrict ourselves to the dominant proportional feedback.

In Figure 2.6 as in the remainder of this work, positions are denoted by x , velocities by v , accelerations by a , and forces by F . K_{px} and K_{pv} are proportional controller factors for position-error and speed-error feedback. The model of the controlled system shown in this figure is explained in Section 2.3.

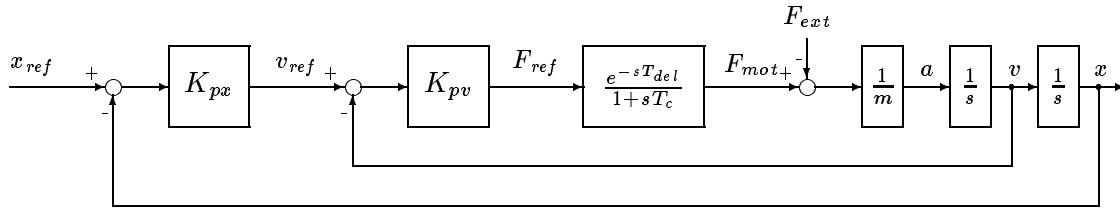


Figure 2.6: Cascade controller structure with speed and position feedback loop.

2.2.4 Performance Requirements and Measures

From the control point of view, machine-tool axes as servo-mechanisms are mainly characterised by speed of response, closed-loop stability, and disturbance sensitivity. Dynamics specifications are expressed by the transfer function from the reference position input x_{ref} to the system output x , disturbance sensitivity considerations by the disturbance transfer function from the disturbance force F_{ext} to x (see Figure 2.6).

An important constant of a cascaded control loop is the *speed amplification* K_{px} . It defines the amplification from the position error to the reference speed value. An increase of speed amplification raises the bandwidth. On the other hand, it leads to a reduction of system damping and thus possibly to overshoot. In practice, the design of the speed amplification is a compromise between high bandwidth and sufficient damping [Stu81]. For a reference trajectory with constant speed, the resulting stationary trajectory error of a proportional cascade controller is equivalent to the ratio between the constant speed and the speed amplification. For high-speed machining, typical speed amplifications are above $150 \frac{1}{s}$ [Zir96].

For second order systems, the *dynamics* is defined by the resonance frequency and the damping ratio. For higher order systems, the frequency with 3dB attenuation and the overshoot ratio define the system dynamics.

The stiffness of a servo-mechanism is related to the disturbance rejection. The *dynamic stiffness* is defined as the inverse of the disturbance transfer function of the controlled system.

$$\text{dynamic stiffness} = \frac{F_{ext}(s)}{X(s)}$$

For a cascade controller with proportional position and speed error feedback, the static stiffness is a good approximation of the dynamic stiffness. Typical values for high-speed machining are $20\text{--}50 \frac{N}{\mu m}$ [Zir96], for other machine-tool applications $300\text{--}700 \frac{N}{\mu m}$ [WV94].

2.3 Components of Linear-Drive Axis

The different components of the controlled systems are briefly discussed and the used model derived. The aim is to give an idea of the elements and their characteristics.

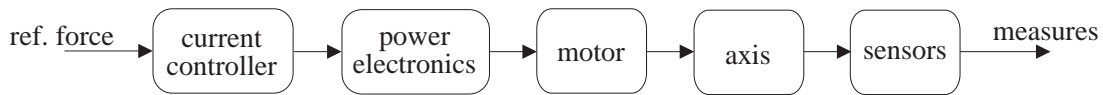


Figure 2.7: Components of open linear axis control loop.

The components of the open loop system from the reference force to the measured motion information are shown in Figure 2.7. The reference force value serves as controlled system input. The current controller together with the power electronics unit supplies the necessary phase currents to generate the desired force. These phase currents depend on the mechanical and hence electrical axis position as well as on the force reference value. The linear drive exerts a force on the slider mass and accelerates it. Sensors measure the motion information for closed-loop control. The mentioned components are now discussed in more detail.

2.3.1 Current Controller and Power Electronics

Power electronics and phase-current control loop are closely related. In this dissertation, we consider the current control and power electronics as a black box with given specifications. A reference force is given as input to this unit, which generates and regulates the phase currents of the motor. The block diagram of the elements interacting in the current control loop are given in Figure 2.8. The *power converter* block converts in a first step the AC power from the power distribution network to an internal direct current or direct voltage. A second power stage within the power converter converts DC current or voltage to the desired phase currents as a function of the commutation signals from the current controller. The *current controller* determines the commutation signals as a function of the reference force value, the measured phase currents, and the actual electrical motor position. The electrical motor position denotes the relative displacement of motor windings and permanent magnets.

For the power converter block, different setups are possible, i.e. direct internal current or voltage. In Figure 2.9, a schematic diagram of the second stage of such a converter is given. In this figure, the conversion from an internal DC-voltage to one phase current of a linear motor, as used in our work, is illustrated. The internal voltage is kept constant by the converter from the power distribution network to the intermediary voltage. The two switches S1 and S2 connect alternately the two phase lines to the upper and the lower voltage level in opposite

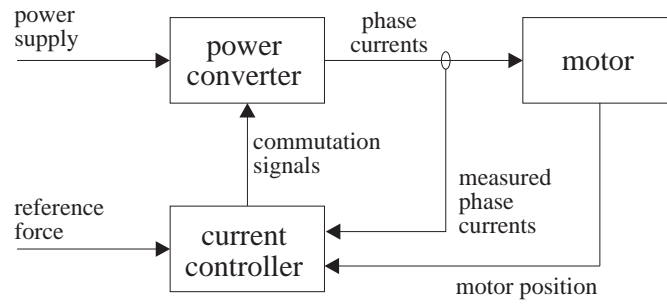


Figure 2.8: Block diagram of power electronics with current controller.

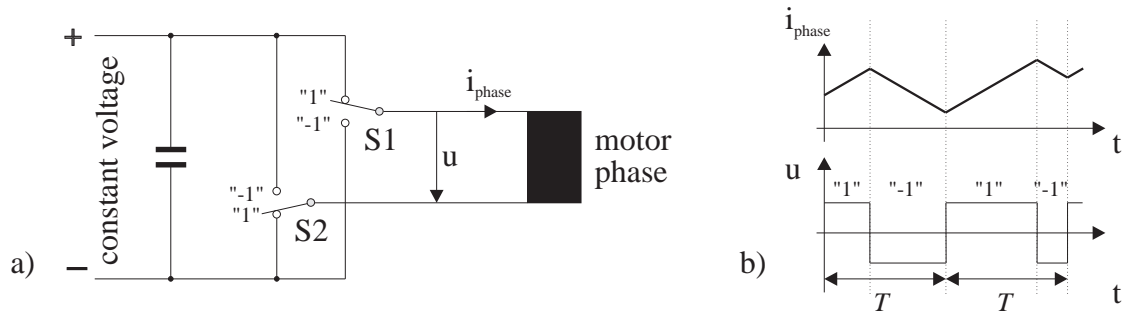


Figure 2.9: (a) Converter from DC-voltage to motor phase currents; (b) Example of phase voltage and current.

direction. Due to the dominant motor phase inductance, the phase current steadily increases if the phase is connected the way to impose a positive phase voltage u and decreases if it is connected in the opposite direction. The phase current can be controlled by the commutation of the switches. The employed semiconductor power-switches commute at high frequencies (some hundreds of hertz to some tenth of kilohertz) to reduce the ripple on the resulting current. The maximum switching frequency is limited by two factors. First, the employed semiconductor switches need some time to commute between off and on switch position. One commutation has to be terminated before another can be initiated. Second, during the transition phase of the commutation, a power dissipation peak is generated in the switch [Ste91]. By increasing the switching frequency, these power peaks with almost constant duration and power dissipation occur more frequently and raise thus the mean power dissipation of the switch. Problems of heat-up arise for high frequencies. From the control point of view, this switching frequency causes delays of the reaction of the phase current to reference values which are equally distributed between zero and the switching period T between two switching actions. This delay is modelled by a constant pure time delay of half the switching period [Ste91].

The current controller block generates the current reference signals which are synchronous to the electrical motor position. In addition, it regulates the actual phase current to follow the generated reference values. The block has as inputs the force reference signal, the motor position measurement, and the measured phase currents. The phase-current reference values are generated to obtain a resulting current vector with exactly 90-degree phase shift to the electrical motor position. The sinusoidal relationship between this phase shift and motor force assures that the ratio between generated force and current vector amplitude is maximum and that the motor is used with maximum efficiency. With φ denoting the phase shift between motor windings

and permanent magnets, the equations for the two reference values of a two-phase motor are as follows:

$$I_{ref1} = F_{ref} \cdot \frac{I_{max}}{F_{max}} \cdot \sin(\varphi + 90) \quad I_{ref2} = F_{ref} \cdot \frac{I_{max}}{F_{max}} \cdot \cos(\varphi + 90)$$

A current feedback loop regulates the real current value to follow the above reference values based on measured phase currents. Current controllers can be implemented in analog and digital technology. Often, hybrid electronics is employed.

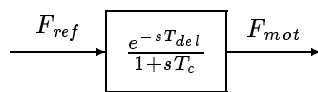


Figure 2.10: Transfer function of current controller and power electronics model.

It is assumed that the intermediary voltage of the power electronics is sufficiently high to follow the reference phase current variations. Therefore, the transfer function of current controller and power electronics can be approximated by a pure time delay T_{del} and a time constant T_c representing the dominant current controller dynamics, as illustrated in Figure 2.10. The complete block has the reference force F_{ref} as input and the total motor current (the sum of the two phase current vectors) which is equivalent to the generated motor force F_{mot} as output. Both, T_{del} and T_c , are for linear-axis drives in the range of tenth of milliseconds.

2.3.2 Permanent-Magnet Linear Motor

Linear motors are derived from rotary motors by unwrapping rotor and stator of the motor on a plane. The difference between rotary and linear motor type is exemplified in Figure 2.11. Besides some minor influences at the borders of the linear drive, the basic theory remains the same as the one of rotary AC motors which is described in [Fis86].

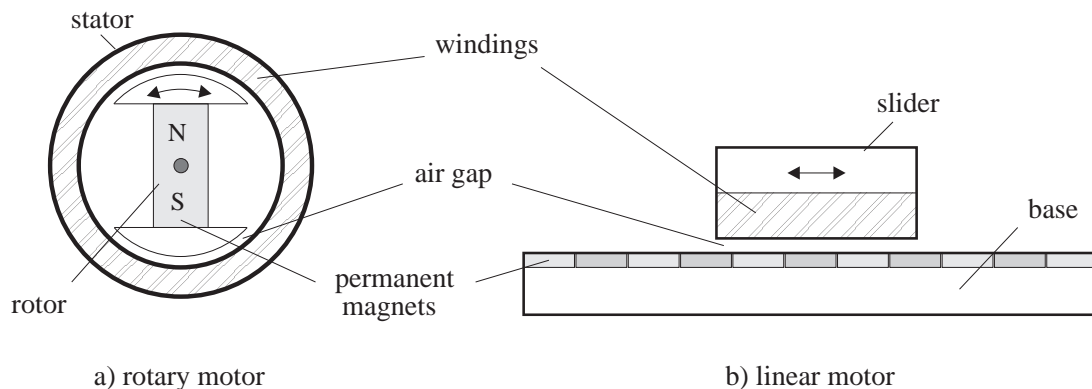


Figure 2.11: Schematic of permanent-magnet (a) rotary and (b) linear synchronous motor.

For machine-tool axes, mainly permanent magnet synchronous [Alt94] and induction linear drives [Phi92] are used. Reluctance drives are more appropriate for positioning purposes than

for machining. Permanent magnet linear drives achieve high efficiency and high force dynamics due to the quality of the permanent magnets [Wav94]. These motors are also called brushless DC drives with electronic commutation. For this work, two phase permanent magnet synchronous motors from ETEL are employed. They are described in Appendix C.1.

The electrical phase angle φ depends on the relative displacement between the permanent magnets and the windings. The relationships are equivalent to the rotary permanent magnet synchronous motor. In case of zero phase angle between the revolving field generated by the phase currents and magnetic field of the magnets, no force is exerted by the drive. In case of phase shift, the force varies with the sine of the phase angle. At 90 degrees phase shift, maximum force is exerted for a given absolute value of the two phase currents. Therefore, this operating point is chosen, because of its maximum ratio between force and current amplitude and thus maximum motor efficiency.

A linearised model of linear permanent-magnet drives is given in Figure 2.12. It is the same as for a permanent-magnet synchronous rotary drive. Underlined symbols in this figure denote vectors of rotating fields. The motor is modelled as a resistance R , an impedance X and a voltage source \underline{U}_{ind} in series connection.

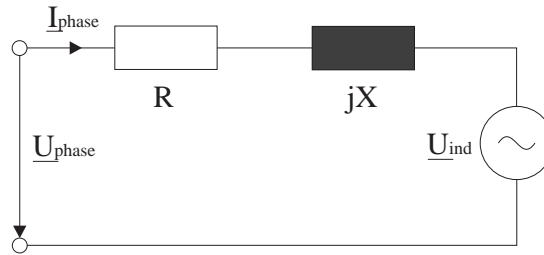


Figure 2.12: Linear model of synchronous motor phase in vector notation.

The induced voltage \underline{U}_{ind} is proportional to the drive speed. The exerted force of the drive is proportional to the total phase current amplitude. The acceleration of the axis results as the difference between exerted force and disturbance forces divided by the mass to be accelerated. The equations of a brushless linear DC motor (permanent-magnet synchronous drive) are summarised in Table 2.1. In this table, underlined variables denote vectors, not underlined variables denote scalars.

phase voltage	$\underline{U}_{phase} = \underline{U}_{ind} + R \cdot \underline{I}_{phase} + L \cdot \frac{d\underline{I}_{phase}}{dt}$
induced voltage ^a	$U_{ind} \propto v$
motor force	$F_{mot} \propto I_{phase}$ $F_{mot} \propto \sin(\varphi)$

^a \propto — proportional to

Table 2.1: Equations of permanent-magnet synchronous linear motor.

An important constant for the design of linear-drive applications is the ratio between maximum force and motor mass (only slider part). This ratio is equivalent to the maximum acceler-

ation of the drive without any load. For drives with simple air-cooling, this value is in the range of $25\text{--}40\frac{N}{kg}$; for drives with fluid cooling, in the range of $50\text{--}170\frac{N}{kg}$ [Zir96]. The maximum force is limited by motor heat-up restrictions. In general, active cooling is necessary for machine-tool applications.

2.3.3 Disturbances Acting on the Controlled System

Different external disturbance forces act on a linear-drive axis. They act directly on the drive forces. In contrast to lead-screw drives, their influence is not reduced by the gearing. Possible disturbance forces are:

- *Friction forces* are mainly caused by the bearings of the axis. Generally, the total friction force composed of dry friction and viscous friction for linear drive axes is in the range of 5% to 30% of the nominal drive force [Phi92]. For our experimental axis (see Appendix C.1.2), viscous friction is around 10%, dry friction about 5–15% higher than viscous friction. For the second experimental drive with air cushion bearings, frictions forces can be neglected.
- *Inertial forces* are proportional to slider mass and acceleration. They are important in the case of high axis dynamics.
- *Machining forces* are forces between tool and workpiece of a machine-tool axis. Depending on the kind of machining, they may have quite different characteristics. For instance, high-frequency forces are generated by the blades of a milling tool.

The importance of the inertial force component depends on the dynamics of the system. For highly dynamic direct drive axes, inertial forces are dominant. In contrast to the other two disturbance forces, this force is deterministic and known for control action. Therefore, it is easily compensated in the feed-forward path of the controller.

2.3.4 System State Acquisition

The problem of system state measurement and estimation is the main topic of this dissertation. In Chapter 3, possible sensors for linear-axis motion control are discussed. Enhanced speed estimation methods are presented in Chapter 4. Here, we just summarise that position measurement only is normally used for machine-tool axes. The position resolution is chosen in the range of tenth of micrometers. Higher resolutions would be possible, but they limit the maximum speed. This is not desired for high speed machining applications.

The position is measured by optical encoders with output signal periods of some micrometers. The resolution is increased by a special interpolation electronics which outputs an incremental signal in digital form. By counting the increments, the position is directly available as discrete value.

2.3.5 Model of the Controlled System

Cascade controller structures are often employed for machine-tool axis control, as already mentioned in Chapter 1. The cascade controller consists of an outer position control loop and an inner speed control loop. The third and innermost current-control loop is closely related to

power electronics and drive characteristics. Its design is normally done by the drive manufacturer. Therefore, in this dissertation, it is considered as a black box with a known but fixed transfer function. In Figure 2.13, the complete linear model composed of the above presented blocks power electronics, current control loop, and drive is given. It should be noted that the reference force F_{ref} of the model corresponds to the reference phase current input of the power electronics.

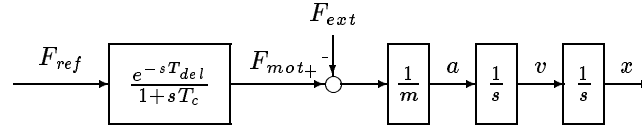


Figure 2.13: Complete model of power electronics and linear drive.

One important characteristic of servo drives, namely *actuator saturation*, is neglected in the presented axis model. This problem is thoroughly discussed in [Büh94]. The influence of the induced voltage \underline{U}_{ind} is also neglected. As this voltage considerably reduces the drive force for high speeds, this simplification only holds for low speeds (e.g. typical working speeds of machine tools).

2.4 Problems due to Position Quantisation

In Section 1.1, it is stated that speed estimation causes problems due to the increased sampling frequency which is necessary for high bandwidth control. In the following, the problem is illustrated on a typical example of a real linear-drive axis. The influence of sampling frequency on position quantisation noise is explained.

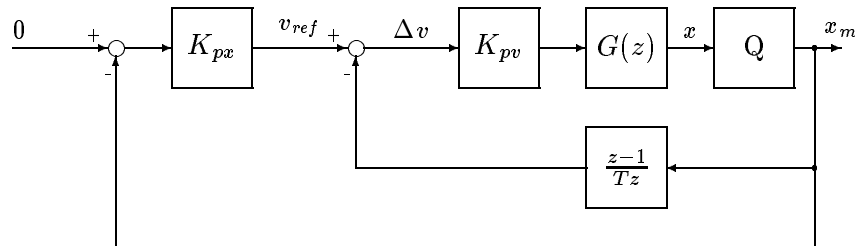


Figure 2.14: Cascade controller structure with quantisation and position differentiation ($\frac{z-1}{Tz}$).

In Figure 2.14, a cascade controller structure with a proportional speed and a proportional position control loop is illustrated. The discrete motor transfer function is denoted by $G(z)$. The measurement quantisation is added as a special block Q , which has the measured position x_m as output. The speed estimation of the speed loop is obtained by direct differentiation ($\frac{z-1}{Tz}$) of the position. To quantify the position quantisation noise, quantisation is modelled as a uniformly distributed stochastic variable. Successive position samples are not correlated for usually employed sampling periods in the order of $100\mu s$. The variance of the reference speed due to position quantisation is calculated based on the formulae explained in Appendix A.1.

The difference between reference speed and measured speed results as:

$$-\Delta v = x_{m,k} \cdot K_{px} + \frac{x_{m,k} - x_{m,k-1}}{T_{sampl}}$$

The variance σ^2 of this speed difference Δv as a function of the position quantisation q is:

$$\sigma^2 = \frac{q^2}{12} \left[\left(K_{px} + \frac{1}{T_{sampl}} \right)^2 + \left(\frac{1}{T_{sampl}} \right)^2 \right] = \frac{q^2}{12} \left[K_{px}^2 + \frac{2K_{px}}{T_{sampl}} + \frac{2}{T_{sampl}^2} \right]$$

Table 2.2 shows how the variance increases when using a higher sampling frequency while leaving the speed amplification K_{px} ($200\frac{1}{s}$) and the position quantisation q ($0.1\mu m$) constant. The rightmost column indicates by what degree the position resolution has to be increased to compensate this increased variance compared to the values with $500\mu s$ sampling period. The

T_{sampl}	f_{sampl}	Variance of v_{ref} $\left[\frac{m^2}{s^2} \right]$	Compensation factor
$500\mu s$	2kHz	$29 \cdot 10^{-9}$	1
$200\mu s$	5kHz	$173 \cdot 10^{-9}$	6
$100\mu s$	10kHz	$680 \cdot 10^{-9}$	23

Table 2.2: Variance σ^2 of v_{ref} as a function of sampling period or sampling time and necessary increase in position resolution to compensate the increased variance (for $K_{px} = 200$; $q = 0.2\mu m$).

employed value of 200 for K_{px} is selected according to the derivation in Section 5.1.2.3. It constitutes the limit value for which our linear drive axis (see Appendix C.1.1) is stable for a $500\mu s$ sampling period. For shorter sampling periods, the system would remain stable for even higher feedback gains. In [PFST95] values of $200\text{--}500\frac{1}{s}$ are indicated as current values of speed feedback gains. However, the sampling period T_{sampl} has the major influence on the variance and the feedback gain K_{px} has only minor influence on the result. Therefore, the speed feedback loop with speed estimation has a major influence on the variance of the speed error signal Δv . For shorter sampling periods, it makes thus greater demands on position resolution than the position loop. Typically, the variance increases with the inverse square of the sampling period.

A high bandwidth of speed measurement is important to ensure a high closed-loop bandwidth. Decreasing the variance on the speed estimate would increase the delay or the time constant on the obtained speed signal and thus limit the achievable closed-loop control bandwidth.

In [LVP91], the problem of the inner speed loop having higher feedback gains and thus demanding higher position resolution than the outer position feedback loop is discussed. The authors state there that the higher gain requirement for the velocity loop has a significant influence on the variance of the torque producing command. This causes problems for AC-drives, where the current loops need to have a high bandwidth for a proper field generation. This is exactly the case for our direct drives. The authors state in [LVP91] that filtering is unacceptable because the resulting phase lag degrades the closed-loop performance. They propose observer solutions to reduce the problem of quantisation noise. But they also conclude that the tuning of the observer feedback gains is always a trade-off between dynamic performance and quantisation noise.

2.5 Experimental Environment for Validation

2.5.1 Digital Controller

For the control of high-precision, high-dynamic axes, digital controllers are employed, because they offer the necessary flexibility. Higher sampling frequencies are used for linear drive axes than for conventional machine-tool axes, where frequencies of less than 1kHz are usually sufficient. For high-speed machining, sampling frequencies of at least 2kHz are desirable. Due to their performance, digital signal processors are often employed for axis control. They are programmed in high-level programming languages. Optimising compilers generate almost time optimal machine code for real-time control. There exists a wide variety of processors with fixed and floating point arithmetic. Their instruction set is well adapted to signal processing and thus to digital control, where mainly the same types of operations are performed.

Experimental validation is very important in this dissertation, because the assumed sensor noise, external disturbance influences, and delays on measured signals have to be verified on real measurements. Two different approaches for experimental validation are differentiated:

- *On-line evaluation*: the measured variables are evaluated during control action and measurement and are directly displayed. This method is adapted for evaluating slow processes and medium to long-term characteristics. The process can be directly adapted depending on the evaluations results.
- *Off-line evaluation*: the measured data are only recorded during control action and measurement. They are evaluated afterwards. This method is appropriate for evaluating highly dynamic processes which cannot be evaluated on-line.

For this dissertation, we choose the off-line evaluation, because the process is highly dynamic and because we are interested in testing the influences of design parameters on exactly the same measured data. However, the closed-loop characteristics and performance cannot be directly influenced by off-line evaluations and results of the evaluations can only be considered in later test series. The following steps describe controller design, implementation, and off-line evaluation:

- The *design and simulation* of a controller is done off-line with specialised software tools (e.g. Matlab, Simulink).
- The *programming* of the controller on the digital signal processor is usually carried out with a cross compiler on a separate host computer. Programming languages are C and assembler.
- The *control with recording* of the interesting process variables is done on the signal processor. The recorded variables are stored into random access memory (RAM) during control action for later off-line evaluation.
- The *storing* of the recorded values in a file on the host computer is done after terminating the control action.
- The *evaluation* of the recorded process variables is performed off-line with software tools (e.g. Matlab, Excel).

For this dissertation, a TMS320C40 32-bit floating-point signal processor from Texas Instruments has been employed. This processor executes floating point operations with a cycle time of $50ns$. The experimental environment which we have developed is composed of a main processor board, an interface board, and a memory extension board. It provides the analog and digital interfaces for the control of two machine-tool axes. The developed software comprises digital controller, reference trajectory generation, a terminal-based user interface, and emergency routines which intercept instable controller action. Even without taking too much care of calculation time during software development, sampling frequencies of more than $10kHz$ are easily obtained for the mentioned tasks.

More technical aspects of the developed digital controller environment are given in Appendix C.2. To summarise, the software development, debugging, and retrieval of the recorded data is done on a separate host computer (PC, Sun workstation), which is connected to the signal processor. The user interface is in a terminal window on the host computer. It provides the basic user-interface functions, such as controller start/stop, parameter changes, and so on. For recording experimental data during control, a memory board with 2M-Bytes of 32 bit large data words is available.

2.5.2 Linear-Drive Axes

Two different linear-drive axes are used for experimental validation. The first one is a 75N peak-force drive with a slider mass of $1.6kg$, air cushion bearings, and a position resolution of $0.4\mu m$. The second is a 2200N drive with a mass of $100kg$, roller bearings, and a position resolution of $0.1\mu m$. These two drives are further described in Appendix C.1.1 and Appendix C.1.2, respectively.

2.6 Conclusion

The setup of linear-drive machine-tool axes has been discussed and the basic notions of motion control introduced. The components of the axis control loop have been presented and the models derived. The problems of speed estimation for axis control has been identified and the experimental environment for the validation of the theoretical results presented.

Machine-tool axes require a high stiffness (up to $700\frac{N}{\mu m}$), i.e. a low sensitivity to external disturbances. Inertial, friction, and machining forces are the main disturbances acting on linear-drive axes. For high system dynamics, inertial force influence is dominant.

Linear-drive machine-tool axes provide an almost ideal model. Their linear model consists of a pure time delay from power electronics, a time constant from the current controller, and a double integration describing the complete system dynamics.

Linear-drive machine-tool axes can achieve a bandwidth which is a factor of 5 to 10 above conventional machine-tool axes. The controller sampling frequency has to be adapted to the increased control bandwidth and thus raised. The variance on the purely position-based speed estimation due to position quantisation error increases with the square of the sampling frequency. To compensate this increase the position resolution would have to be increased by the same factor as the bandwidth. However, an increase in resolution is usually coupled with a reduction of the maximum speed. This is not desired for high-speed machining.

References

- [Alt94] D.M. Alter. *Control of Linear Motors for Machine Tool Feed Drives*. PhD thesis, University of Illinois at Urbana-Champaign, 1994.
- [ÅW84] Karl J. Åström and Björn Wittenmark. *Computer controlled systems*. Prentice-Hall, Englewood Cliffs, N.J., 1984.
- [Büh94] Hansruedi Bühler. *Theorie du réglage de systèmes d'électronique de puissance*. Cours d'électronique industrielle, EPF Lausanne, October 1994.
- [DC93] A. De Carli. Motion control: an emergent technology. *Control Engineering Practice*, 1(3):485–491, 1993.
- [Fis86] Rolf Fischer. *Elektrische Maschinen*. Hanser Verlag, München, 6th edition, 1986.
- [Lon95] Roland Longchamp. *Commande numérique de systèmes dynamiques*. Presses polytechniques et universitaires romandes, Lausanne, 1995.
- [LVP91] Robert D. Lorenz and Keith W. Van Patten. High-resolution velocity estimation for all-digital, ac servo drives. *IEEE Transactions on Industry Applications*, 27(4):701–705, July/August 1991.
- [PFST95] G. Pritschow, C. Fahrbach, and W. Scholich-Tessmann. Elektrische Direktantriebe im Werkzeugmaschinenbau. *Antriebstechnik*, 137(3/4):76–79, March/April 1995.
- [Phi92] W. Philipp. *Regelung mechanisch steifer Direktantriebe für Werkzeugmaschinen*. Springer Verlag, Berlin, 1992.
- [See94] Michael Seehuber. *Automatische Inbetriebnahme geschwindigkeitsadaptiver Zustandsregler*. PhD thesis, TU München, 1994.
- [Ste91] H. Stemmler. *Leistungselektronische Systeme 1-2*. Vorlesungsskript, ETH Zürich, 1991.
- [Stu81] G. Stute. *Regelung an Werkzeugmaschinen*, volume 5. Carl Hanser Verlag, München, 1981.
- [Unb89] H. Unbehauen. *Regelungstechnik*, volume 1. Verlag Vieweg & Sohn, Wiesbaden, 6th edition, 1989.
- [Wav94] Nicolas Wavre. *Hochdynamische elektrische Linearantriebe*. ISW Lageregelseminar, Stuttgart, 1994.
- [WV94] Nicolas Wavre and Jean-Marc Vaucher. Direct drive with servo linear motors and torque motors. In *Symposium on Electric Drive Design and Applications*, pages 151–155, Lausanne, 1994.
- [Zir96] Oliver Zirn. *Beitrag zum Entwurf von Vorschubantrieben für die Hochgeschwindigkeitsbearbeitung*. PhD thesis, ETH Zürich, 1996.

Chapter 3

Sensors for Linear Axis Control

Sensors play a major role in control system design. They are as important as actuators and controllers. In order to achieve precise control action, they have to provide accurate information about the system's controlled variables. This fact holds even more in the presence of external disturbances acting on the system. Often, such disturbances are not deterministic and are only statistically known. Therefore, they cannot be completely modelled. The only way to detect them for compensation is to measure their effect. The quality of the sensor data is thus a limiting element of the achievable closed-loop system performance.

The aim of this chapter is to discuss the state of the art of commercially available sensors for linear axis motion control. Moreover, a survey of the different sensors, their performance and limitations is provided. In general, movement is expressed in terms of position, speed, and acceleration. The corresponding sensors are discussed in Section 3.3, Section 3.5.1, and Section 3.4, respectively. External force measurement is briefly reviewed in Section 3.5.2.

This chapter is mainly based on literature and manufacturer information about the specific sensors. Focusing on commercially available sensors, it provides the basis for the motivation of the central idea of this dissertation, i.e. adding low cost acceleration measurement to reduce the requirements on position measurement.

3.1 Introduction

An appropriate choice of the employed sensors in a control system is crucial. Such a choice has, on the one hand, to meet the requirements for the overall system performance to be achieved. On the other hand, economic reasons limit the choice. Bradley summarises in [Bra92] this compromise:

What is the most inaccurate measurement which would be acceptable given the purpose of the measurement?

The control of conventional machine-tool axes with lead-screw drives makes less demands on the system state measurement. The mechanical transmission from the rotary motor movement to the linear axis movement limits the achievable closed-loop bandwidth. Measurement of axis position and rotary motor position are sufficient to perform accurate control action. For direct-drive machine-tool axes, the situation is quite different. Due to the absence of a gear box, they have a simpler mechanical structure and achieve higher control-bandwidths. As explained

in Section 2.4, given higher controller bandwidths and thus higher sampling frequencies, the purely position-based speed control loop makes greater demands on position resolution than the position loop. Therefore, to achieve the same precision at higher bandwidths, higher position encoder resolution would be necessary. As the additional position information is only used to determine the speed more accurately, a study of other sensor solutions is necessary.

According to [NWN94], sensors represent the weakest link in the development of next-generation instrumentation, data-acquisition, and control systems. They are often unreliable, rarely accurate, and often too expensive. In addition, they provide almost no fault-tolerance or fault-detection capabilities. Today, the available technology enables the manufacturers to integrate signal processing locally on the sensor and add powerful communication interfaces which are adapted to the used sensors. This is clearly visible in recent developments of accelerometers. Each new generation of such sensors provides increased bandwidth, precision and integrated signal processing components at lower prizes. Local signal-processing leads to the development of “smart sensors” [Bra92], with functionalities such as error compensation (e.g. temperature), self-calibration, and diagnostics. We can also think of more complex functions, such as data compression or data fusion.

In recent years, sensor technology relevant to linear axis control has mainly evolved in two directions. First, interferometry position measurement devices for machine-tool axes control are commercially available; they are complex and expensive devices, and hence, their application is only justified for very high demands on resolution and precision. Second, accurate acceleration sensors have become available at low prices. The widespread use of accelerometers for monitoring, modal analysis, testing, and control in different fields has significantly driven their development. Due to the progress in manufacturing technology, complex micro-machined structures are possible on the same chip as micro-electronic elements. The progress in this sector does not seem to have reached a point of saturation yet. Some of the employed manufacturing technology is quite recent. More precise and cheaper sensors are to be expected in the future.

3.2 Quality of Measured Signals

When assessing the “quality” of a sensor, one considers the following parameters [Bra92]: accuracy, resolution, repeatability, linearity, response time, and maximum uncertainty. They all influence the control system performance. For the design of systems, parameters such as environmental conditions and system cost are of major importance. We briefly define the terms which are important for the remainder of this chapter. They are visualised in Figure 3.1

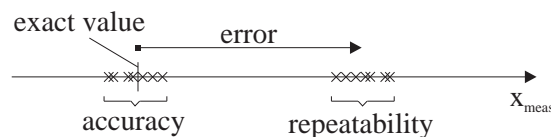


Figure 3.1: Definition of accuracy and repeatability.

- The *repeatability* indicates the closeness of the measurements when a static signal is repeatedly measured. A good repeatability only guarantees that in this case the values are close to each other, but not that they are exact. In accordance with the literature [HSW89], we also use the term *precision* in this work synonymously for repeatability.

- The *accuracy* denotes the closeness of the measured data to its real value.
- The term *resolution* is used here in the context of digital control. It indicates the equivalent physical value of one least-significant bit in the numerical representation of a measured variable.

3.3 Linear Position Measurement

Position is the most important variable to be measured for motion control of machine-tool axes. Its accuracy limits the maximum achieved accuracy in closed-loop control. Its resolution, which is normally an order of magnitude higher than its accuracy, is important for the calculation of speed by differentiating the position.

Three major concepts are used for linear motion position measurement in the sub-millimetre to sub-micron range. The lowest resolutions in the millimetre range are obtained with magnetic encoders. Optical encoders reach signal periods of some microns. Their accuracy lies in the range of 1%–2% of these signal periods. Their concepts and possibilities to increase their resolution by interpolation are the topic of Section 3.3.1. Measurement devices based on laser interferometry offer accuracies in the range of 1ppm (part per million) of the measured distance. For a position range of $1m$, this means an accuracy of at least $1\mu m$. This is especially the case for interferometers in the lower price segment, more accurate devices being far beyond the limit of what can be paid for machine-tool axis measurement. The concept of laser interferometry is described in Section 3.3.2. Rotary encoders are not used in this context due to the lack of precision of the necessary conversion from linear to rotary motion.

3.3.1 Magnetic and Optical Position Measurement

Position measurement devices based on magnetic and optical principles generally output incremental signals with relative position information. These signals are analog and of sinusoidal shape. Absolute position encoders, based on the optical principle, are also available, but have been used less commonly for machine-tool axes so far. There exist different methods for absolute measurement. We do not discuss these methods in greater detail. We are only interested in the available resolution and accuracy, which are equal for incremental and absolute sensors.

3.3.1.1 Position Sensors

Figure 3.2 illustrates the general setup of an optical encoder. The sensing part, composed of a light source, a sensing plate and light sensors, moves with reference to a ruler with gratings. The light source sends the light through the grated sensing plate. The grated ruler plate reflects the light to the sensors as a function of the relative position between sensor and ruler. Four light-sensing elements finally detect incremental position changes.

A Moire effect [Kun93] results from placing sensing plate and ruler gratings at a slightly different angle [Bra92]. This provides sinusoidal output signals. A pair of 180-degree phase-shifted signals is used to generate one output signal. By taking the difference between the two sensor values, the measurement offset is eliminated and the signal amplitude is doubled. Two sensor groups are placed with 90-degree phase difference in order to generate two 90-degree phase-shifted output signals a and b . Therefore, four sensors are necessary to provide the two

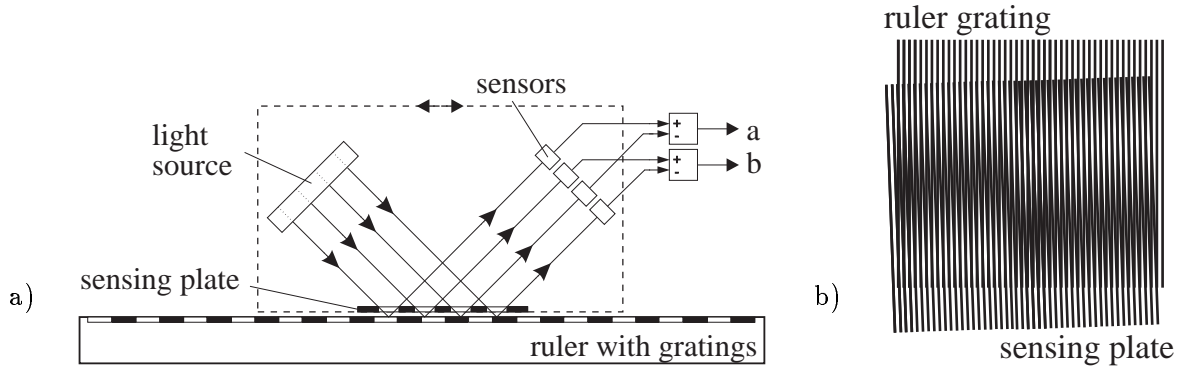


Figure 3.2: (a) Setup of optical encoder [Wal85]; (b) Moire effect.

output signals. The incremental position information, which consists of the moved distance and direction, is extracted from these signals. This extraction is based on the sequence of zero crossings and on the amplitudes of the two signals.

In the remainder of this section, position encoders of HEIDENHAIN, one of the main linear encoder manufacturers, are discussed in detail. We summarise information from [Hag96], which provides us with a recent description of the state of the art of commercially available HEIDENHAIN sensors.

Three main types of position encoder sensors are available. The first type, magnetic sensors, has the lowest precision. The other two types are based on optical principles. One of them uses a light beam and the other one diffraction. Position sensors are available in an open and an encapsulated version. The open version is more precise and has no friction. With the encapsulated version, the sensor is protected against environmental influences, such as lubricants and material from machining. The open version is mainly used for precision machine tools, measurement systems, and production equipment for chip manufacturing. The encapsulated version, in contrast, is used for metal-cutting machine tools.

Table 3.1 summaries signal period and maximum deviation within one signal period of the three types. The maximum position deviation is specified relatively to the signals period. For the open systems this value is 1%, for encapsulated systems 2%.

Principle	Signal period	Maximum deviation
magnetic	$200\mu m$ to $10mm$	$\pm 2\mu m$ to $\pm 100\mu m$
light beam	$10\mu m$ to $200\mu m$	$\pm 0.1\mu m$ to $\pm 2\mu m$
diffraction	$128nm$ to $4\mu m$	$\pm 1nm$ to $\pm 40nm$

Table 3.1: Available signal period and maximum deviation within one period [Hag96].

Encapsulated encoders have eigen-frequencies in the range of 2kHz. This is a factor of at least 4 above the first mechanical mode of the machine. These eigen-frequencies have therefore less influence than the mechanical modes of the axis and are usually neglected. Due to some flexibility of the encoder, dynamic deviation of the position is encountered at periods of high acceleration. With $1g$ constant acceleration and 2kHz eigen-frequency, dynamic errors are around 60nm for all these encoders.

3.3.1.2 Interpolation for Increasing Resolution

Position sensors of the magnetic and optical type have an accuracy of about 1%–2% of their output signal period. Therefore, counting only the zero crossings of the two 90-degree phase-shifted sinusoidal output signals would result in a significant loss of resolution. A variety of methods to improve the resolution of these sinusoidal signals by interpolation has been developed. Interpolation devices are commercially available. They are usually part of the measurement system and are delivered with the corresponding sensor. So far, these interpolation boxes have mainly been separate devices, which have the analog encoder signals as input and digital incremental signals as output. There is, however, a tendency toward the integration of interpolation with the numerical controller electronics.

Theoretical aspects of interpolation. Based on the two sinusoidal phase-shifted signals of the sensor, denoted by a and b , the actual angle φ within the signal period has to be calculated. By defining the first measured output signal as $a = \sin(\varphi)$, the second output signal results as $b = \sin(\varphi + 90^\circ) = \cos(\varphi)$. Vice versa, the angle φ is expressed as the following function of the two measured signals a and b :

$$\varphi = \arctan\left(\frac{a}{b}\right)$$

By taking the periodicity of the trigonometric functions with the explicit signs of a and b into consideration, the angle φ is obtained in the range $[0..2\pi]$. In robotics, this function is known as *4-quadrant arc tangent function*. Different hybrid analog and digital methods have been developed for calculating the output angle in numerical form. We do not go into details because they are not important for our purposes.

Interpolation electronics is usually implemented as sampled system. In order to always trace the absolute position of the incremental signals exactly, the maximum distance moved between two interpolation samples has to be lower than half an encoder signal period. Therefore, the following relationship results between encoder sampling time $T_{encoder}$, the maximum axis speed v_{max} , and the position encoder resolution $X_{encoder}$:

$$X_{encoder} > 2 \cdot T_{encoder} \cdot v_{max} \quad (3.1)$$

Accuracy and resolution of interpolation. Hiller investigates in [Hil96] errors which can occur due to interpolation for a rotary axis and a linear-drive axis. We summarise his explanations and results in the following. It should be noted that his results have been obtained by both simulations and measurements.

The main sources of interpolation errors are perturbations on the two sensor signals a and b , such as offsets, different amplitudes, high-order resonances, time constants, and noise. These perturbations degrade the resulting position values in so far as the position errors are a multiple of the theoretical values of the interpolated position resolution. This fact is clearly visible when calculating the drive speed by differentiating the drive position.

Nowadays, interpolation factors up to 4096 are possible to achieve with specialised chips. Hiller, however, shows the limits of interpolation due to measurement inaccuracies with the following example: The position signal of a $20\mu m$ encoder is interpolated with the factor 1024, leading to a position resolution of about $20nm$. By sampling the signal with $200\mu s$ sampling time and calculating the speed with direct differentiation, there results a theoretical speed

quantisation of $100\frac{\mu m}{s}$, i.e. a maximum quantisation error of $\pm 50\frac{\mu m}{s}$. Due to inaccuracies on the measured position, the errors on the speed, based on measured position, is in the range of $\pm 600\frac{\mu m}{s}$. According to Hiller, this difference is mainly due to harmonics and noise on the sensor signals.

It is certainly possible to adjust some values as offsets and signal amplitudes automatically. Hiller states, however, that measurements with different position encoders show that often it is not possible to have an adjustment for the whole position and speed range at once. Therefore, compensation methods become very complex. Noise and resonance compensation is only partially possible.

We conclude that it is not useful to go far below the accuracy of the encoder (1%-2% of encoder signal period) by interpolation. In this case, measurement noise becomes too important. The influence of this noise on a speed estimated by position differentiation is significant, and therefore, higher interpolation factors cannot be recommended only for improved speed determination. Thus, quantisation noise would inevitably be replaced by measurement noise, and the result would not be improved.

Design issues. The theoretical relationship (3.1) between encoder sampling time $T_{encoder}$, the maximum axis speed v_{max} , and the position encoder resolution $X_{encoder}$ will now be applied to two examples from the practice. For a controller-integrated interpolation electronics with arctan-interpolation, the sampling period $T_{encoder}$ is around $1\mu s$ (see example in [Hil96]). When using a separate interpolation unit, as the described EXE-boxes from HEIDENHAIN (see Appendix B.1), the maximum input signal frequency is further limited. For these two solutions, the following relationships between maximum speed and encoder resolution are defined by:

$$\begin{aligned} \text{Integrated interpolation: } & X_{encoder} > 2\mu s \cdot v_{max} \\ \text{EXE-box interpolation: } & X_{encoder} > 20\mu s \cdot v_{max} \end{aligned}$$

As a result, given the fixed interpolation sampling period, the choice of a certain encoder resolution is a trade-off between position resolution and maximum speed. Hence, the maximum speed constitutes the main limitation when using interpolators. The price of position encoders does not vary significantly for different resolutions, except for very high resolutions and accuracy. Therefore, economic arguments do not influence this trade-off.

3.3.1.3 Signal Transmission

The signal transmission from a position encoder to the numerical controller should not be a matter of concern for our purposes. But the quasi-standard for this transmission shows some severe drawbacks when working with sampling periods in the range of $100\mu s$ (10kHz) as we do. Therefore, we briefly discuss the characteristics of this interface and possible solutions for the future.

Figure 3.3 illustrates two different setups for the placing of the interpolation unit. In the upper one, the interpolation unit is an extra device between the encoder and the controller. In the second one, it is integrated into the numerical controller. Today, the interpolation unit, as a part of the measurement system, is often a device which is independent of the numerical controller (see EXE-box in Appendix B.1). It is placed somewhere near the optical encoder in order to make the analog signal path as short as possible. It interpolates the encoder signals with an internal cycle time of around $2\mu s$ (500kHz). After each interpolation, the position increments

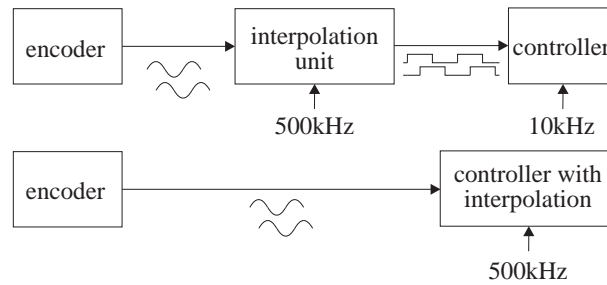


Figure 3.3: Placing of interpolation electronics.

are transmitted to the numerical controller by two 90-degree phase-shifted rectangular signals. These signals have to be counted in the controller in order to obtain the absolute position. Resetting the counters at startup is done by an additional signal from a special zero marker on the position sensor. No signal is present to synchronise the numerical controller to the interpolation unit.

Another possibility is to transmit the analog signal to an interpolation unit which is integrated in the numerical controller. In general, the analog signal transmission path is longer, what possibly induces noise problems. However, the complexity for rectangular signal generation and counting as well as the problem of synchronisation are reduced.

According to our experiences, two major problems arise when using the setup with extra interpolation unit, as we did. First, the missing synchronisation between interpolator and numerical controller with a factor of 50 ($500\text{kHz}/10\text{kHz}$) between the two sampling periods generates unwanted interferences. Second, in earlier interpolation units, the position increments are not equally distributed during the interpolator sampling period, but transmitted by bursts with a fixed output frequency. Figure 3.4 illustrates the two variants: the output increments of the solution on top are equally spaced, the increments of the second solution are output as bursts. The latter solution has severe drawbacks because of the missing synchronisation between the

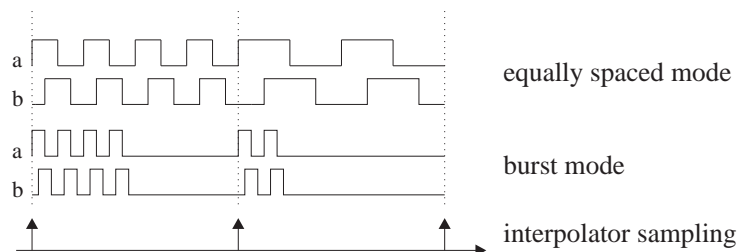


Figure 3.4: Digital output modes of interpolation units.

two sampling operations of interpolator and controller. When sampling occurs exactly during a burst, the sensitivity of the result on the exact moment of sampling is enormous, given the high burst output frequency. However, the former method adds a delay of one interpolator sampling period for signal transmission only. Both solutions are not suitable for the calculation of the actual speed by measuring the time between two encoder increments. This time is influenced by the interpolation unit and hence adds noise to the speed signal.

We expect that in the nearer future, this data transmission will be done by field buses with the possibility of synchronisation. It is not understandable why two different digital components,

both working with microprocessors, should communicate by other means than by buses. Field buses simplify cabling, configuration, synchronisation, commissioning, and add flexibility. They are already successfully implemented for similar control problems in other fields. The fact that they are not more widely used for machine-tool control seems to be a marketing problem rather than a technical one. But the pressure to migrate in this direction will surely raise with the highly-dynamic direct-drive axes.

3.3.2 Laser Interferometers for Linear Position Measurement

Laser-interferometry position measurement devices provide an excellent means to measure position with high accuracy. They are complex measurement systems comprising error compensation components. Therefore, they are very expensive, probably too expensive for machine-tool applications. Nevertheless, for very sophisticated motion control problems with high requirements on accuracy, they might be the only solution to meet the requirements.

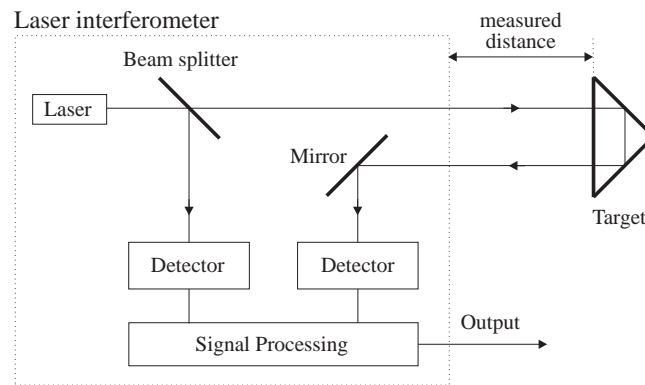


Figure 3.5: Principle setup of laser interferometer [Bra92].

The principle of the measurement is illustrated in Figure 3.5. A laser, which is well-stabilised and temperature-compensated, sends out a light-beam at a specific frequency. A so-called beam splitter reflects a part of the light to a reference detector. The measuring beam which passes the beam splitter is sent out from the basic device to the mobile target. This target acts as a mirror which reflects the beam in a direction towards the basic device, where it is captured by a second detector. By observing the phase differences between the two detected signals, incremental movement information is obtained. The accuracy mainly depends on the frequency stability of the laser. Environmental conditions, as e.g. temperature or humidity, change the propagation of the light and cause additional errors. The resulting errors are proportional to the measured distance. Therefore, the accuracy is specified in ppm.

The specifications of one commercially available laser interferometer in the lower price segment are given in Appendix B.2. The device has an accuracy of about 1ppm. The maximum range is 1m. A conventional version of this device costs around \$20.000, the OEM (Original Equipment Manufacturer) version with functionalities adapted to the requirements costs about one third of this price.

We think that the use of interferometers cannot be generally recommended for position measurement of highly dynamic machine-tool axes. They are an order of magnitude more expensive than comparable optical encoders and need well defined environmental conditions.

In addition, the maximum speed is also limited. Nevertheless, for very high requirements on accuracy, their use can be justified.

3.4 Acceleration Measurement

Adding acceleration measurement to a motion control system significantly improves the knowledge of the movement of the controlled system. Acceleration is proportional to the sum of all forces acting on a linearly moved mass. Therefore, accelerometers are also able to detect external disturbance forces, such as machining forces and friction forces. In contrast to measuring speed or position for disturbance force detection, the obtained signal is not attenuated by the integration relationship between acceleration, speed, and position. Hence, external disturbances are compensated for more directly.

At the beginning of their development, accelerometers have been used to measure only dynamic accelerations [BdRK94]. Piezoelectric accelerometers have been employed as vibration sensors, e.g. for modal analysis. It has only been recently that sensors which also measure static acceleration have been required. Accelerometer technology has significantly evolved in recent years. This development has mainly been driven by two factors. First, manufacturing technology in the field of micro-machining and micro-electronics has made considerable progress. Thus, it is possible today to combine mechanical components with electronic signal conditioning circuitry on one single chip. And second, accelerometers are used in various industrial applications, which means that huge quantities of these sensors are manufactured. Accelerometers are available in a wide range of accelerations, bandwidths, and prices. Today, even low cost products guarantee high precision.

In the following, the main accelerometer types are briefly explained. Their characteristics are outlined and the different types are compared. We restrict ourselves to inertial accelerometers which are commercially available. The technical data of two low cost accelerometers are summarised in Appendix B.3. Other sensor types, as e.g. sensors for direct measurement of relative accelerations based on eddy currents [Hil96], are under development and will possibly provide interesting alternatives to the inertial sensors.

3.4.1 Mechanical Characteristics of Accelerometers

Most of today's accelerometers are based on a mass-spring system. In this setup, a mass is suspended with a spring. Without acceleration, the mass is in neutral position. In the presence of a constant acceleration, the mass moves and remains at that point of deflection where the spring force is equivalent to the inertial force due to the acceleration of the mass. To measure the acceleration, the deflection is transformed into an electric signal.

The mass-spring system is modelled as a second order system with the main parameters being resonant frequency and damping. For the derivation of this model, the reader should refer to [DRM93]. The design of the sensor is a compromise between sensitivity and operational frequency range [BdRK94]. A higher sensitivity, obtained by a bigger mass, lowers the resonant frequency and hence the usable bandwidth. From the theory of second-order systems it is known that the highest usable bandwidth can be achieved when the movement is critically damped. Over-damping would lower the usable bandwidth, and under-damping could generate mechanical resonances. The damping of accelerometers is determined by the viscosity or pressure of the

medium in which the mass is placed, and by the dimension of gaps in which the mass can freely move in [KdR94].

Accelerometers have to be robust against very high acceleration peaks due to shocks, which occur during transport, mounting, or even during measurement. Therefore, accelerometers have overrange protection and bear for accelerations which exceed the maximum measurement range by more than an order of magnitude.

Most small-size accelerometers are silicon sensors, manufactured by micro-machining and photo fabrication. They often have a monolithic structure, i.e. the sensor is basically one single element. This structure reduces assembly costs for producing high-performance sensors [BdRK94]. The main matters of concern when fabricating acceleration sensors are temperature coefficient, non-linearity, cross-axis sensitivity, overrange protection, and other reliability problems [BdRK94].

The accelerometer weight often influences the measurement, as mentioned in [BdRK94] and [Bra92]. This problem does not occur in the case of machine-tool axis control due to the relation between accelerometer mass (some grams) and the axis slider mass (some tenths of kilograms).

3.4.2 Detection Methods

As we have seen in the previous section, a mass inside the accelerometer is displaced in the presence of an acceleration. Here, we summarise the possible detection methods to transform this deviation into an electrical signal. The detection of the displacement is mainly based on two different methods. A first one monitors the strain in the spring caused by the acceleration. The following effects are used for strain detection [BdRK94].

- *Piezoresistive* elements change their resistance when stress or strain is applied to them. Piezoresistive sensors also detect static accelerations. They are further discussed in Section 3.4.2.1.
- *Piezoelectric* elements induce charges on their surface, when pressure is applied by the inertial mass. Due to leakage currents, these charges do not persist with constant accelerations. Therefore, no static accelerations can be measured with this method, which is briefly discussed in Section 3.4.2.3.
- *Resonant* sensors are based on a mechanical oscillator that changes its natural frequency as a function of the applied acceleration. In the case of vibrating beam accelerometers, the natural frequency of the beam is changed by the inertial mass suspended on the beam. The mechanical structure is actively excited and the natural frequency detected. Different methods for excitation and detection are possible [BdRK94]: Electrostatic excitation and capacitive detection, thermal excitation by periodic heating and piezoresistance detection, piezoelectric excitation and detection, and electro magnetic excitation and detection.

A second type of monitoring the acceleration measures the deflection of the mass-spring system caused by accelerations directly [BdRK94]:

- *Capacitive*: The capacitance varies with the distance between the two electrodes of a capacitor. In the case of capacitive accelerometers, the deflected mass and a metal plate on the substrate form a capacitor. For further details, see Section 3.4.2.2.

- *Optical*: The light intensity as measurand is modified by the acceleration-caused deviation of the mass.
- *Permanent magnet*: In this setup, the mass is a permanent magnet. Magnetic sensors, e.g. Hall elements, detect its displacement. The precision is rather limited.
- *Inductive*: The displacement is detected by a differential transformer.

From these different detection methods, mainly the piezoresistive, the capacitive and the piezoelectric are widely applied. Highly precise sensors are commercially available, most of them at low cost. Therefore, only these three detection methods will be further discussed in the following.

3.4.2.1 Piezoresistive Accelerometers

Piezoresistive accelerometers measure the strain on the spring induced by the acceleration acting on a mass. They have been developed for more than a decade [KdR94]. They are capable of measuring static as well as dynamic accelerations up to medium frequencies and provide medium sensitivity at low cost.

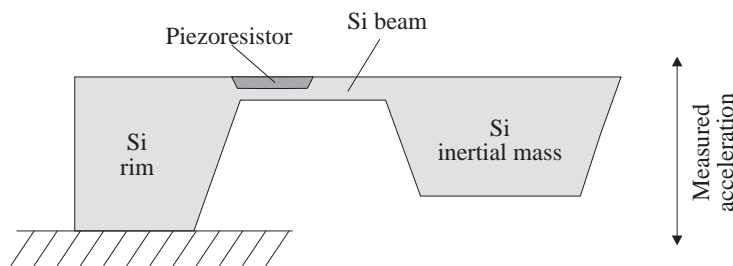


Figure 3.6: Schematic of piezoresistive accelerometer [KdR94].

Figure 3.6 illustrates the basic setup of a piezoresistive accelerometer. The sensor is composed of three components: a base, a beam, and an inertial mass. All these components are made of silicon. The base serves for fixing the structure on the housing of the sensor. The beam acts as spring. Accelerations acting on the inertial mass deflect the beam. Piezoresistors for detecting the strain are mounted on the beam near the base part, where the strain is maximum. By diffusing the piezoresistive element on the beam, a small monolithic accelerometer structure is obtained [BdRK94].

Piezoresistive accelerometers have a low output impedance. Therefore, the output signals can be used without on-chip signal conditioning circuitry [BdRK94]. However, the piezoresistors are sensitive to temperature changes. Sometimes, active temperature compensation is required. Much of the temperature-drift problems can be solved by using a Wheatstone bridge configuration.

In the following, some characteristics of the *Wheatstone bridge* are briefly reviewed. This paragraph is a summary of the discussion in [KdR94]. For more details the reader is to refer to this reference. In general, two opposite resistances of the bridge are placed on the sensor in order to have the current flow in the direction of the stress, and the two other resistances in order to have it perpendicular to the stress. Therefore, stress on the beam decreases the resistance of the two former resistances and increases the one of the two latter ones. This setup

increases the sensitivity. The Wheatstone bridge configuration directly outputs a voltage. If the bridge is perfectly balanced, common-mode temperature influences are not visible at the differential bridge output. Often, passive temperature compensation techniques are sufficient. An interesting method of sensing the internal temperature for active compensation is to observe the relationship between the bridge voltage and the total bridge current. Thus, the piezoresistors act as temperature sensors.

To specify the performances obtained by purely passive temperature compensation, three different coefficients are defined:

- The *Temperature Coefficient of Offset (TCO)* indicates the relationship between temperature and output offset. With the Wheatstone bridge setup, the temperature dependency of the piezoresistors is not of major influence on the TCO. Residual stresses on the resistors and their temperature dependency are more important and have to be reduced by a careful sensor design. Manufacturers usually define a setup for the electronic circuit to be used including exact values of compensation resistances given for each sensor individually. When using this electronics, they guarantee a certain TCO for their devices.
- The *Temperature Coefficient of Sensitivity (TCS)* defines the dependence between temperature and output sensitivity of the bridge. The temperature dependence of the piezoresistors has the main influence on this coefficient. Manufacturers also provide a maximum TCS for a certain electronic circuitry and a specific sensor. By using a constant bridge current instead of a constant bridge voltage, this phenomenon is partially compensated for, depending on the respective bridge resistance values.
- The *Temperature Coefficient of Resistance (TCR)* defines the relationship between temperature and total bridge resistance.

Piezoresistive type accelerometers have been used in this work. A summary of their data sheets is given in Appendix B.3. In addition to the general sensor information, the manufacturer provides a special calibration data sheet for each sensor. It specifies sensitivity, offset, bridge resistance, damping ratio, resonant frequency, TCO, TCS, TCR, and temperature compensation resistor values to be used.

3.4.2.2 Capacitive Accelerometers

Capacitive accelerometers directly measure the deflection of the mass-spring system due to acceleration by transforming the deflection into a capacitance change. Their measurement range comprises static accelerations as well as high frequency accelerations. In general, they are more sensitive than the piezoresistive types, but need more complex signal conditioning electronics.

The general setup illustrated in Figure 3.7 is similar to the piezoresistive type. A silicon mass is fixed on a base part by a silicon spring. The mass acts on the same time as inertia and as one electrode of a capacitor. A second electrode is fixed on the base of the accelerometer. When the mass gets out of its neutral position due to accelerations, the distance between the two electrodes and thus the capacitance changes. An oscillator with the varying capacitor as timing element detects the capacitance and generates an output frequency as a function of the capacitance.

A detailed description of the peculiarities of these capacitive sensors is found in [BdRK94]. We summarise only the most important points. As in general the relative capacitance change is

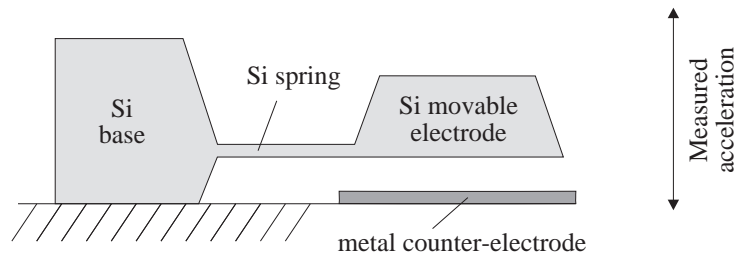


Figure 3.7: Schematic of capacitive accelerometer [KdR94].

greater than the relative resistance change, capacitive sensors have a higher sensitivity than their piezoresistive counterparts. Nevertheless, given the small size of the sensors, their capacitances are very low. The influence of parasitic capacitance and noise is thus significant. Therefore, the detection electronics has to be placed near the sensor, or better, integrated on the sensor. Usually, CMOS electronics is used for detection due to its high impedance. Different output signal types are possible. Frequency output provides good noise immunity. Voltage output is the most commonly used today. Digital output will be important in the future. The advantages of capacitive sensors compared to piezoresistive sensors are summarised in [NWN94] as follows: their sensitivity is higher and they consume less power; they have smaller temperature coefficients, because they do not have the temperature sensitive piezoresistors.

Another detection technique for capacitive accelerometers than simple capacitance measurement is *force feedback*. With this configuration the capacitor is used as sensor as well as an electrostatic force actuator. The idea behind this method is to generate an opposite equal force to the inertial force of the acceleration. A control loop exerts the necessary force to completely compensate for the inertial force, and thus keeps the mass at its neutral position, independently of the acceleration. By knowledge of the exerted force, the equivalent inertial force is known. This setup has the advantage that non-linearities of the mass spring system do not influence the result, as only small deviations from the zero force point are possible and are directly compensated for. The sensor switches periodically between a measurement phase and a force phase.

Force feedback offers different advantages. The operating range is increased [BdRK94]. These accelerometers have a high sensitivity and very high precision at moderate bandwidths [NWN94]. The force-feedback method provides the possibility of self-testing and calibration. The necessary more complex signal-conditioning circuitry and a higher current supply are the drawbacks of this solution.

3.4.2.3 Piezoelectric Accelerometers

Piezoelectric accelerometers also consist of a mass-spring system. Accelerations of the mass induce stress on a piezoelectric element, which thereby induces charges on its surface. A signal conditioning circuitry measures these charges.

The following description is taken from [DRM93], where more detailed information on this sensor type can be found. Piezoelectric material, most often single crystal quartz, contain molecules with asymmetrical charge distributions. In the presence of pressure on the element, the crystal is deformed. Positive and negative charges are relatively displaced within the crystal. This internal displacement generates external charges of opposite sign on the external surfaces of the crystal. By metallic electrodes, the external charge is detected as a voltage. The piezo-

electric sensor is modelled as a charge generator in parallel with a capacitor and a resistance. This resistance causes a leakage current which lowers the charge in the case of constant pressure on the piezoelectric element, equivalent to constant acceleration. Therefore, static accelerations cannot be measured precisely with this type of sensors. The dynamic response of the piezoelectric element itself is very high. However, the dynamic response of the complete piezoresistive accelerometer is limited by the resonant frequency of the mass-spring system of the accelerometer.

3.4.2.4 Comparison of Accelerometer Types

When focusing on commercially available products, three different detection types, namely piezoresistive, capacitive, and piezoelectric accelerometers, have to be considered possible solutions. Table 3.2, extracted from a table in [KdR94], compares their main characteristics with regard to axis control.

Parameter	Accelerometer type		
	Piezoresistive	Capacitive	Piezoelectric
Linearity error	Low	High	Medium
DC response	Yes	Yes	No
AC response	Medium	Wide	Wide
Sensitivity	Medium	High	Medium
Local electronics required	No	Yes	Yes
Cost	Low	Medium	High

Table 3.2: Comparison of piezoresistive, capacitive, and piezoelectric accelerometers [KdR94].

The *piezoelectric sensors* do not provide DC response. As low frequencies or constant accelerations are well possible in axis control, this type of sensor does not match well the requirements of the linear axis control problem and is not further considered in this work.

In general, the necessary electronics for external signal conditioning of *capacitive sensors* is complex. Compared to piezoresistive sensors, this is not a drawback any more, due to the integration of signal conditioning on chip. As an example, the capacitive sensor specified in Appendix B.3 has the same bandwidth as the comparable piezoresistive one at a lower price. In addition, it offers a direct voltage output. Capacitive type accelerometers have a higher sensitivity than piezoresistive ones. The high linearity error of capacitive type accelerometers mentioned in Table 3.2 has been reduced by the manufacturers. Low cost accelerometers with a good linearity are available today.

In [BdRK94], it is stated that *piezoresistive type sensors* are generally simpler than their capacitive type counterparts and have a better frequency response. This is in contradiction to Table 3.2. With today's manufacturing technology, both types have a very similar mechanical structure. Therefore, performance criteria such as damping, bandwidth, and precision depend more on manufacturing precision and hence on the price than on the readout technique. We completely agree with Bradley when he states in [Bra92] that in either configuration, the conditioning of the output signal is of great importance, and when he adds that the development of smart sensors and transducers with the initial signal conditioning located on the same chip as the sensor itself is likely to be of major importance. Operations such as linearisation, filtering, and scaling are implemented by the manufacturer and hence adapted to the sensor that way.

3.4.2.5 Accelerometer Inaccuracies

Let us briefly discuss some error sources which occur when measuring acceleration. The different errors are seen in the context of linear-axis control.

- *Non-linearities* generally add new frequency components to the output signal. This is not wanted on an acceleration signal. Therefore, sensors with high linearity have to be used. Time invariant non-linearities can be identified and compensated by look-up tables.
- *Temperature drift* is mainly a problem of the piezoresistive type sensors. Temperature changes cause, for this sensor type, *gain drifts* and *offset drifts*. When working at variable temperatures, drift effects have to be adaptively compensated for.
- *Transversal sensitivity* denotes the influence of accelerations in other directions than the measuring direction. Linear-drive axes usually have one degree of freedom and, therefore, transversal sensitivity does not pose any problems.
- *Resonance frequencies* of the accelerometers have to be avoided. Their excitation is possible due to structural resonances and as a result of control action. In the presence of high acceleration amplitudes near or at the resonant frequency, the sensor could reach saturation due to the gain, which is often higher than unity at this frequency. Thereby, the measurement becomes unusable.
- *Mounting* of the accelerometers on the structure of the axis is a crucial point, according to our experiences. Due to local mechanical resonances of the axis structure, measured signals can be made unusable, because the amplitudes of the resonance accelerations are bigger than the ones of the axis accelerations. We employ heuristics to determine an optimal position for the sensor. By exciting the axis with a deterministic signal and assessing the measured acceleration, unsuitable places are recognised and better places may be looked for. This method is not scientific; based on heuristics on possible spots of minimum resonances, however, good results are obtained within a short time period and without costly measurement equipment. Of course, modal analysis directly identifies the locations of nodes of the mechanical modes of the structure, which are advantageous for mounting accelerometers. However, this approach necessitates costly measurement equipment, and the expense is not justified.

3.5 Other Measured Variables

3.5.1 Axis Speed

Knowledge of the axis speed is important for feedback control. The speed is usually obtained by differentiation of the position. For high bandwidth control, however, this method leads to quantisation noise and hence to considerable control chatter. Thus, there is a need for direct speed measurement. The only practical solution is the linear-velocity transducer (LVT).

A self-generating LVT is discussed in [DRM93]. This device is based on electro magnetic induction. The output voltage of this transducer is proportional to the axis speed. Its schematic representation is shown in Figure 3.8. A permanent magnet core moves in two windings, which are wired in opposition. This special setup has as its consequence the magnet's ability to move

from its shown initial position half its length to the right and half its length to the left always generating a signal proportional to its speed. In addition, non-idealities in the magnetic field are compensated to a high degree. In [DRM93], it is stated that with this setup linearities of $\pm 1\%$ are achieved.

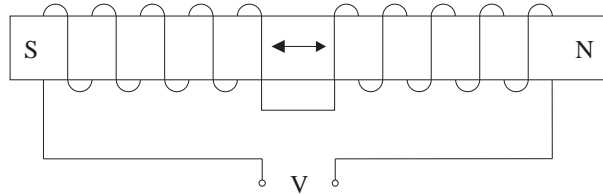


Figure 3.8: Linear velocity transducer (LVT) [DRM93].

Philipp discusses direct speed measurement for linear-drive axes in [Phi92]. He states that this solution poses some problems:

- *Size, cost:* Direct-drive machine-tool axes may move very slowly. Inductive speed sensors adapted to these speeds are large and expensive.
- *Bandwidth:* The high inductance of these sensors limits the usable bandwidth. The necessary anti-aliasing filter further reduces the bandwidth.

Philipp concludes that inductive speed sensors are not well adapted to digital control of direct drives. To our knowledge, no considerable progress in the field of direct speed measurement has been made recently. Therefore, the drawbacks (cost, size, bandwidth) of the inductive solutions persist and we did not pursue this direction any further in this dissertation.

3.5.2 External Force

Sensors for measuring the force between two mechanical pieces are commercially available. Forces acting on these sensors cause shear, which is detected by piezoresistive elements. These sensors usually have a considerable mass. More details are found in [DRM93]. Alter successfully implemented tool force measurement with force feedback control for increasing the stiffness of linear motor machine-tool feed drives [Alt94]. Tool force measurement provides information exclusively on the force between the tool and the axis. Friction forces are not detected and hence not compensated for.

Alter concludes that acceleration instead of force measurement would be advantageous for the following reasons. First, accelerometers need not be placed at the point, where external disturbances have their effect. Second, acceleration sensors do not affect the system dynamics or add a significant mass to the linear axis. Therefore, we do not investigate the use of force sensors any further.

3.6 Summary and Conclusions

Different sensors which are possible for motion control of linear-drive machine-tool axes have been reviewed in this chapter. Their main characteristics are briefly summarised here.

The most important variable to be measured for axis motion control is the *axis position*. Linear encoder rules with signal periods from 128nm to 10mm are available. Their output signals can be interpolated by factors up to 4096. In practice, only factors up to about 200 turn out to be useful, due to measurement noise. The choice of ruler signal period and interpolation factor results from a compromise between high maximum axis speed and high position resolution.

The use of *laser interferometry* is recommended only for special applications with strong requirements on accuracy. First, because these devices are very expensive and provide an accuracy which is beyond what can be obtained by the mechanical setup of machine-tool axes. Second, because they have restrictions on the environmental conditions, e.g. stable temperature. And third, due to their high resolution, the maximum axis speed is rather limited.

Micro-machined low-cost *inertial accelerometers* provide a good means to obtain complementary measured motion information to the position. They are very precise and a variety of different types with different interfaces and performances exists on the market. They are easy to use and do not change the system's dynamics, because of their low mass.

Direct speed measurement with *inductive speed-measurement devices* is not well adapted to linear drive machine-tool axis control due to its complexity and limited bandwidth.

Measurement of *external forces* is well possible, as precise sensors are available. These devices, however, add a considerable load to the system and thus influence its dynamics. In addition, this force measurement provides no information on friction influence, which is a drawback when designing control systems.

Based on this review of sensors, we decide to use optical position measurement with interpolation as the base for linear-axis motion control. These sensors offer the desired accuracy and resolution, are commercially available, and have an adequate cost-performance ratio. They are commonly used for machine-tool applications today. In addition to position measurement, we propose the use of low-cost accelerometers. They provide the additional dynamic information, which is necessary for motion control of high-bandwidth direct-drive axes.

References

- [Alt94] D.M. Alter. *Control of Linear Motors for Machine Tool Feed Drives*. PhD thesis, University of Illinois at Urbana-Champaign, 1994.
- [BdRK94] H.H. Bau, N.F. de Rooij, and B. Kloeck, editors. *Mechanical Sensors*, volume 7 of *Sensors: A Comprehensive Survey*. VCH Verlag, Weinheim, 1994.
- [Bra92] D.A. Bradley. Transducers for motion control. In *IFAC Motion Control for Intelligent Automation*, pages 45–56, Perugia, October 1992.
- [DRM93] J.W. Dally, W.F. Riley, and K.G. McConnell. *Instrumentation for Engineering Measurements*. John Wiley & Sons, Inc., New York, 2nd edition, 1993.
- [Hag96] Rainer Hagl. Längenmesssysteme für Linearmotoren. ISW Lageregelseminar, Stuttgart, 1996.
- [Hil96] Bernhard Hiller. Hochgenaue Messung von Zustandsgrößen an NC-Achsen. ISW Lageregelseminar, Stuttgart, 1996.

- [HSW89] J.A. Haslam, G.R. Summers, and D. Williams. *Engineering instrumentation and control*. Edward Arnold, London, 1989.
- [KdR94] B. Kloeck and N.F. de Rooij. *Semiconductor Sensors*, chapter 4: Mechanical Sensors, pages 153–204. John Wiley & Sons, Inc., New York, 1994.
- [Kun93] Murat Kunt. *Traitement numérique des images*. Presses polytechniques romandes, Lausanne, 1993.
- [NWN94] K. Najafi, K.D. Wise, and N. Najafi. *Semiconductor Sensors*, chapter 10: Integrated Sensors, pages 473–530. John Wiley & Sons, Inc., New York, 1994.
- [Phi92] W. Philipp. *Regelung mechanisch steifer Direktantriebe für Werkzeugmaschinen*. Springer Verlag, Berlin, 1992.
- [Wal85] Hans Walcher. *Winkel- und Wegmessung im Maschinenbau*. VDI-Verlag, Düsseldorf, 2nd edition, 1985.

Chapter 4

High-Precision Speed Estimation

Highly dynamic direct-driven machine-tool axes require controllers with a high closed-loop bandwidth and an excellent disturbance rejection in order to take full advantage of their increased dynamic performance. High controller bandwidth with its resulting high sampling frequency makes great demands on the system state measurement and estimation. As already mentioned in Section 2.4 and more detailed in Section 5.1, the accurate estimation of the axis speed is one of the key issues of the control of highly dynamic machine-tool axes. As a result of design, the accuracy of the employed position encoder is adapted to the required axis precision. However, with a high bandwidth, the position-only speed estimation requires higher position resolution. Therefore, it imposes restrictions on the digital control of high-bandwidth axes. The different possibilities of speed estimation, their limitations, and possible enhancements are the topic of this chapter. They will be analysed and compared concerning the delay on the signal and their output noise caused by quantisation. The influence of these two factors on the closed-loop performance is discussed in Chapter 5.

The remainder of this chapter is structured as follows. After a brief introduction to the speed estimation problem in Section 4.1, Section 4.2 compares different, commonly used position-only methods to estimate drive speed. In Section 4.3, a novel fusion method to combine position and acceleration measurement to a highly accurate speed estimation is proposed. After a review of related work, the algorithm is developed and analysed. The proposed method includes on-line identification of accelerometer gain and offset. Experimental results demonstrate its successful implementation and advantages. Section 4.4 finally compares the different speed estimation approaches.

4.1 Introduction

The use of position-only speed estimation raises the problems of quantisation noise and delay on the resulting speed signal. Both effects reduce the closed-loop performance of the speed control loop. Noise leads to control chatter which unnecessarily heats up the motor, may excite system modes and hence, deteriorate the surface quality of the machined pieces. Delay, on the other hand, reduces the maximum possible bandwidth of a stable closed-loop system. All designs of position-only speed estimation algorithms lead to an inherent trade-off between noise and delay on the resulting signal: reducing chatter by filtering increases the delay on the signal. The use of state observers does not solve this problem because their design always involves a compromise between noise reduction, bandwidth, and disturbance detection. As explained in Section 3.5.1,

direct axis-speed measurement sensors do not meet the requirements of the high bandwidth and the large speed range of direct-drive axes. Therefore, they are not further considered in this chapter.

The use of more precise position measurement is a promising alternative to avoid the mentioned trade-off between noise and delay. However, today's machine-tool axes already work at the limits of the available optical encoders. Increasing the resolution and maintaining a high maximum axis speed at the same time is in fact not possible with the actual encoder technology. Therefore, more complex and more expensive measurement systems, based on laser interferometry, would have to be used. Besides the fact that this solution also limits the maximum speed, it turns out to be too expensive.

The two main arguments for the use of direct drives for machine-tool axes are a high closed-loop bandwidth and an excellent disturbance rejection. Since position encoders do not output the necessary signal quality, we propose to improve the measurement of the system state by additional acceleration measurement. This dissertation argues that by using low-cost accelerometers, the demands on the resolution of the position measurement can be considerably reduced. By fusion of the measured position with measured acceleration, a highly accurate speed estimate is obtained. The resulting output signal is of a high quality with low noise and almost no phase lag even at very high sampling rates. The success of our implementation is based on two facts. First, acceleration measurement provides, to a high degree, complementary speed information to the position signal. Second, today's acceleration measurement sensors are very cheap and accurate because of their widespread use for different industrial applications. In addition, the acceleration measurement employed to obtain an enhanced speed estimate can also be directly fed back as an acceleration feedback loop, which considerably increases closed-loop stiffness. This is further studied in Section 5.2 within the context of the control of the axes.

4.2 Position-Based Solutions

This section presents different, common methods to estimate the speed which is purely based on position measurement. In this dissertation, these methods are called *position-only methods*. An overview of algorithms basically performing a differentiation operation on the measured position will be given; they have different transfer functions and hence different noise/delay characteristics. State observers based on position measurement and on the reference force as control variable will then be analysed. Their design always leads to a trade-off between noise reduction and speed. Both have their influence on the maximum feedback gains and therefore limit the maximum available closed-loop bandwidth.

For the two methods of speed estimation discussed above, the resolution of the position measurement can be improved by oversampling the position. An implementation adapted to the specific controlled system will be developed.

4.2.1 Introduction

Before considering the use of additional sensors to standard position measurement, which inevitably increases the complexity and the cost of the measurement system, the limitation of position-only speed estimation has to be analysed. For normal motion control applications, with less requirements on bandwidth due to less dynamic actuators, there exists a variety of such algorithms which are widely applied.

Philipp in [Phi92] investigates different methods of speed estimation for direct-drive machine-tool axes. First, given enough CPU power and considering the overall system performance, it is often advantageous to estimate the speed by a discrete differentiation of the position signal with a high sampling frequency. Unfortunately, a high sampling frequency deteriorates the signal to noise ratio of the estimated speed, because of the quantisation of the position measurement. The quantisation step size thus becomes the limiting element for bandwidth, stiffness and the overall performance of an axis. Second, employing state observers is only of very limited use for this specific control problem. The main disadvantages are their sensitivity to model errors and external disturbances. Finally, direct speed measurement devices for direct drives all have some major drawbacks, in particular complexity and limited bandwidth (see Section 3.5.1).

For comparing different position-only speed estimation algorithms, two criteria are important:

- *Delay*: almost all numerical position-only speed estimation methods introduce a certain delay on the estimated speed signal. This delay is usually in the range from half a sampling period up to a few sampling periods.
- *Quantisation noise*: the position-based speed estimation algorithms inherently execute a differentiation operation. This operation amplifies errors on the measured signal, such as quantisation noise and other types of measurement noise. Quantisation noise is normally expressed by the *quantisation step size* or the *variance*.

In the following section, the different methods will be characterised. The influence of the two above-mentioned criteria on the closed-loop system will be evaluated in Section 5.1. All methods presented below are based on a regular sampling in a digital control system. Speed estimation methods based on measuring the time between two encoder steps are excluded. As previously mentioned, the interpolation units output the encoder increments as a function of an internal clock which is only approximately proportional to the actual speed. Therefore, the quality of the obtained speed would not be satisfactory.

All results are given as a function of the position resolution, offering the possibility to directly determine the benefits to speed signal quality by resolution improvement. It should be noted, however, that increasing the resolution always leads to a further reduction of the maximum speed, independently of the employed encoder type, as explained in Section 3.3.

4.2.2 Survey of Position Differentiation Algorithms

In the field of numerical control systems, the method most frequently used to determine the actual drive speed is the differentiation of the measured position. This applies to rotary encoder signals as well as to linear encoder signals. Therefore, there exists a variety of methods for differentiation with different characteristics, which will be analysed in terms of variance and delay. In this thesis, the discussion will be restricted to the four most important methods, which are taken from [Föl85] and [CS92].

- A. The *direct differentiation* is the most commonly used method. It calculates the speed as the simple difference between the actual position and the last position measurement divided by the sampling period. Therefore, it is very sensitive to position quantisation for short sampling periods. Its output has a delay of half a sampling period.

- B. The *mean speed method* is based on the last four position measurements. The mean position \bar{x}_k at the point in time $(k - 1.5)$ is the basis for the calculation.

$$\bar{x}_k = \frac{1}{4} (x_k + x_{k-1} + x_{k-2} + x_{k-3})$$

The speed estimate is calculated as the average of the differences between the four points and the mean position divided by the respective time differences:

$$v_k = \frac{1}{4} \left[\frac{x_k - \bar{x}_k}{1.5 \cdot T_{sampl}} + \frac{x_{k-1} - \bar{x}_k}{0.5 \cdot T_{sampl}} + \frac{\bar{x}_k - x_{k-2}}{0.5 \cdot T_{sampl}} + \frac{\bar{x}_k - x_{k-3}}{1.5 \cdot T_{sampl}} \right]$$

This solution is less sensitive to position quantisation due to the mean value generations, but it has an increased delay.

- C. The *delayed differentiation* is a direct differentiation which additionally takes into account the last speed estimate weighted by a factor (τ) . It has the structure of an IIR filter. Increasing the time constant τ reduces the quantisation noise, but increases the delay. The special case with $\tau = 0$ is equivalent to the direct differentiation. The two cases where $\tau = T_{sampl}$ and $\tau = 2 \cdot T_{sampl}$, denoted C1 and C2 respectively, will be analysed below.
- D. The *quadratic interpolation* method is a special case of the more general n-th order polynomial interpolation. This method assumes the measured value to have the form of a second order polynomial. The polynomial crossing the last three position samples is determined. Its gradient at the last position sample is equivalent to the speed at this point. This method provides a speed estimate with no delay, but a high sensitivity to position quantisation.

	Formula	Variance	Delay
A	$v_k = \frac{x_k - x_{k-1}}{T_{sampl}}$	$\frac{q^2}{12} \frac{2}{(T_{sampl})^2} = 0.17 \cdot \frac{q^2}{T_{sampl}^2}$	$0.5 \cdot T_{sampl}$
B	$v_k = \frac{x_k + 3x_{k-1} - 3x_{k-2} - x_{k-3}}{6T_{sampl}}$	$\frac{q^2}{12} \frac{0.56}{(T_{sampl})^2} = 0.05 \cdot \frac{q^2}{T_{sampl}^2}$	$1.5 \cdot T_{sampl}$
C1 ^a	$v_k = \frac{x_k - x_{k-1} + \tau v_{k-1}}{T_{sampl} + \tau}$	$\frac{q^2}{12} \frac{2}{(\tau + T_{sampl})(2\tau + T_{sampl})} = 0.03 \cdot \frac{q^2}{T_{sampl}^2}$	$1.5 \cdot T_{sampl}$
C2 ^b		$= 0.01 \cdot \frac{q^2}{T_{sampl}^2}$	$2.3 \cdot T_{sampl}$
D ^c	$v_k = \frac{3x_k - 4x_{k-1} + x_{k-2}}{2 \cdot T_{sampl}}$	$\frac{q^2}{12} \frac{6.5}{(T_{sampl})^2} = 0.54 \cdot \frac{q^2}{T_{sampl}^2}$	$\cong 0 \cdot T_{sampl}$

^aValues for $\tau = T_{sampl}$

^bValues for $\tau = 2T_{sampl}$

^cZero delay is only correct for exact quadratic position evolution

Table 4.1: Comparison of variance and delay of position-only speed estimation methods.

The variances of the different position-only speed estimation methods presented in Table 4.1 are based on the theory of Appendix A.1. The delays of the methods A and B are easily obtained from the respective formulae. The estimation of the delay for the two examples of method C are approximations because their IIR structure does not fit well with the used scheme of pure

time delays. The indicated values have been obtained by comparison of their phases with the phase of method B in the lower frequency range. The indicated zero delay for method D is only correct when the position evolves in an exact quadratic polynomial shape.

The term *variance* is defined in Appendix A.1. Here, only an intuitive interpretation of variance is given. The mean square value $\overline{x^2}$ denotes the expected value of the square of a random variable. This indicates the expected total power of the signal described by the variable. It is composed of two summing terms, the square of the mean value $(\overline{x})^2$, and the variance σ^2 , as follows: $\overline{x^2} = (\overline{x})^2 + \sigma^2$. In the case where the mean value is zero, the variance equals the mean square. Therefore, the variance can be seen as a kind of “noise power”. Of course, in the presence of a mean value, this noise power is not physically measurable, but it is present as a disturbance on the signal.

Variance and delay generated by a certain differentiation method provide a general measure of its performance over the whole frequency range. As not all the discussed methods fit well into the used variance/delay scheme, their discrete transfer functions will now be compared. We are interested in the *total transfer functions* of the respective algorithms, i.e. the transfer function from the unknown real speed v_{real} to the output speed v_k of the algorithm. Figure 4.1

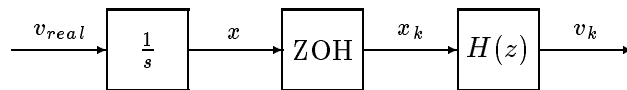


Figure 4.1: Elements of differentiation algorithm.

shows the elements which compose this total transfer function. The measured position x_k is the sampled real position x , which is the integral ($\frac{1}{s}$) of the real speed. The discussed differentiation methods are applied on this measured position x_k . Their discrete transfer functions $H(z)$ are easily derived from the formulae of Table 4.1. The employed numerical software MATLAB [Mat94] calculates the Bode plots of discrete and continuous transfer functions directly, with the gain transfer functions at the top and the phase transfer function at the bottom of the figure. Usually, a logarithmic frequency scale is used for these Bode plots. The gain factors are indicated in decibels (dB).¹ Negative phase angles denote phase lag, positive ones denote phase lead. By numerically combining the continuous Bode plot of the integral term with the discrete Bode plot of the algorithms, the plots of the total speed transfer functions are obtained. It is important to note, that no phase lead is possible for the total speed transfer function due to the causality of the signals.

The resulting total speed transfer functions from the real speed v_{real} to the calculated speed v_k are depicted in Figure 4.2. The sampling period T_{sampl} is normalised in this figure to 1s. Hence, the indicated frequencies are all relative to the sampling frequency. The Shannon frequency is $0.5 \cdot T_{sampl}$. It is important to note that, in this case, the ideal transfer functions would be straight lines with unity gain² and zero phase shift.

From Table 4.1 and Figure 4.2, it can be concluded that the direct differentiation (A) constitutes a good compromise between quantisation noise amplification and phase lag. It causes an average delay of half a sampling period on the speed. Compared to this method, the mean speed (B) and the delayed differentiation (C1) have only half its variance but at the expense

¹Equivalent to $20 \cdot \log_{10}(\text{gain})$.

²Equivalent to 0dB in Figure 4.2.

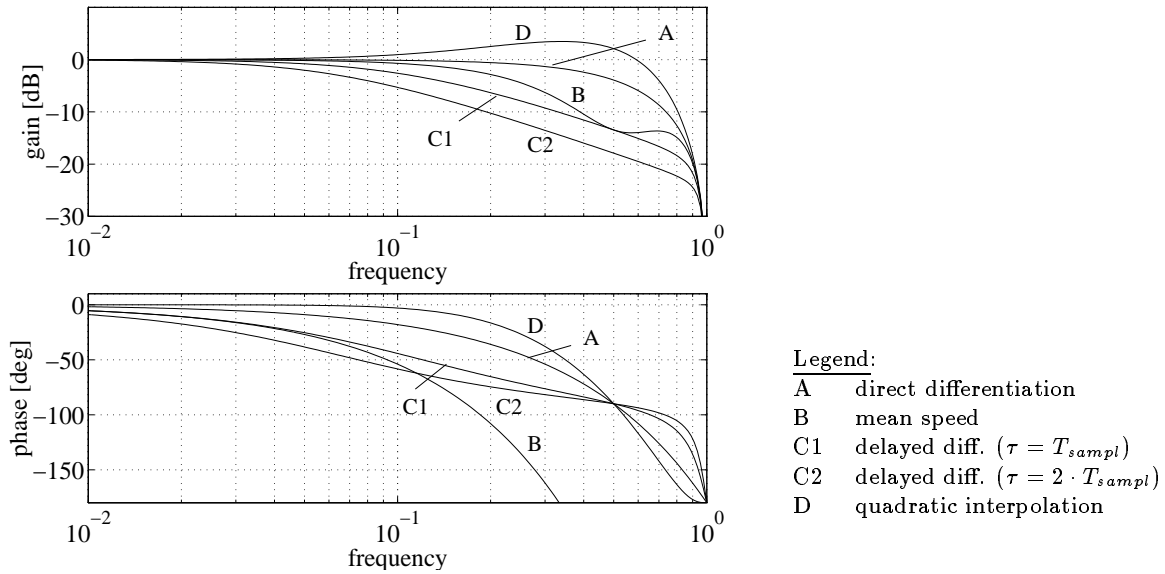


Figure 4.2: Total speed transfer function of different differentiation methods.

of a tripled phase lag. The delayed differentiation (C2) has furthermore reduced variance but increased phase lag. The two examples (C1) and (C2), with $\tau = T_{\text{sampl}}$ and $\tau = 2 \cdot T_{\text{sampl}}$ respectively, have been selected to show solutions which are comparable to the other methods. Tuning the design parameter τ determines the trade-off between variance and phase lag. The direct differentiation may be seen as a special case of the delayed differentiation with $\tau = 0$. The quadratic interpolation (D) is not well adapted to this problem despite its minimum phase lag. By putting a parabolic curve across the last three position samples, quantisation noise on these samples becomes too dominant. The result is a high variance which is a factor of about three higher than the variance of the direct differentiation.

The variance of all the discussed methods varies with the square of the position resolution q and the inverse square of the sampling time T_{sampl} . In order to give an idea of the order of magnitude of the speed quantisation for a practical example, the direct differentiation is analysed with data of the 75N experimental drive (see Appendix C.1.1). With a controller sampling time of $T_{\text{sampl}} = 100\mu\text{s}$ and an encoder resolution of $q = 400\text{nm}$, a speed quantisation of $\frac{400\text{nm}}{100\mu\text{s}} = 4\frac{\text{mm}}{\text{s}}$ results. Although this speed quantisation does not seem to be very large compared to the maximum speed of about $1\frac{\text{m}}{\text{s}}$, it generates well audible control chatter for reasonable controller feedback gains.

Of course, there exist many other solutions by which the differentiated value of a measured value can be obtained, e.g. direct differentiation with filtering afterwards. Indeed, they all lead to a trade-off between phase lag and variance because the position signal quantised in time and amplitude does not contain more information and thus constitutes the limiting element.

4.2.3 State Observers

State observers [Ise87a] for the speed estimation are also discussed in this section dealing with position based estimators since the position is the only measured variable they need. They estimate system states based on known system inputs and measured system outputs. Their design is based on knowledge of the dynamics of the controlled system, called the model. Therefore,

their accuracy depends to a high degree on well known dynamics.

In state-space representation, a plant is characterised by the input matrix \mathbf{B} , the dynamics matrix \mathbf{A} , and the output matrix \mathbf{C}^T . The structure of the state observer for such a plant is shown in Figure 4.3. In parallel to the plant, a model of the plant with the same matrices estimates the internal system state $\hat{\mathbf{x}}_k$ of the system based on the system input $u(k)$ and the last estimated system state $\hat{\mathbf{x}}_{k-1}$. In addition, the estimated system output \hat{y}_k is compared to the measured output value y_k . The estimation error Δe_k is fed back into the observer via appropriate feedback gains in \mathbf{H} to reduce the long-term estimation error to zero. This feedback loop gives the observer its own dynamics, which has, in general, to be an order of magnitude faster than the closed-loop control system dynamics. Thus, estimation errors decay faster than controller errors and the controller bases its control action not on transient errors of the observer. The choice of the feedback poles for the calculation of \mathbf{H} constitutes a compromise between sensitivity to measurement noise and fast reduction of estimation errors.

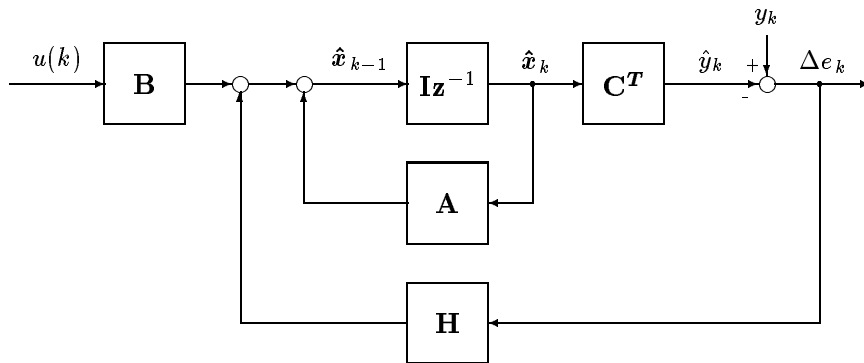


Figure 4.3: State observer structure.

Two different structures of observers will now be briefly reviewed with respect to the linear-drive axis control problem, and the reasons for not considering them further for this control problem will be given. After the discussion of ordinary state observers, based on the model of the controlled system, a special kind of observers, a form of disturbance observers will be looked at.

4.2.3.1 Conventional Observers

The use of conventional observers as shown in Figure 4.3 for linear-drive machine-tool axes has already been discussed in [Phi92] and [Zir96]. Both authors conclude that the design of the observer implementation, usually done by pole placement, leads to a limiting trade-off between reachable closed-loop bandwidth and quantisation noise reduction. For fast poles, quantisation effects are well audible [Zir96].

For linear-drive machine-tool axes with considerable external disturbances as friction and machining forces, conventional observers have some major drawbacks. In the presence of important unmodelled disturbances, they output incorrect state estimations [Büh83]. Hence, state observers are not appropriate for the necessary disturbance rejection of direct-drive machine-tool axes.

4.2.3.2 Disturbance Observers

The disturbance observer adds terms for disturbance estimation to the conventional observer structure. These estimations are taken into consideration when estimating the state variables. Therefore, stationary disturbances do not generate stationary estimation errors on the state variables. Transient disturbance effects are only compensated for if they do not exceed the disturbances observers dynamics imposed by pole placement during design.

Hori investigates in [Hor93] the use of an *instantaneous speed observer* based on a low-precision shaft encoder for rotary drives and the current measurement of the DC motor. This observer is a discretised form of the continuous disturbance observer. It observes speed as well as disturbance torque based on two sampling activities which work at different frequencies:

- The *fast sampling* is the controller sampling with update of the controlled variable and stepwise calculation of the actual speed by integrating observed speed, disturbance torque, and motor torque.
- The *slow sampling* is the observer sampling with readout of position to adjust observed speed and disturbance torque based on measured position.

An observer for speed and disturbance torque works with the slow sampling rate and is based on position and motor current input. The speed for the faster sampling rate between the observation steps is obtained by integration of speed and disturbance torque at the time of the last observation. For this integration, the observer needs information of the inertia of the rotating part. In the case of inertia variations, the inertia has to be identified on-line, as described in [Hor93].

The disturbance torque is observed with the slower sampling rate. The poles of the observer have therefore to be chosen in such a way as to have much slower dynamics than the dynamics possible with the high sampling rate. Hence, high frequency disturbances which are typical of axes with stiction and machining forces are not sufficiently well rejected. Therefore, an application of this solution to our linear-drive control problem is not further studied here.

4.2.4 Oversampling

Oversampling consists of sampling a measured variable with a higher frequency than the controller sampling frequency, thus measuring the variable several times in one controller sampling interval. The finally used measure is then obtained once per sampling interval by a decimation operation [ASvdS96] which performs low-pass filtering and down-sampling to the controller frequency. The aim of this method is to reduce the variance due to measurement noise. Thus, oversampling provides an alternative to reducing the variance on a speed estimate by increasing the position resolution.

4.2.4.1 Principle

The principle of oversampling is adapted to the application of position encoder measurement enhancement. The measured position at the output of the encoder interpolation unit is over-sampled to reduce the variance on position based speed estimates. The scheme is very similar to increasing the resolution of A/D -converters by oversampling [BG90].

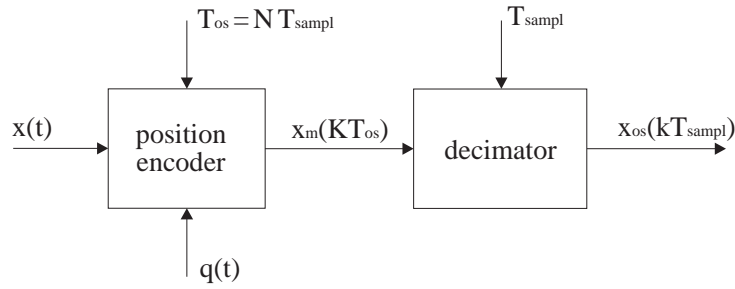


Figure 4.4: Setup of position oversampling.

Figure 4.4 shows the setup of oversampling the axis position. The output of the position encoder interpolation unit is sampled with a frequency $\frac{1}{T_{os}}$, which is a factor N , denoted *oversampling ratio*, higher than the controller sampling frequency $\frac{1}{T_{sampl}}$. The measured position x_m is quantised. The input $q(t)$ on the figure denotes the quantisation error. The oversampled position x_m is fed through the decimator block, which outputs the value $x_{os}(kT_{sampl})$, the position measurement which is improved by oversampling.

The low-pass filtering will be implemented as a simple mean value calculation, as it is proposed in [BG90]. In contrast to the cited solution, we propose the use of *oversampling in bursts* at the beginning of each controller sampling period instead of continuous oversampling. Figure 4.5 exemplifies the employed principle of oversampling in burst mode. At the beginning of each sampling interval, the position value is read several times at a high frequency. Then, the mean value of the sampled position values is calculated.

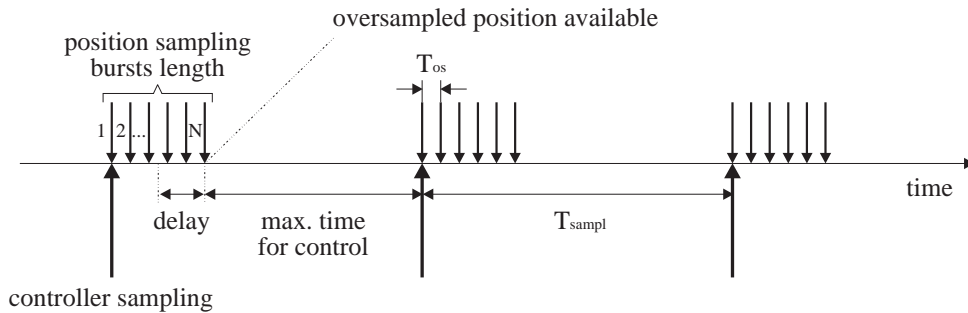


Figure 4.5: Position oversampling in burst mode.

The employed burst mode offers the advantage that the variance of the position signal is reduced without adding a long delay. It should be noted that the mean value calculation causes an average delay of half a burst length. Interpolation techniques applied to the individual position samples would probably reduce this delay, but they are sensitive to quantisation noise. Therefore, this approach is not further considered. Other filter approaches are not further detailed neither, because the aim of this section is only to test the general principle.

The final oversampled position signal $x_{os}(t)$ is obtained at the end of each burst. Only at this point in time, the controller can start to calculate its output value. Therefore, the sum of burst length and necessary controller calculation time must not exceed the controller sampling time T_{sampl} . The maximum oversampling frequency $\frac{1}{T_{os}}$ is limited by the maximum cycle time of the position interpolation unit. As this interpolation sampling frequency is not extremely high, it turns out to be advantageous in practice to use this frequency directly as oversampling

frequency. The design of the burst length N consists in finding a compromise between delay, maximum burst length and a maximum oversampling ratio.

4.2.4.2 Analysis of Burst Mode Oversampling

For sampled systems, the quantisation error of analog signals is usually a uniformly distributed quantisation noise because consecutive samples are not correlated. When sampling with very high frequencies, as is the case with oversampling, this assumption does not necessarily hold anymore. Therefore, oversampling is analysed in the following in burst mode, where the position is sampled several times in very short intervals. As a mathematical modelling of this type of oversampling would become very complex, and the benefits of such a model are rather limited, the following analysis is based on simulation.

The aim of the simulation is to know the probability of having a certain position quantisation error on the output signal and to know how the error probability is influenced by the oversampling ratio. The simulation is based on the following assumptions, which determine how the quantisation errors on the individual measured position samples are distributed during a burst:

- The speed of the axis remains constant during a burst. Therefore, maximum acceleration during a burst must not influence the speed significantly.
- The quantisation error of the first sample of the burst is uniformly distributed.
- The constant speed modulo one position-encoder-step per oversampling period is uniformly distributed. The modulo condition is based on the fact that in the case of a speed which is exactly one encoder-step per oversampling period higher than a comparable speed, the distribution of the quantisation errors during one burst remains the same.

In the simulation, a large number of examples which satisfy the above-made assumptions are generated. In these examples, burst-mode oversampling with mean value calculation is applied to different burst lengths. In Figure 4.6, the probabilities to have a certain absolute position error (normalised with encoder steps) are plotted. From these simulation results, it can be concluded that oversampling with even a low oversampling ratio, such as $N = 5$, significantly reduces the probability of having a high absolute position error. As intended, it appears that for higher oversampling ratios, the probability to have almost no quantisation errors increases. Comparisons of the presented simulations with simulations assuming non-correlation of consecutive input samples within a burst showed significant differences. Therefore, with respect to quantisation error, the taken simulation approach is well justified.

In addition to quantisation error, the interpolated measured position also contains other measurement errors. Possible sources are noise or calibration problems in the measurement electronics. These errors are not correlated with successive position samples within a burst. Therefore, its variance is reduced by a factor N by oversampling [BG90].

4.2.4.3 Typical Application

In order to demonstrate the feasibility of the proposed oversampling algorithm, experiments are performed on the 75N test bench described in Appendix C.1.1. We are interested in the gain of signal quality for the position-based speed estimates. Therefore, we directly analyse the quality

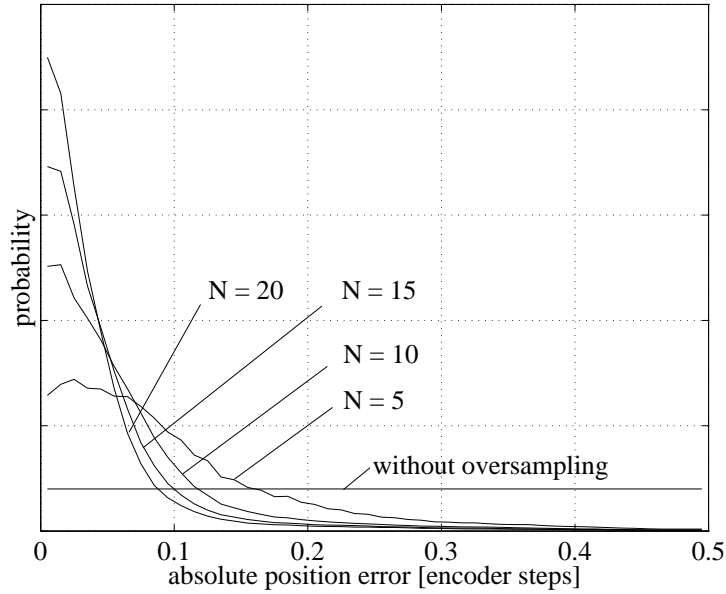


Figure 4.6: Probability to have a certain absolute error for different oversampling burst lengths.

of the final speed signals. The above-discussed variance reduction on the measured position is expected to lead to an equivalent variance reduction on the speed estimation. Table 4.2 summarises the main characteristics of measurement device and controller.

controller sampling time	$T_{s\,ampl}$	$100\mu s$
interpolation sampling time	$T_{encoder}$	$2\mu s$
position resolution	q	$400nm$
maximum acceleration	a_{max}	$47\frac{m}{s^2}$

Table 4.2: Characteristics of 75N experimental drive.

The assumptions of the above-made analysis section are examined in order to demonstrate that they can be met with a real test bench. We discuss them in the same order as above.

- The maximum deviation of the position from a straight line (constant speed) due to maximum drive acceleration results for a burst length of $N = 10$ as: $\Delta X_{max} = a_{max} \frac{\Delta t_{burst}^2}{2} = 47\frac{m}{s^2} \frac{(20\mu s)^2}{2} = 10nm$. This is in the range of $\frac{1}{40}$ position quantisation step-size.
- Consecutive burst starts are separated by $100\mu s$. It is generally accepted that, in this case, successive position samples are uncorrelated with respect to quantisation and measurement noise.
- The constant speed during the bursts has to be uniformly distributed in the range of modulo $0.2\frac{m}{s}$. Given the maximum axis speed of $1\frac{m}{s}$ and speed steps of $0.1\frac{m}{s}$ in common reference trajectories of commercial numerical axis controllers, these assumptions are met.

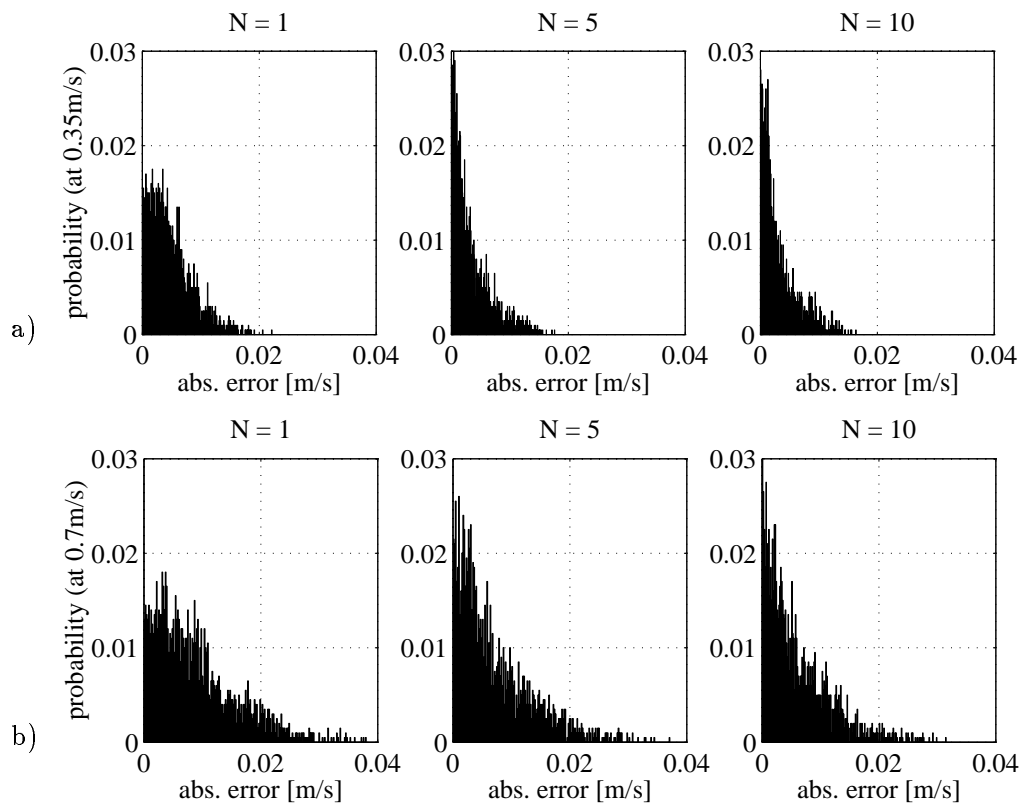


Figure 4.7: Experimental results with oversampling for constant axis speeds and for different oversampling ratios N : (a) $0.35 \frac{m}{s}$; (b) $0.7 \frac{m}{s}$.

In Figure 4.7, the results of two experiments with the 75N drive are summarised. The drive moves at two different, almost constant speeds. The probability of a certain speed error is given for different oversampling periods. The diagrams for $N = 1$ depict the results without oversampling. The scales indicating the density do not represent specific absolute values. They only show that all examples use the same scale. Two facts are important to note when looking at the two graphs on the left. First, the maximum absolute error is significantly above the expected absolute speed quantisation error of $0.002\frac{m}{s}$. Second, speed error increases with speed. The reasons for these results are measurement noise and the special signal transmission mode (burst mode) of the used interpolation box (see Section 3.3.1). In addition, the oversampling cycle cannot be synchronised with the interpolation unit. This further deteriorates the quality of the position measure, thus leading to the shown results.

As a general result, the probability of large speed errors is decreased by increasing the oversampling rate. The effective gain in quality cannot be quantified because speed errors cannot be exactly determined by these measurements since an exact speed reference is lacking. Therefore, the shown examples of Figure 4.7 give only approximative results. However, it can be clearly seen from the experimental results that measurement errors are considerably reduced by oversampling.

From the implementation of this oversampling method we draw the following conclusions: oversampling in the explained burst mode is feasible and easily implemented by minor software modifications; it needs no additional hardware. For oversampling with the numerical controller, a high performance processor is necessary. It would certainly be better to do oversampling directly in the interpolation unit and to transmit the improved position signal to the numerical controller.

4.3 Accelerometer-Enhanced Speed Estimation

In Section 2.4 it is stated that for highly dynamic machine-tool axes, a very accurate high-bandwidth speed estimation is essential to guarantee the desired performance. The review of position-only speed estimation methods in Section 4.2 concludes that the variance on the resulting speed signal increases proportionally to the square of the quantisation step size and proportionally to the square of the sampling frequency. All numerical methods for reducing the variance lead to a bigger phase lag. The discussion of linear position sensors in Section 3.3 concluded that today's machine tool-axes already work at the sensor's limits. Improving sensor resolution would inevitably lead to a further limited maximum speed. As an alternative to increasing position resolution, we propose the use of additional acceleration measurement to enhance speed estimation.

This choice of acceleration measurement is advantageous for the following four reasons. First, very accurate accelerometers are available on the market at low cost. Second, the acceleration has to be integrated to obtain a speed signal, in contrast to the position which has to be differentiated. The discrete integration of a measured variable is much less sensitive to measurement noise than the discrete differentiation. Third, the combination of both, acceleration and position measurement, leads to a very accurate speed estimation, as the two signals contain complementary information to a high degree. Theoretically, position and acceleration contain redundant speed information. By using only position measurement, the main problem is quantisation, by using only acceleration measurement, offset leads to a drift of the speed signal. By combining both measurements, the high value information of both sensors is extracted and the measure-

ment errors are suppressed. Forth, low-cost acceleration measurement lowers the demands on the position measurement, and therefore, a much cheaper position encoder system may be used, which constitutes an excellent economic argument for this alternative.

Nevertheless, acceleration measurement has some drawbacks, whose influence on the system performance have to be taken into consideration. Accelerometers are analog devices and usually output analog signals. Therefore, considerable noise on the output of these very sensitive devices cannot be excluded and an acceptable signal to noise ratio has to be verified by experiments. In addition, these analog sensors have temperature-dependent offset and gain, which have to be identified.

A novel method for combining position and acceleration measurement to a highly accurate speed estimation will be proposed. The key criteria for the development of the algorithm are a simple design, harvesting the advantages of the two different sensors, and minimising the influence of their weaknesses. Earlier solutions to this data fusion problem will be discussed. The algorithm with its numerical implementation will be developed. Algorithms for the on-line estimation of the accelerometer parameters [Gee96], namely offset and gain factor, will be derived and problems related to the implementation of the algorithm discussed. Experimental results will demonstrate the feasibility and accuracy of the proposed approach.

4.3.1 Related Work

4.3.1.1 Theoretical Aspects and Aerospace Applications

The fusion of position and acceleration measurement to an enhanced system state estimation is a common problem in the field of aerospace applications. This problem is generally solved by *complementary filtering* [Mer96] of the two measurements. Normally, simple high-pass filters and low-pass filters are employed. Their sum has an exact all-pass characteristic. For the implementation of position and speed estimation based on position and acceleration measurement, the setup of Figure 4.8 is commonly used. The accelerometer signal a_m is integrated twice, and the difference e between the estimated position x and the measured position x_m is fed back by feedback gains k_1 and k_2 . The internal states of the two integrators correspond to the estimated speed v and the estimated position x . Note that with this solution no accelerometer offset com-

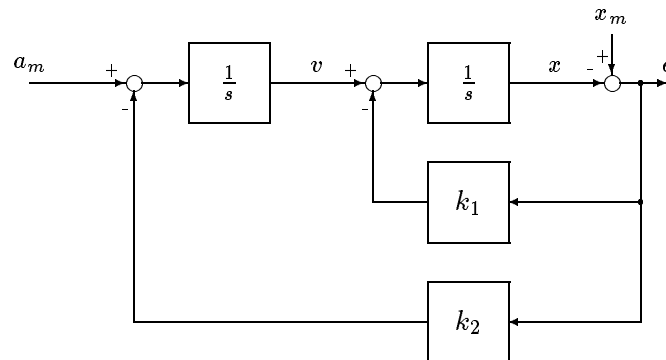


Figure 4.8: Complementary filter implementation.

pensation is provided. By adding a third integrator with a third feedback gain, however, this problem is solved [Mer96]. The estimated speed of this complementary filter implementation is

composed of an acceleration component and a position component. The complementarity of the two filter transfer functions is expressed in the following equation. Acceleration and position are transformed in speed signals by integration ($\frac{a_m}{s}$) and differentiation ($x_m \cdot s$), respectively.

$$v = \underbrace{\frac{a_m}{s} \cdot \frac{s^2}{s^2 + k_1 s + k_2}}_{\text{from acceleration}} + \underbrace{x_m \cdot s \cdot \frac{k_1 s + k_2}{s^2 + k_1 s + k_2}}_{\text{from position}}$$

The design of the complementary filter solution consists in finding appropriate feedback gains. One solution is to design the complementary filters explicitly in the frequency domain. However, the classic solution is to use Kalman filter design [Mer96]. The structure of Figure 4.8 is transformed into Luenberger observer state space representation. Common *Kalman filter* design methods [Bra94] are employed in order to minimise output signal variance as a function of the known variance of the two measured variables. Note that the Kalman design approach for this estimation problem minimises the output variance, but only with respect to the specific structure. Therefore, it is well possible that other structures lead to further reduced variance on the output.

Compared to our linear axis control problem, aerospace applications have quite different sensor performances. Inertial navigation systems are well compensated highly linear devices and have certainly higher precision than our low cost acceleration measurement. On the other hand, linear encoders are very precise compared to aerospace position measurement systems based on GPS (Global Positioning System) or barometric altimeters. These aerospace sensors usually have much lower sampling rates for the position and have considerable time lag due to physical constraints and complex calculations to be performed on-line.

4.3.1.2 Robotics and Linear Axis Applications

For robotics and machine-tool control, the use of additional acceleration measurement to enhance the system state measurement compared to the position-only method is not as widespread as it would be expected. This has two main reasons. First, adding sensors increases the complexity of the control system. It is only employed if the conventional sensors, in this case the position measurement, are not sufficiently accurate. For most motion control problems this is not the case, seen the high resolution of today's position encoders. Second, accelerometers have become much more accurate and much less expensive in recent years. Therefore, it is only now that they constitute a technically and economically interesting alternative.

Nevertheless, successful implementations of fusion of position and acceleration measurement for robot and axis control have already been discussed in the literature, although the use of direct feedback of the measured acceleration (see Section 5.2) is employed much more often. Shaw and Srinivasan propose in [SS90] acceleration measurement to improve position and speed estimation of a robot arm, especially to enhance their bandwidth. They consider in this article only one dimensional motion. Therefore, their approach can be directly adapted to our linear drive problem. Their basic idea is developed for the example of position measurement enhancement. The position measurement and the double integration of the acceleration measurement are fed through complementary filters in order to eliminate the high frequencies from the position component and the low frequencies from the acceleration component. The DC part of the acceleration component is completely cut off. Therefore, uncompensated accelerometer offsets

do not influence the results. The main problem of this approach lies in the design of the two filters. Despite their susceptibility to quantisation effects, Shaw and Srinivasan use IIR filters, which apparently leads to different problems as a proper choice of A/D word length, avoidance of aliasing, and so on. They reject the solution with less quantisation susceptible FIR filters because of high computational demands and, even more severe, because of the phase lag. They state that “*the effective time corresponding to the linear phase shift [of FIR filters] is large and would have a destabilising effect in closed-loop applications*” [SS90]. They conclude that the digital implementation raises the position measurement bandwidth from initially 16Hz to 40Hz and that the accelerometer bandwidth constitutes the limiting element of the overall achieved closed-loop bandwidth. In Section 4.3.8 this solution is compared to the one proposed in the next section of this dissertation.

Methods for improving the tracking performance of motion control by acceleration measurement in addition to position measurement are discussed in [Jag94]. Jager compares direct acceleration feedback (see also Section 5.2), called *direct method*, where the acceleration signal is directly fed back in the control loop, with the *indirect method*, where the acceleration signal is used to improve speed and position estimation. He states that both methods reduce the tracking error by about the same degree compared to the position-only approach. He claims that the combined use of both methods does not improve the performance further. We assume that this can be explained with the accelerometer noise becoming too dominant in the case of a combined use. The indirect method employed in [Jag94] is based on Kalman filter theory. Jager concludes that for this problem the assumptions of Kalman filter theory are not satisfied in that process and measurement noise are not exactly white and Gaussian. Therefore, he proposes some detuning of the obtained filter gain matrix to obtain reasonable performance.

4.3.2 Fusion of Position and Acceleration

The aim of our fusion algorithm is to combine a position with an acceleration signal in order to generate a highly accurate speed signal. Measured acceleration and position contain redundant information as the double integration of the former constitutes exactly the latter. Measurement inaccuracies on the two signals have to be taken into consideration when designing the fusion algorithm. To summarise, the fusion algorithm must have the following characteristics:

- *Reduction of accelerometer noise:* accelerometers as analog sensing devices and their analog signal amplification circuitry are very sensitive to noise caused by external electrical disturbances. Noise attenuation within the algorithm reduces the disturbance sensitivity of the algorithm. Hence, it makes less demands on separate analog filtering of the sensor signals.
- *Insensitivity to accelerometer offset:* offset on the analog accelerometer output signal is always present and cannot be completely compensated for. This offset must not lead to drift of the obtained speed signal, as it would be the case when using the simple integration of the accelerometer signal to obtain a speed signal.
- *Insensitivity to position quantisation:* the influence of position quantisation on the noise of the speed signal has to be considerably reduced compared to the direct differentiation of the position. Noise on the speed signal creates control noise, which reduces the maximum possible feedback gains and hence the available controller bandwidth.

- *Minimisation of phase shift:* phase lag of the speed signal also reduces the available controller bandwidth and should be minimised.
- *Simple computation:* the actual speed has to be calculated at each sampling interval of the controller. As highly dynamic direct-drive axes need high sampling frequencies, the algorithm should only contain few calculations so as not to exceed the processor's performance.

The main idea behind the presented algorithm is as follows. Position and acceleration measurement are observed over a fixed past observation time period Δt_i , and the actual speed at the end of the period is estimated on the basis of this information. For explanatory purposes, we first present the idea for the case where the speed at the beginning of the observation period is calculated. The formulae for calculating the speed at the end of the observation period are derived thereafter. Figure 4.9 illustrates an example of axis movement in terms of acceleration, speed, and position. The curves depending on the initial speed $v(t_i)$ at the beginning of Δt_i are drawn in dark grey, whereas the ones depending on the accelerations during Δt_i are drawn in light grey. The integration of the acceleration $a(\tau_a)$ leads to the light grey curve in the speed graph, its double integration to the light grey curve in the position graph.³ The integration of the initial speed $v(t_i)$ gives the dark grey position ramp in the position graph. The sum of both curves in the position graph determines the total movement Δx_i during Δt_i , which is measured by the position encoder. The acceleration component ΔX_a , the double integration of the acceleration, is obtained from acceleration measurement. The difference $\Delta x_i - \Delta X_a$ together with Δt_i defines the slope of the dark grey position ramp, which is equivalent to the desired initial speed $v(t_i)$.

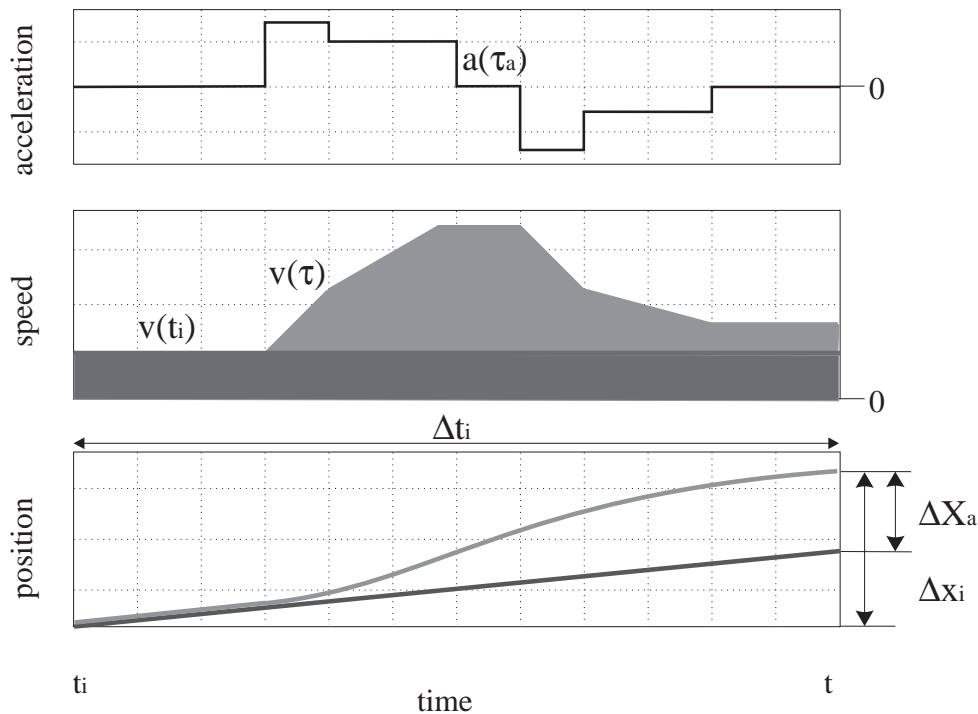


Figure 4.9: Example of axis movement.

³ τ_a is equivalent to τ , but is used here to distinguish between different integration variables.

This proposed solution satisfies the above defined specifications. It has the following characteristics:

- The proposed algorithm adds absolutely no phase lag, provided there are no delays on the measured signals.
- The accelerometer noise is considerably attenuated by the double integration. This reduces the influence of the measurement noise which is always present.
- The influence of the position encoder quantisation is reduced, as only the difference between start and end position is used, and divided by a much longer time period as for direct position differentiation.
- The influence of accelerometer offset is limited by the limited observation period. Accumulation of offset leading to a speed drift is impossible.
- No model of the system is needed for design.

Based on this idea, a formula for the calculation of the speed at the end of the observation period can be derived.

4.3.2.1 Fusion Algorithm in Continuous Time Domain

Our novel algorithm for position- and acceleration-based speed estimation is derived first for the continuous time domain. Its discretisation will be given thereafter.

The presented algorithm evaluates *acceleration* $a(\tau_a)$ and *position* $x(\tau_a)$ over a given *observation time period* $\Delta t_i = [t_i..t]$, starting at the time t_i and ending with the actual time t , and calculates the *speed* $v(t)$ at the end of the period.⁴ The calculations are based on the integration relationship between acceleration, speed, and position. The considerations made in the sequel are based on linear movements. They apply, however, in exactly the same manner to rotary movements.

The speed $v(\tau)$ for any τ within the observation time period ($t_i \leq \tau \leq t$) is expressed in Equation (4.1) as a function of the speed $v(t)$ at the end of the interval $[t_i, t]$, and the integration of the acceleration $a(\tau_a)$.

$$v(\tau) = v(t) - \int_{\tau}^t a(\tau_a) d\tau_a \quad (4.1)$$

The position $x(t)$ at the end of Δt_i is derived from the position $x(t_i)$ at the beginning of Δt_i and the integration of the above obtained speed.

$$x(t) = x(t_i) + \int_{t_i}^t v(\tau) d\tau = x(t_i) + (t - t_i)v(t) - \int_{t_i}^t \int_{\tau}^t a(\tau_a) d\tau_a d\tau \quad (4.2)$$

Solving Equation (4.2) for the actual speed $v(t)$ leads to Equation (4.3), which calculates the speed as the sum of a position component $P_i(t)$ and an acceleration component $A_i(t)$.

$$v(t) = \underbrace{\frac{x(t) - x(t_i)}{t - t_i}}_{P_i(t)} + \underbrace{\frac{\int_{t_i}^t \int_{\tau}^t a(\tau_a) d\tau_a d\tau}{t - t_i}}_{A_i(t)} \quad (4.3)$$

⁴Below, the subscript i will be used to distinguish different observation time periods.

Employing the substitutions (4.4), in which Δt_i denotes the *observation period*, $\Delta x_i(t)$ the *position difference*, and $\Delta X_{a,i}(t)$ the position difference obtained by the backward double integration of the acceleration measurement, finally leads to Equation (4.5).⁵

$$\begin{aligned}\Delta t_i &= t - t_i \\ \Delta x_i(t) &= x(t) - x(t_i) \\ \Delta X_{a,i}(t) &= \int_{t_i}^t \int_{\tau}^t a(\tau_a) d\tau_a d\tau\end{aligned}\tag{4.4}$$

The resulting speed $v(t)$ is composed of a position-based component $P_i(t)$, which is equivalent to the mean speed over the whole observation period, and an acceleration-based component $A_i(t)$ containing the remaining information.

$$v(t) = \underbrace{\frac{\Delta x_i(t)}{\Delta t_i}}_{P_i(t)} + \underbrace{\frac{\Delta X_{a,i}(t)}{\Delta t_i}}_{A_i(t)}\tag{4.5}$$

All derivations are based on the exact integral relationship of acceleration, speed, and position. Therefore, the resulting $v(t)$ is the exact speed at time t without any delays and independent of the length of the observation period. From the structure of Equation (4.3), a reduction of the influence of position and acceleration quantisation is expected due to the long observation period and the double integration operation respectively. An analysis of the algorithm in the frequency domain is given in Section 4.3.3.

4.3.2.2 Discretisation of Fusion Algorithm

In the view of an implementation on a numerical controller with equally spaced sampling intervals, the fusion algorithm, i.e. Equation (4.5), is discretised. After some explanations on the used notation, the discretisations of $\Delta x_i(t)$ and Δt_i are derived. The calculation of $\Delta X_{a,i}(t)$ is then studied in more detail. First, an adequate discretisation of the double integration of the acceleration is developed. This formula is then rewritten in a recursive way to reduce the number of operations to be executed during real-time control action.

Notation In the following, the sample numbers of sampled variables are always given as subscripts, as opposed to the notation in some literature, where they are indicated in brackets. Therefore, x_k is equivalent to notations such as $x(k)$ or $x(k \cdot T_{sampl})$. Where other subscripts are used in addition, the sample number is always at the last position separated by a comma. An example of this notation is provided by the speed difference $\Delta x_{N_i,k}$, where N_i represents the duration of observation period and k the sample number.

Discretisation of observation period and position difference The calculations of $\Delta x_i(t)$ and Δt_i are both very simple to discretise. The observation period Δt_i is chosen as a multiple N_i of the sampling period T_{sampl} , leading to $\Delta t_{N_i} = N_i \cdot T_{sampl}$. The position difference results in $\Delta x_{N_i,k} = x_k - x_{k-N_i}$.

⁵Backward — because the integration starts at time t and integrates back to t_i .

Discretisation of the double integration In the following, the discretisation of the double integration is developed. $\Delta X_{a,i}(t)$ backward integrates the measured acceleration twice, beginning with the actual time t and integrating back to the beginning of the observation time t_i , as follows:

$$\Delta X_{a,i}(t) = \int_{t_i}^t \int_{\tau}^t a(\tau_a) d\tau_a d\tau$$

For the discretisation of the integration of regularly sampled measured data, there exist various sophisticated solutions [BSMM95]. As the algorithm has to be implemented on a real-time controller, a simple method is chosen. The two used methods, based on rectangles and trapezoids, are illustrated in Figure 4.10. The former method, denoted *backward rectangular integration*, sums up the areas composed of rectangles of width T_{sampl} and of height of the function value at the end of the rectangle. From Figure 4.10a it is easily derived that this method compensates well for an average measurement delay of half a sampling period. The *trapezoidal integration method* integrates the measured values based on trapezoidal areas composed of the function value at the begin and at the end of the blocs. This method is based on a polynomial of first degree. The use of methods which are based on higher order polynomials are less favourable, because the noise on the acceleration signals cannot be modelled as a signal of the form of such polynomials.

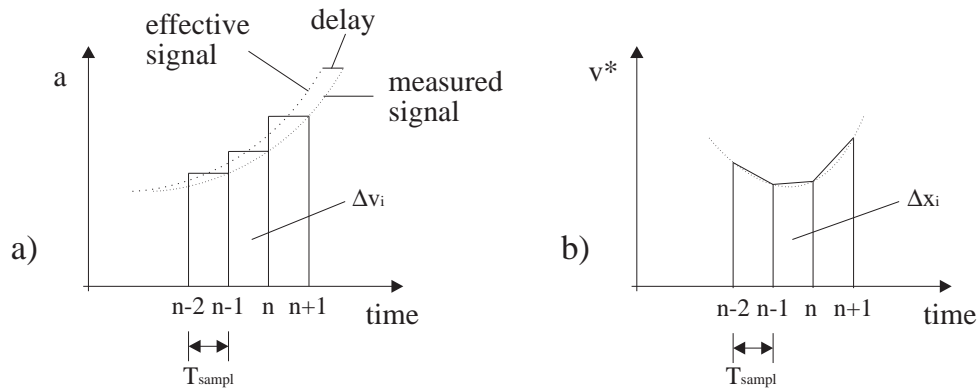


Figure 4.10: (a) Backward rectangular and (b) trapezoidal discrete integration method.

For the first integration of the acceleration we apply the rectangular integration algorithm. The second integration to finally obtain the values equivalent to a position are carried out using the trapezoidal rule. The difference between this choice and using twice the trapezoidal rule is illustrated in Figure 4.15 on page 66.

In the following, the double integration over N -times the sampling interval is developed step by step. The speed variation Δv_i is calculated in Equation (4.6), based on the the rectangular method. Afterwards, the backward cumulative sum of the speed variations is obtained in Equation (4.7).

$$\Delta v_n = T_{\text{sampl}} \cdot a_n \quad (k - N_i < n \leq k) \quad (4.6)$$

$$v_n^* = \sum_{j=n+1}^k \Delta v_j \quad (k - N_i \leq n < k) \quad (4.7)$$

Equation (4.8) describes the position variation, based on the trapezoidal method. Equation (4.9) finally calculates the backward cumulative sum of the position change, which equals the position change induced by the acceleration during the observation period.

$$\Delta x_n = \frac{T_{sampl}}{2} (v_{n-1}^* + v_n^*) \quad (k - N_i < n \leq k) \quad (4.8)$$

$$\Delta X_{a,N_i,k} = \sum_{n=k-N_i+1}^k \Delta x_n \quad (4.9)$$

After some mathematical transformations of the summing terms, $\Delta X_{a,N_i,k}$ is expressed directly in terms of the measured accelerations a_i .

$$\Delta X_{a,N_i,k} = \frac{T_{sampl}^2}{2} \sum_{n=1}^{N_i} (2n-1) \cdot a_{k-N_i+n} \quad (4.10)$$

This formula for the calculation of the acceleration component consists of a weighted sum of the measured acceleration values. This representation is equivalent to the form of discrete FIR filters.

To sum up, the speed can be estimated on the basis of position and additional acceleration measurement by the following formula.

$$v(t) = \frac{\Delta x_i(t)}{\Delta t_i} + \frac{\Delta X_{a,i}(t)}{\Delta t_i}$$

The different components of the formula to calculate the speed, based on position and acceleration measurement are summarised in Table 4.3.

Component	continuous case	discrete case
observation time	$\Delta t_i = t - t_i$	$\Delta t_{N_i} = N_i \cdot T_{sampl}$
position component	$\Delta x_i(t) = x(t) - x(t_i)$	$\Delta x_{N_i,k} = x_k - x_{k-N_i}$
acceleration comp.	$\Delta X_{a,i}(t) = \int_{t_i}^t \int_{\tau}^t a(\tau_a) d\tau_a d\tau$	$\Delta X_{a,N_i,k} = \frac{T^2}{2} \sum_{n=1}^{N_i} (2n-1) a_{k-N_i+n}$

Table 4.3: Summary of the different components of the proposed speed estimation algorithm.

Recursive implementation of double integration The direct implementation of Equation (4.10) results in a certain number of floating point instructions to be executed at each sampling interval. Given the observation period as N_i sampling intervals, $\Delta X_{a,N_i,k}$ is obtained as the sum of N_i measured acceleration values, weighted with a set of N_i constant values. This leads to a total of $(2N_i - 1)$ floating point instructions per sampling interval for a single calculation of $\Delta X_{a,N_i,k}$. For a reasonable practical example of $N_i = 50$, 99 floating point operations seem to be a lot. However, given the calculation power of the digital signal processor (DSP) explained in Appendix C.2, which use approximately 50 cycles of 50ns for these operations, the

calculation time is, with less than $3\mu s$, relatively fast. Nevertheless, for less powerful processors or for cases where different integrals of this type have to be calculated, as e.g. for the parameter identification algorithm of Section 4.3.4, a recursive implementation is well justified.

For preparation of a recursive implementation Equation (4.10) is rewritten, replacing n by $j := k - N_i + n$:

$$\Delta X_{a,N_i,k} = \frac{T_{sampl}^2}{2} \sum_{j=k-N_i+1}^k (2(j + N_i - k) - 1)a_j$$

The difference between two successive double integrations $\Delta X_{a,k} - \Delta X_{a,k-1}$ based on the above formula results in

$$\Delta X_{a,N_i,k} - \Delta X_{a,N_i,k-1} = \frac{T_{sampl}^2}{2} \left[\sum_{j=k-N_i+1}^k (2(j + N_i - k) - 1)a_j - \sum_{j=k-N_i+1}^{k-1} (2(j + N_i - k) - 1)a_{j-1} \right]$$

which can be simplified by transforming the summing terms into

$$\Delta X_{a,N_i,k} - \Delta X_{a,N_i,k-1} = \frac{T_{sampl}^2}{2} \left[(2N_i - 1)a_k - a_{k-N_i} - 2 \underbrace{\sum_{j=k-N_i+1}^{k-1} a_j}_{I_{N_i,k}} \right]$$

The remaining term $I_{N_i,k}$ is simply the direct sum of the acceleration values. It is rewritten in a recursive form by taking the difference between two successive values.

$$I_{N_i,k} - I_{N_i,k-1} = \sum_{j=k-N_i+1}^{k-1} a_j - \sum_{j=k-N_i}^{k-2} a_j = a_{k-1} - a_{k-N_i}$$

1. Initialise $I_{N_i,N_i-1} = \sum_{j=0}^{N_i-2} a_j$
2. Initialise $\Delta X_{a,N_i-1} = \frac{T_{sampl}^2}{2} \sum_{j=0}^{N_i-1} (2j + 1)a_j$
3. Starting with $k = N_i$, carry out the following iteration:
 - (a) $I_{N_i,k} = I_{N_i,k-1} + a_{k-1} - a_{k-N_i}$
 - (b) $\Delta X_{a,N_i,k} = \Delta X_{a,N_i,k-1} + \frac{T_{sampl}^2}{2} [(2N_i - 1)a_k - a_{k-N_i} - 2I_{N_i,k}]$
 - (c) Go to (a)

Table 4.4: Recipe for recursive implementation of double integration.

The derived recursive implementation is summarised in Table 4.4 in form of a recipe. This recursive form of the double integration considerably reduces the number of arithmetic operations per sampling interval. Less than ten arithmetic operations remain per cycle, independently

of the observation period length. Therefore, this period can be freely chosen based on other criteria than the calculation power of the processor. The influence of the observation period on the characteristics of the algorithm is the topic of the subsequent section.

Rounding errors have not been considered so far. When working with integer data representation, standard error estimation schemes [OS92] for the non-recursive FIR structure of our algorithm of Equation (4.10) can be used. The recursive representation consists of addition, subtraction, and multiplication with integer operands. All these operations do not lead to additional calculation error, if taking care not to generate data overflow. Therefore, the analysis of Equation (4.10) holds also for the recursive representation. For a floating point implementation, data representation problems could cause rounding errors on $I_{N_i,k}$, which lead to undesired drifts of $\Delta X_{a,N_i,k}$. By a proper choice of the used word length, these problems can be avoided.

4.3.3 Analysis of Algorithm in Frequency Domain

The above-proposed data fusion algorithm will now be analysed. The influence of the choice of the observation period Δt_i , the only design parameter of the method, on the resulting speed estimate is of major interest. It will be determined which frequency components of the speed are based on acceleration measurement and which ones on position measurement. The transfer function of the speed estimate is also derived to compare the algorithm with the position-only methods of Section 4.2.2.

Sensors and algorithmic components of the speed estimation algorithms can be modelled as linear systems in the continuous and discrete domain respectively. The following considerations are based on the analysis of their transfer functions. Numerical simulation and calculation software, as the here used MATLAB software, provide Bode plots of continuous as well as discrete systems. The frequency-gain and frequency-phase vectors resulting from these Bode plots can be directly used to obtain total transfer functions of serial and parallel setups of the initial transfer functions, independently whether the latter are discrete or continuous ones.

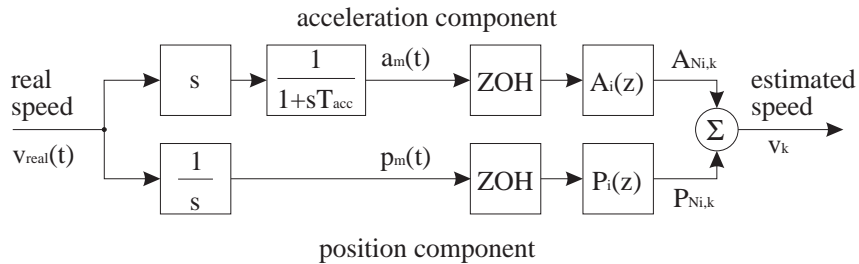


Figure 4.11: Block diagram of proposed speed estimation algorithm.

The different components of the proposed speed estimation algorithm are found in the block diagram of Figure 4.11. Beginning with the unknown real speed $v_{real}(t)$ on the left, the measured position $p_m(t)$ and the measured acceleration $a_m(t)$ is obtained by the continuous transfer functions $\frac{1}{s}$ and $s \cdot \frac{1}{1+sT_{acc}}$ respectively. The time constant T_{acc} is in the range of about $50\mu s$. Both, position and acceleration component are sampled with a zero-order-hold (ZOH) element, each of them followed by the discrete algorithm, denoted $A_i(z)$ and $P_i(z)$, respectively. A final addition of the two components results in the estimated speed v_k at time $t = k \cdot T_{sampl}$.

Based on the derived formulae (see Table 4.3), the z-domain transfer functions of the position

component $P_i(z)$ and the acceleration component $A_i(z)$ result as:

$$P_i(z) = \frac{1 - z^{-N_i}}{N_i \cdot T_{s\text{ampl}}}$$

$$A_i(z) = \frac{T_{s\text{ampl}}^2}{2} [(2N_i - 1) + (2N_i - 3)z^{-1} + \dots + 3z^{-N_i+2} + z^{-N_i+1}]$$

In the remainder of this section, the different transfer functions are given and commented for one specific design example of the speed estimation algorithm to exemplify the method's general characteristics. The question of how to choose the observation period for a specific design is the topic of Section 4.3.5. Here, only its general influences are of interest. The aim is to show the characteristics of the algorithm based on parameters from real systems which are also used to get the experimental results in Section 4.3.7.

In the example, the sampling frequency is set to $f_{s\text{ampl}} = 10\text{kHz}$ and the observation period to $N_i = 50$, i.e. 5ms. Figure 4.12 shows the resulting total transfer functions for the acceleration component on the left and the position component on the right. Total transfer function in

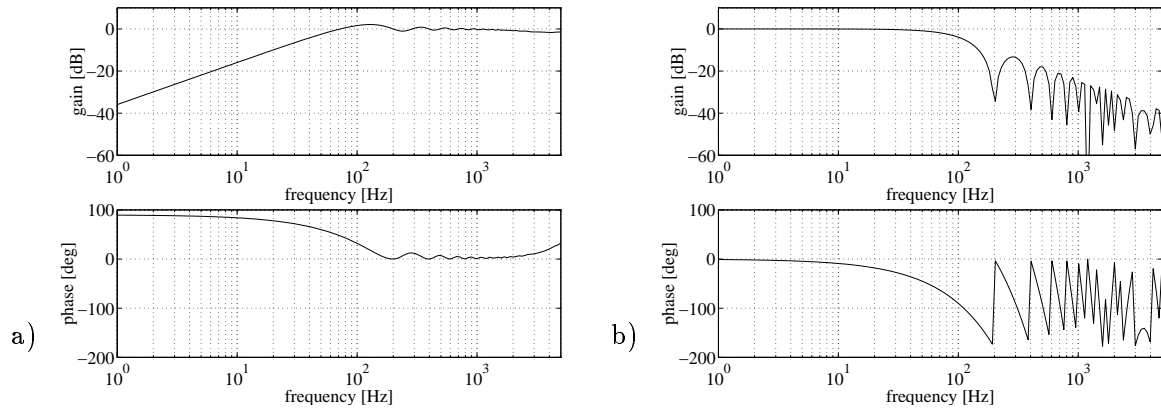


Figure 4.12: Total transfer function of (a) acceleration and (b) position component.

this context means the transfer function from the unknown real speed v_{real} to the respective component $P_{N_i,k}$ and $A_{N_i,k}$. As intended, the position component mainly contributes to the low frequencies and the acceleration component to the high frequencies of the speed signal. Both components have no significant phase shift in the regions where they are not attenuated, and however mainly constitute the speed signal. In the region of attenuation, the position component exhibits phase lag and the acceleration component phase lead.

Figure 4.13 exemplifies in one plot how position and acceleration component are attenuated as a function of the speed signal frequency. The break-even of the two curves is at about 60Hz. We denote this frequency as *edge frequency* f_{edge} of the two components. The position component decreases above f_{edge} by 20dB per decade, the acceleration component does so below it.

The influence of the length of the observation period on the contribution of the acceleration signal to the speed component is visualised in Figure 4.14. The numbers given in the figure correspond to the number of sampling periods of $T_{s\text{ampl}} = 100\mu\text{s}$, which constitute the observation period. It turns out that the -3dB point of the acceleration contribution lies at a frequency of

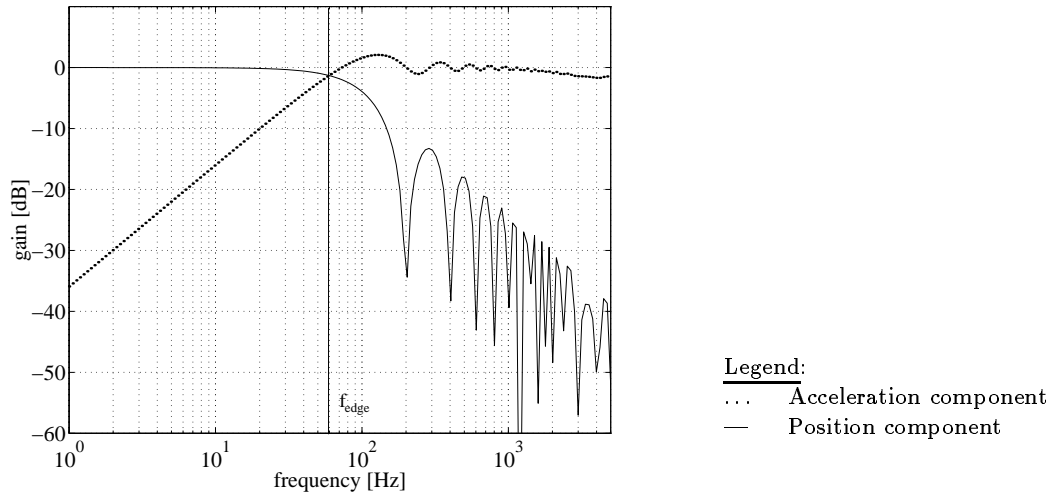


Figure 4.13: Total transfer gain of position and acceleration component.

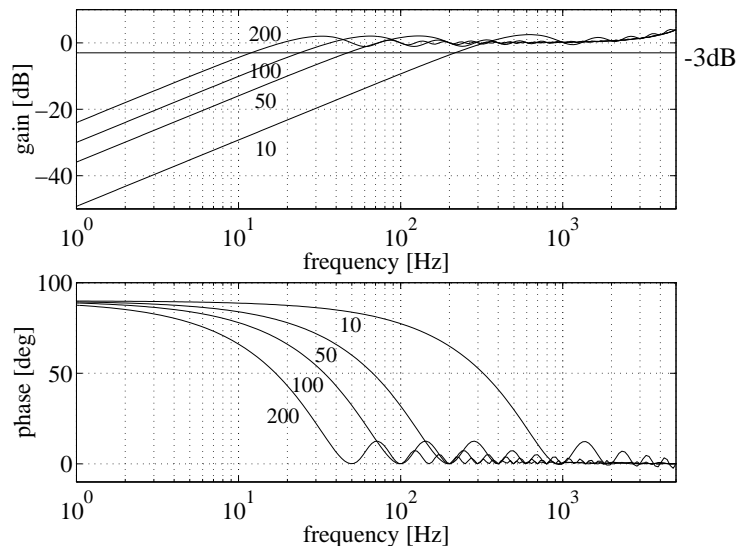


Figure 4.14: Influence of observation period (N_i) on acceleration component.

about a quarter of the inverse of the observation period. This relationship is further discussed for design purposes in Section 4.3.5. Here, it is sufficient to understand that by means of the observation period length Δt_i , the edge frequency f_{edge} of the two components can be influenced and hence adapted to the bandwidth of the sensors.

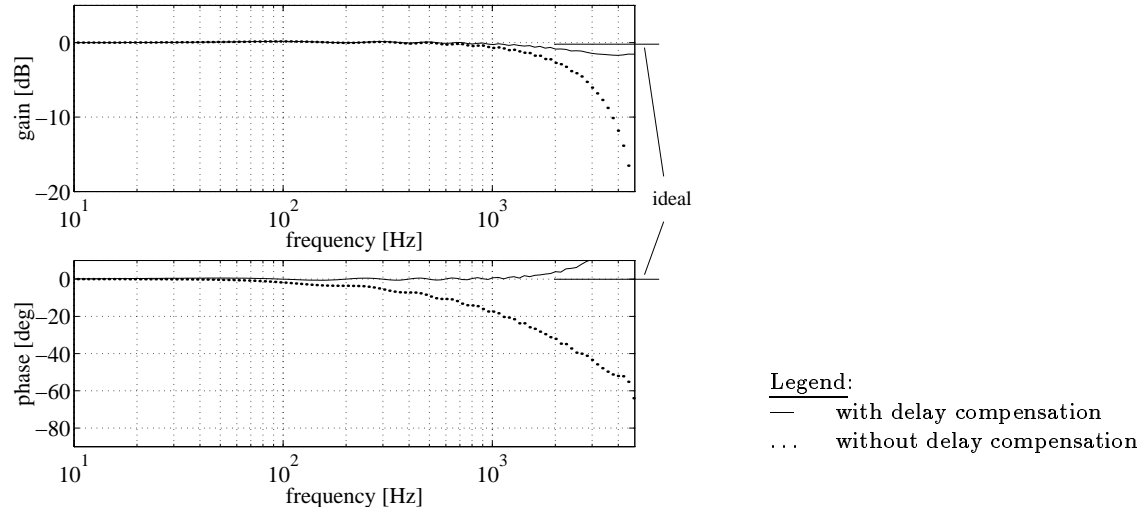


Figure 4.15: Total speed transfer function of the algorithm for different integration methods.

In order to compare the speed estimation algorithm to the position-only methods of Section 4.2.2, its total transfer function is shown in Figure 4.15. Acceleration and position components of Figure 4.13 are added to obtain this figure. This addition is performed by transforming the two transfer functions in the complex plane, adding them, and transforming them back in the gain/phase representation. Ideal results would have unity gain (0dB) and no phase shift over the whole frequency range. The solid lines in Figure 4.15 are the result based on the acceleration component obtained by applying once the backward rectangular method and once the trapezoidal method for numerical integration, as explained on page 59. For comparison, the dotted curves are obtained by employing twice the trapezoidal integration rule. The figure clearly demonstrates the ability of the adapted double integration of compensating for the time constant T_{acc} on the acceleration measurement. The difference between the two algorithms is also clearly visible in the results of real measurements. Without the compensation algorithm, the obtained speed signal contains an additional delay, and the results of the parameter estimation algorithm explained in Section 4.3.4 considerably deteriorate. With the compensation algorithm, there results a speed signal with almost no phase shift over the whole frequency range up to the Shannon frequency of 5kHz. Without this compensation, a considerable phase shift for speed signals with frequencies higher than 500Hz is present. The increase in gain of the compensation algorithm for frequencies towards the Shannon frequency is compensated by the limited bandwidth of the accelerometer.

4.3.4 Accelerometer Parameter Identification

The motivation for the accelerometer parameter identification presented in this section is based on the fact that accelerometers are analog sensors. Their output is an analog signal that has to be transmitted and converted to a digital value for numerical control. All elements of this measurement chain have their specific transfer gain and often add an offset to the signal. Therefore,

identification algorithms for both, gain factor and offset of the acceleration measurement are proposed. The identifications are based on the digital values at the end of the chain, and hence, the identified values globally include the influences of all elements in the chain. Automatic identification of the parameters is useful for the following reasons. First, the process of commissioning an axis including acceleration measurement is much easier. Second, temporal parameter variations due to temperature changes and ageing are taken into account in the speed estimation algorithm, which guarantees stable long-term performance of the drive. And third, maintenance of the system is simplified because in case of a necessary exchange of an accelerometer, the new sensor is automatically calibrated.

The remainder of this section is composed as follows. First, the influence of offset and gain errors (in the acceleration measurement) on the quality of the estimated speed is shown. Thereafter, the measurement setup for the parameter-identification algorithm is defined. Then, the identification of accelerometer offsets based on zero long-term mean value of the acceleration measurement is described. Finally, a novel gain parameter identification algorithm is developed. This algorithm is based on the redundancy of position and acceleration measurement as well as on the speed estimation algorithm of Section 4.3.2. All considerations in this section are based on the continuous case, but the results can be translated to the discrete case by using the discretisation of the speed estimation algorithm already given.

4.3.4.1 Influence of Offset and Gain Errors on Speed Estimation

The influence of offset and gain errors on the proposed algorithm is now being analysed. Error terms for position quantisation q , as well as accelerometer offset a_0 and gain error ϵ are added to the ideal values of Equation (4.5) on page 59. Measured values are marked with the subscript 'm'. Assuming ideal measurements, the observation period Δt_i has no influence on the resulting speed. In the presence of measurement inaccuracies, however, a proper choice of Δt_i has affects the obtained results.

The *measured acceleration* a_m differs from the real acceleration by an *offset* a_0 and a *gain error* ϵ . Due to the *quantisation step size* q of the position measurement, the maximum absolute error of the position difference Δx is q . Accelerometer non-linearities, accelerometer quantisation, as well as time measurement errors are sufficiently low to be neglected. Substituting the ideal values of Equation (4.5) with the measured values in Equation (4.11) leads to Equation (4.12) for the speed calculation.

$$a_m(t) = (1 \pm \epsilon) a(t) \pm a_0 \quad \Delta x_{m,i}(t) = \Delta x_i(t) \pm q \quad (4.11)$$

$$v_m(t) = \frac{\Delta x_i(t) \pm q}{\Delta t_i} + \frac{(1 \pm \epsilon) \Delta X_{a,i}(t) \pm \frac{1}{2} a_0 \Delta t_i^2}{\Delta t_i} \quad (4.12)$$

The maximum absolute speed error is limited by:

$$|v(t) - v_m(t)| \leq \frac{q}{\Delta t_i} + \frac{\epsilon \Delta X_{a,i}(t)}{\Delta t_i} + \frac{1}{2} a_0 \Delta t_i$$

The three error sources q , ϵ , and a_0 can be evaluated separately since they are completely independent of each other. Their influence is summarised as follows:

- The *accelerometer offset* a_0 adds a constant offset to the estimated speed value. Its influence depends proportionally on Δt_i .

- The *accelerometer gain error* ϵ depends to a high degree on the movement of the drive. Its influence cannot be quantified in a general way. The maximum absolute value of $\epsilon \frac{1}{2} a_{max} \Delta t_i$ is reached in the case where the drive performs maximum acceleration a_{max} during the whole observation period. $\Delta X_{a,i}(t)$ acts only on parts of the frequency components of the speed signal. Therefore, ϵ leads to a nonlinear deformation of the resulting speed. The rule “the longer Δt_i , the bigger the influence of ϵ ” holds for most of the expected axis movements.
- The *position quantisation* q has a reduced influence with increased Δt_i .

To sum up, the optimisation of the observation period Δt_i leads to a trade-off between low influence of position quantisation and a low influence of accelerometer gain and offset error. Nevertheless, by accurately identifying accelerometer gain and offset, the observation period can be chosen sufficiently long to reduce position quantisation noise considerably. Therefore, an automatic estimation of gain and offset is useful.

4.3.4.2 Measurement Setup

The question of the measurement setup has not been raised during the explanation of the speed estimation algorithm in Section 4.3.2. It is supposed there that both position and acceleration sensors measure the relative displacement between the base part and the sliding part of the axis. This is the case for position encoder which measure the relative position between the two parts. However, inertial accelerometers always measure the absolute acceleration of the part on which they are mounted. In Figure 4.16, the employed measurement setup is illustrated. The position

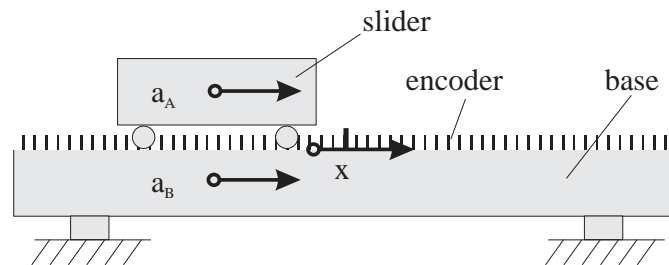


Figure 4.16: Position and acceleration measurement setup.

encoder measures the relative position x between the base and the sliding part of the axis. For the acceleration measurement, two cases have to be distinguished. In the *one-accelerometer case*, the base of the drive is immobile. Therefore, the measured absolute acceleration a_A is equivalent to the desired relative acceleration between base and slider. In the *two-accelerometer case*, the base also performs some movements. Therefore, the relative acceleration has to be determined as the difference between the two measured accelerations a_A and a_B . When working with highly dynamic direct-drive axes, the assumption of a, to some degree, mobile base part is well justified, because a very high base mass would be needed to assure complete immobility. The influence of such a mobile base on the measurement is demonstrated in Section 4.3.7, which presents experimental results.

4.3.4.3 Offset Identification

Acceleration measurement offset can be caused by the sensor, the signal transmission, the amplification electronics, and the A/D-conversion. As shown above, this offset is directly visible as offset in the estimated speed, and increases with increasing observation period. Hence, it has to be compensated for. The offset varies only slowly in time and the linearity of the used accelerometers is excellent. Therefore, this offset can easily be identified as a quasi static value by calculating the mean value of the measured data over a long time period. As concerns the problem of determining static components of measured variables, there exist well established solutions in literature, e.g. [Ise87b]. Therefore, implementation issues are not further studied here. The interest of the following considerations lies in establishing error bounds for the mean value calculation of the acceleration measurement on a machine-tool axis. The worst case error estimations are made for FIR implementation of the mean value calculation, because IIR methods generally provide lower error bounds.

The fact that the acceleration is measured on a machine-tool axis with limited absolute speed v_{max} and limited absolute position x_{max} , enables one to easily estimate the error bounds. For the estimation of the accuracy of the obtained offset value, the measured acceleration $a_m(t)$ is considered as the sum of a signal part $a(t)$ without offset and a quasi static offset part a_0 . The mean value \bar{a}_m of the measured acceleration over the time period $[t_a..t_b]$ is calculated as follows:

$$\bar{a}_m = \frac{1}{t_b - t_a} \int_{t_a}^{t_b} (a(t) + a_0) dt$$

The resulting absolute difference between mean value and offset is therefore:

$$|\bar{a}_m - a_0| = \left| \frac{1}{t_b - t_a} \int_{t_a}^{t_b} a(t) dt \right| \quad (4.13)$$

The integral term of the right hand side of Equation (4.13) is less than or equivalent to the change of speed between the two points of time t_a and t_b . The absolute value of this change is bounded by twice the maximum speed v_{max} , assuming a change from maximum negative to maximum positive speed as the worst case. The bound for the absolute error

$$|\bar{a}_m - a_0| \leq \frac{2v_{max}}{t_b - t_a}$$

varies as a function of the mean value calculation period $t_b - t_a$. The error can be made as small as needed by increasing this period.

Typically, the maximum speed lies in the range of $1 \frac{m}{s}$ and the time constants of the offset variations in the range of some minutes. This leads to deviations of the identified offset from the real offset of some $\frac{mm}{s^2}$, equivalent to $10^{-4}g$, which is much lower than the maximum acceleration of the drives of 1–2g. Therefore, an accurate offset identification can be obtained by this method. The considerations made above apply, in the same way, for all accelerometers for the one- as well as for the two-accelerometer case, because all accelerometers fulfil the underlying assumptions.

4.3.4.4 Gain Identification

This section describes a method for identifying the accelerometer gains based on the redundancy between position and acceleration measurement. The method is based on the algorithm developed in Section 4.3.2. The main idea behind it is to calculate the actual speed $v(t)$ with different

observation periods. The calculated speed is always the same, independent of the observation period. Two different observations lead to a set of two equations, which enable one to calculate drive speed and accelerometer gain. Note that the explained gain identification algorithm is based on the assumption that accelerometer offsets have been previously compensated for.

The one- and the two-accelerometer case are discussed separately because of the different number of used observations. Moreover, it is not possible to treat the one-accelerometer case as a special case of the two-accelerometer case with one acceleration always having the value zero. The derivations with the measurement setup defined in Figure 4.16 on page 68 are based on the measurement of *position* x , *slider acceleration* a_A , and *base acceleration* a_B .

The One-Accelerometer Case As derived in Equation (4.5), the estimated speed is composed of a position component $P_i(t)$ and an acceleration component $A_i(t)$:

$$v_i(t) = \underbrace{\frac{x(t) - x(t_i)}{t - t_i}}_{P_i(t)} + \underbrace{\frac{\int_{t_i}^t \int_{\tau}^t a_A(\tau_a) d\tau_a d\tau}{t - t_i}}_{A_i(t)}$$

The unknown *accelerometer gain* K_A is defined as the factor of *real acceleration* a_A and *measured acceleration* $a_{A,m}$:

$$a_A = K_A \cdot a_{A,m}$$

A new variable $M_i(t)$ is defined equivalent to $A_i(t)$, but based on the measured instead of the real acceleration. The relationship between M_i and A_i is described in Equation (4.14).

$$\begin{aligned} M_i(t) &= \frac{\int_{t_i}^t \int_{\tau}^t a_{A,m}(\tau_a) d\tau_a d\tau}{\Delta t_i} \\ A_i(t) &= K_A \cdot M_i(t) \end{aligned} \quad (4.14)$$

By applying the speed estimation algorithm at time t for two different observation periods Δt_0 and Δt_1 , the following two equations are obtained.

$$\begin{aligned} v_0(t) &= P_0(t) + A_0(t) = P_0(t) + K_A \cdot M_0(t) \\ v_1(t) &= P_1(t) + A_1(t) = P_1(t) + K_A \cdot M_1(t) \end{aligned} \quad (4.15)$$

The resulting speeds $v_0(t)$ and $v_1(t)$ correspond to the estimation of the real speed $v_{real}(t)$. Assuming a compensated accelerometer offset, a linear accelerometer and a marginal influence of position quantisation, the estimated speed is independent of the observation period. Hence, $v_0(t)$ and $v_1(t)$ must be equal, independently of the observation period. With the condition $v_0(t) = v_1(t)$ and Equations (4.15), one obtains the gain factor K_A :

$$K_A = \frac{P_0(t) - P_1(t)}{M_1(t) - M_0(t)}$$

The gain factor K_A results as the difference between two position components divided by the difference between the two acceleration components. At each sampling interval, a new gain estimate is calculated. In practice, problems of this formula can arise due to insufficient excitation

of the drive, leading to a fraction with numerator and denominator which both tend towards zero. By dropping all samples of K_A which do not satisfy Equation (4.16), this problem can be eliminated.

$$|P_0(t) - P_1(t)| > \Delta P_{min} \quad (4.16)$$

The value of ΔP_{min} is the result of a trade-off between the percentage of the used gain estimates and the variance on the used gain estimates. Low-pass filtering of the individual gain estimation samples with a time constant adapted to the slow possible variation of the gain K_A reduces the influence of measurement noise and inaccuracies and leads to a very accurate gain estimation. This low-pass filtering leads, as does the offset identification, to the problem of identifying a constant value. Possible implementations are found in [Ise87b].

An appropriate choice of the two observation periods is required to ensure that the resulting speed estimates provide usable output. Fixing one of these periods to half the length of the other one, turns out to give accurate results in practice (see Section 4.3.7.1).

The Two-Accelerometer Case For the two-accelerometer case, exactly the same derivation strategy as for the one-accelerometer case is applicable. In this case, the relative acceleration a has to be expressed by the acceleration difference $a_A - a_B$ and the speed estimation algorithm has to be employed with three different observation periods. Based on the three resulting equations, drive speed and the two accelerometer gains are identified.

The term $\Delta X_{a,i}(t)$ of Equation (4.5) is rewritten as the difference of two terms $\Delta X_{a_A,i}$ and $\Delta X_{a_B,i}$, which exclusively depend on a_A and a_B , respectively. They are calculated in the same way as $\Delta X_{a,i}(t)$ is calculated from a . Hence, the actual speed is the result of three components:

$$v_i(t) = \underbrace{\frac{\Delta x_i(t)}{\Delta t_i}}_{P_i(t)} + \underbrace{\frac{\Delta X_{a_A,i}(t)}{\Delta t_i}}_{A_i(t)} - \underbrace{\frac{\Delta X_{a_B,i}(t)}{\Delta t_i}}_{B_i(t)}$$

Special attention has to be paid to the sign of the contribution of accelerometer B. This part has to be subtracted, since the directions of both accelerometers are the same (see page 68). K_B and $M_{B,i}$ for accelerometer B are defined in the same way as K_A and $M_{A,i}$ for accelerometer A:

$$\begin{aligned} a_A &= K_A \cdot a_{A,m} & A_i(t) &= K_A \cdot M_{A,i}(t) \\ a_B &= K_B \cdot a_{B,m} & B_i(t) &= K_B \cdot M_{B,i}(t) \end{aligned}$$

The use of three different observation periods Δt_1 , Δt_2 and Δt_3 leads to the following three equations:

$$\begin{aligned} v_0(t) &= P_0(t) + K_A \cdot M_{A,0}(t) - K_B \cdot M_{B,0}(t) \\ v_1(t) &= P_1(t) + K_A \cdot M_{A,1}(t) - K_B \cdot M_{B,1}(t) \\ v_2(t) &= P_2(t) + K_A \cdot M_{A,2}(t) - K_B \cdot M_{B,2}(t) \end{aligned}$$

By applying the condition $v_0(t) = v_1(t) = v_2(t)$ to this set of equations, the two accelerometer gains K_A and K_B are obtained:

$$K_A = -\frac{P_0(M_{B,1} - M_{B,2}) + P_1(M_{B,2} - M_{B,0}) + P_2(M_{B,0} - M_{B,1})}{M_{A,0}(M_{B,1} - M_{B,2}) + M_{A,1}(M_{B,2} - M_{B,0}) + M_{A,2}(M_{B,0} - M_{B,1})} \quad (4.17)$$

$$K_B = +\frac{P_0(M_{A,1} - M_{A,2}) + P_1(M_{A,2} - M_{A,0}) + P_2(M_{A,0} - M_{A,1})}{M_{B,0}(M_{A,1} - M_{A,2}) + M_{B,1}(M_{A,2} - M_{A,0}) + M_{B,2}(M_{A,0} - M_{A,1})} \quad (4.18)$$

Sufficient excitation has to be supervised the same way as in the one-accelerometer case, this time taking the numerators or denominators of (4.17) and (4.18). A proper choice of the minimum value, whether a sample is dropped or not, is difficult to make. One possible solution is to determine these values by simulations of the drive with the chosen observation periods.

A proper choice of the three observation periods is very important. It is crucial to choose all of them in such a way that each provides a usable output signal. In addition, it is important that the three periods are not too similar. In practice, good results are obtained with the choice where the second and third observation period are twice and three times the first one (see Section 4.3.7.2).

4.3.4.5 Influence of Acceleration-Measurement Inaccuracies

In this section, the most important inaccuracies which might occur on the acceleration measurement are briefly reviewed and commented. The importance given to each of the inaccuracies is determined by the practical experiences with accelerometers mounted on machine-tool axes.

- *Delay* generally adds a small delay on the obtained speed signal. Since only the acceleration signal contains delay, position and acceleration measurement are no longer synchronous. This deteriorates the quality of the gain estimation algorithm to a high degree, because the accelerometer gain factors are estimated on the two measurements. This problem is solved by adding an artificial delay to the position signal in the gain estimation algorithm in order to re-synchronise position and acceleration measurement for gain estimation. In practice, this considerably reduces the variance on the estimated gains.
- *Noise* is for reasonable observation period lengths considerably reduced by the double integration operation. The attenuation may even eliminate the need of an anti-aliasing filter for the accelerometer input. Practical experiments show that the phase lag of an anti-aliasing filter influences the result more than the aliasing in absence of a filter.
- *Saturation* of the acceleration sensor and the signal transmission electronics has to be avoided because it deteriorates the quality of the estimated speed, estimated offset and gain factor.
- *Resonance modes* at the mounting place of the accelerometer have to be avoided. In practice, they can reduce the benefits of acceleration measurement to a high degree. Therefore, a proper placing of the accelerometers is crucial.
- *Non-linearities*, which are here understood as deviation from an exact linear relationship between acceleration and measurement output, are very low for the used accelerometers; they can be neglected.

Note that the above-made comments are given for the case where the accelerometers are used for an enhanced speed estimation. In case of direct acceleration feedback, some of the inaccuracies may be weighted quite differently.

4.3.5 Design Guidelines

The position and acceleration based speed estimation algorithm presented in Section 4.3.2 depends on one single design parameter. It has already been stated there that the choice of the

observation period influences the frequency, where the resulting speed changes from being mainly composed of the position component to depending only on the acceleration component. In the sequel, this influence will be clearly identified and commented upon in order to give adequate design guidelines for the application of the fusion algorithm.

The analysis of the transfer functions of the two components will be restricted to their magnitudes since this enables one to clearly identify the frequency ranges where the speed is mainly composed of one or the other component. As shown in Figure 4.13 on page 65, below the edge frequency f_{edge} , the speed is practically only composed of the position component, and above it, the influence of the position decreases by 20dB per decade. The acceleration component is exactly complementary to the position component. The phases of the two components ensure that the sum of the two components has almost no phase shift over the whole frequency range from DC up to Shannon frequency.

The analysis in Section 4.3.2 considers the total transfer function of position and acceleration component. The total transfer function is defined as the transfer function from the unknown real speed to the respective estimated speed component. This total transfer function is necessary for analysing the quality of the resulting speed. In the following, only the transfer functions of the position and acceleration component from the measured inputs to the speed components are of interest. This is to exemplify which frequency bands of the measured signals are attenuated by what degree.

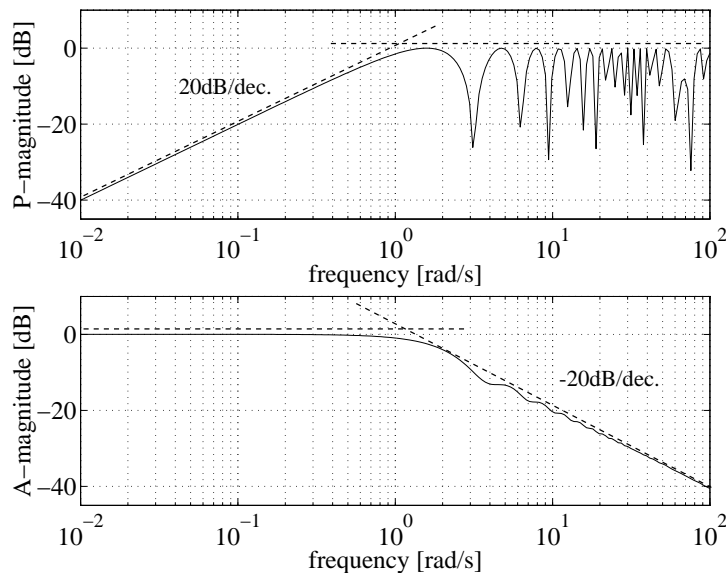


Figure 4.17: Magnitudes of transfer functions from position (P) and acceleration (A) measurement to the respective speed component (observation period: 2s).

The magnitudes of the position (P) and acceleration (A) transfer functions, i.e. from the measured position and acceleration to the respective speed component, are drawn in Figure 4.17. High-pass characteristics results from the position component and low-pass characteristics from the acceleration component. Note that an observation time period of 2 seconds is especially chosen to obtain exactly 0dB attenuation for the pass-band frequencies of the two transfer functions. To simplify the analysis, the two exact gain transfer functions are now replaced by straight lines. Placing the straight lines always above the real values ensures that the damping is always stronger than supposed by the simplification. Without adding significant errors, the position

transfer function can be replaced below a certain frequency $\omega_{edge} = 2\pi f_{edge}$ by a straight line which increases by 20dB per decade, and above ω_{edge} by a straight line at 0dB. The acceleration transfer function results in a 0dB straight line for frequencies below ω_{edge} and decreases by 20dB per decade above. The frequency ω_{edge} is at $1\frac{\text{rad}}{\text{s}}$ for the observation period of 2s. One can interpret this figure in an intuitive manner. The P-magnitude corresponds to a limited band differentiation and the A-magnitude to a limited band integration. The cut-off frequency of these two limited band components corresponds to ω_{edge} .

Observation periods used in practice are much shorter than the mentioned 2s. Therefore, the transfer functions are now analysed for different periods. The edge frequency varies with the reciprocal value of the observation time, which is easily understood by looking at the formula of the position component.

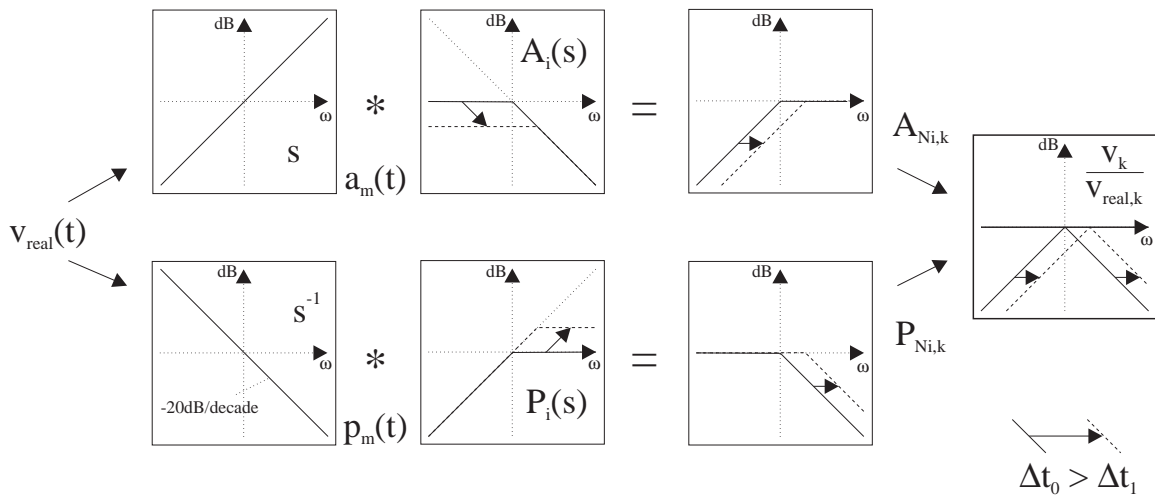


Figure 4.18: Combination of transfer functions to final transfer function $\frac{v_k}{v_{real,k}}$.

The relationships between the different transfer functions are now intuitively explained by means of Figure 4.18, where the influence of the observation period on the transfer functions of position and acceleration component is illustrated. Figure 4.18 has the same principal structure as Figure 4.11 on page 63, but this time with respect to the magnitudes of the transfer function Bode plots. We start the explanation with the resulting total speed transfer function $\frac{v_k}{v_{real,k}}$, the rightmost box on Figure 4.18. Ideally, this total transfer function has unity gain over the whole frequency range, expressed by a fat solid line at 0dB. It is composed of the two components (position and acceleration), the thin solid lines at angles of ± 45 degrees, equivalent to $\pm 20\frac{\text{dB}}{\text{decade}}$. Reducing the observation period length raises the edge frequency f_{edge} . The shift of the two transfer functions is indicated by the short arrows and leads to the dashed lines. The sum of the two components remains the same, independently of the observation period. The six boxes on the left of the figure indicate how the two components are obtained. For example, the acceleration component is composed of a differentiation of the real speed, leading to the measured acceleration, and of the algorithm's transfer function itself. It can easily be seen from the figure, that an increase of ω_{edge} of one decade raises the pass band of the position of the position component transfer function $P_i(s)$ by 20dB and lowers the one of the acceleration component $A_i(s)$ by 20dB.

The gain factor k_{gain} and the edge frequency $f_{edge} = \frac{\omega_{edge}}{2\pi}$ in Hz can be approximated as

follows, based on the observation time period Δt :

$$k_{gain} = 20 \log \left(\frac{2[s]}{\Delta t} \right) \quad f_{edge} \approx \frac{1}{2\pi} \cdot \left(\frac{2[s]}{\Delta t} \right) \quad (4.19)$$

To give an idea of the order of magnitude of gain factor and edge frequency, Table 4.5 summarises the results for practical values of the observation period Δt .

observation period Δt	acceleration attenuation $-k_{gain}$	position amplification k_{gain}	edge frequency f
0.5ms	-72dB	72dB	640Hz
1ms	-66dB	66dB	320Hz
5ms	-52dB	52dB	64Hz
10ms	-46dB	46dB	32Hz

Table 4.5: Characteristics of position and acceleration component for typical observation periods.

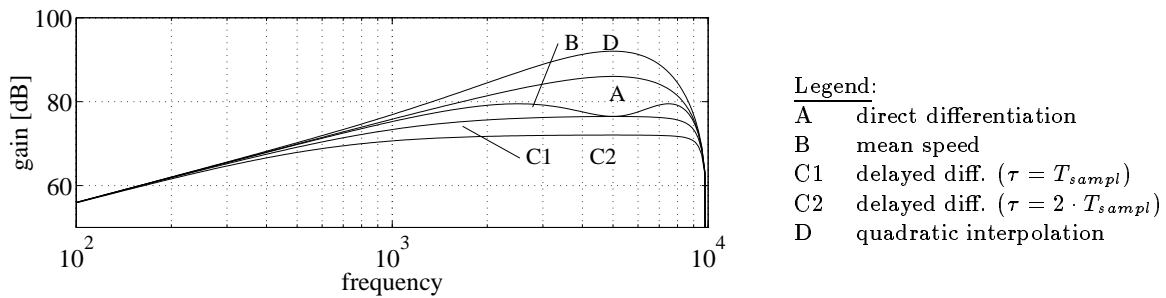


Figure 4.19: Position-to-speed transfer function of position-only methods with $T_{sampling} = 100\mu s$.

For comparison, the gains of the different position based speed estimation methods, discussed in Section 4.2.2, are shown in Figure 4.19. All the results in this figure are based on a sampling period of 0.1ms. For the example of 5ms, there results a reduction of the gain on the position of about 20dB compared to the position-based methods. The speed above 64Hz is mainly constituted of the accelerometer component.

4.3.6 Sensor Failure Detection

The above-derived algorithm for an enhanced speed estimation is based on redundant information obtained from the position and the additional acceleration measurement. In addition to using this redundancy for an enhanced speed estimation, it may also be useful in the case of failure and partial failure of one of the sensors. Different scenarios for failure detection and reaction to such deficiencies are possible. They depend to a high degree on the specific application and their safety concepts. In the following, a failure detection mechanism, based on the proposed algorithm, will be introduced, and possible reaction on failures will be listed.

A possible failure is easily detectable if the gain estimation algorithm — sufficient excitation provided — leads to accelerometer gain factors which are out of a certain tolerance around the nominal gain value. Sufficient excitation has to be tested based on numerator and denominator

of the gain factor calculation formula in order to avoid the case where a faulty position measurement, e.g. a constant measured position despite movement of the axis, always signals insufficient excitation. However, this method allows one only to decide whether or not a sensor failure has occurred, but not whether it is a position encoder or an accelerometer failure. For this more detailed discrimination, if information about the source of failure is also needed, the dynamic behaviour of the system has to be taken into consideration. A simple state estimator based on the control variable and the actual system state is able to decide whether the last few position measurements are plausible or not.

The simplest reaction to any kind of detected failure is to stop the axis by breaking resistances without any external energy. In some cases, it is moreover advantageous to finish a movement in a controlled way due to process constraints, e.g. to stop an axis in a safe position.

Three types of sensor faults of position/acceleration measurement can occur. They are listed here with appropriate reactions:

- *Accelerometer failure:* the axis can be controlled only when based on position measurement. The controller parameters have to be adapted to the new measurement performance. Hence, dynamic stiffness is reduced, but accurate control is possible.
- *Position encoder failure:* position and speed can be estimated based on the last correct position measurement and on the integration of the acceleration measurement. This is only possible during some seconds, due to the always present offset on the accelerometer signals, which is, however, sufficient to perform a controlled stop of the axis at a desired position.
- *Combined accelerometer and position encoder failure:* the drive has to be stopped immediately by braking resistances.

4.3.7 Experimental Results

The fusion algorithm derived in Section 4.3.2 needs measurement of the acceleration. As the accelerometers are analog devices with noise on the output, the algorithm is tested on real axes with measurement errors and disturbances in order to demonstrate its usefulness and accuracy in an industrial environment. As the real speed cannot be measured for reference, the results of the accelerometer-enhanced speed estimation is only compared to the position based ones. For this comparison, we choose the simplest one, i.e. the direct differentiation of the position. This method is independent of knowledge of the controlled system, has a delay of half a sampling interval, and is very sensitive to position quantisation.

Furthermore, the quality of the gain estimation algorithm is demonstrated by experimental results. The estimation of the accelerometer offset is not discussed here, because successful implementations already exist for this common problem of sensor offset compensation. Our measurements showed the expected good results.

The algorithms have been implemented on two different platforms, first, on the DSP of the axis controller in C programming language, and second, on a PC and workstation with MATLAB [Mat94]. The former implementation proves the feasibility under real time constraints. The latter offers the possibility of evaluating off-line the same recorded measurements with different observation periods. The results obtained by both implementations are identical, as expected given the use of exactly the same algorithms, the numerical stability of the algorithms, and the use of floating point numbers for both implementations.

A first series of measurements for the one-accelerometer case is performed on the 75N linear drive (explained in Appendix C.1.1) with almost friction-less air cushion bearings and an immobile base. For the two-accelerometer case, a second series is carried out with the 2200N linear drive machine-tool axis, which is explained in Appendix C.1.2.

In the following, the results of the measurements are presented, first for the one-accelerometer case, and second for the two-accelerometer case. For all experiments, the sampling frequency is set to 10kHz. For both drives, low cost piezoresistive accelerometers are used. Their analog signals are filtered with a first-order anti-aliasing filter with a cut-off frequency in the range of 10kHz. Therefore, the theorem of Shannon is not satisfied. The problem of aliasing does not arise, because the employed algorithm with the double integration of the acceleration signal is less sensitive to aliasing than to the time constant added by a stronger anti-aliasing filter. However, the filter eliminates the main disturbances in the range of 70kHz, caused by the power electronics for the motor phase currents.

4.3.7.1 The One-Accelerometer Case

This section summarises the results obtained on the 75N linear drive axis explained in Appendix C.1.1. This prototype drive glides on air cushion bearings nearly without any friction. The base is fixed to remain completely immobile. Therefore, only one accelerometer measuring the slider acceleration is used. The position encoder resolution is of $0.4\mu\text{m}$.

In the following, two different experiments are performed on this drive. In a first experiment, the slider of the switched-off linear drive is hit by a hammer in order to generate a force impulse. This experiment demonstrates the correct functioning of the speed estimation algorithm for a speed response on a force impulse. In a second experiment, a sinusoidal chirp force reference signal is used as a system input. This open loop configuration tests the algorithm over a wide frequency range and provides also results on the gain estimation algorithm. In the following, representative results of the test series are given for the two experiments.

The reaction of the speed estimation algorithm on a force impulse, caused by a hammer, is

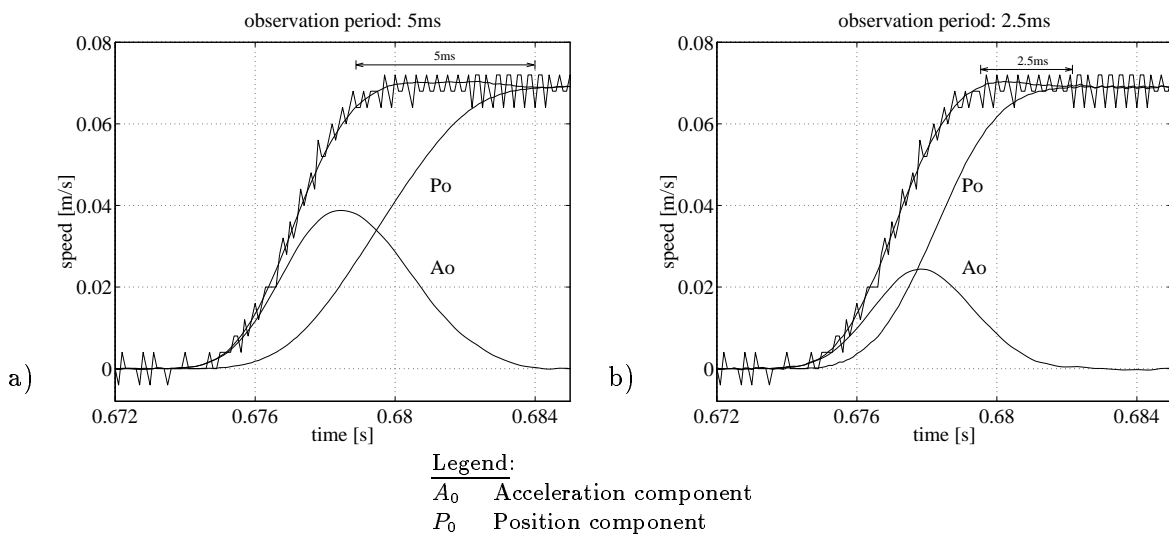


Figure 4.20: Speed response on a force impulse with (a) $\Delta t_i = 5\text{ms}$ and (b) $\Delta t_i = 2.5\text{ms}$.

illustrated in Figure 4.20. For the example on the left, the observation period is set to 5ms, for the one on the right to 2.5ms. The noisy speed signal is the one obtained by direct differentiation of the position. Its speed quantisation step size of $0.004\frac{m}{s}$ is clearly visible. The smoother signal is the one of the accelerometer-enhanced speed estimation algorithm. It is the sum of the position component P_0 and the acceleration component A_0 . The speed response on the force impulse contains high frequency components. Therefore, at the beginning, the accelerometer part A_0 mainly contributes to the speed response. It is clearly visible from the two graphs that A_0 reaches zero and only P_0 constitutes the speed signal at the time Δt_0 after the end of the force impulse. The measurements confirm that the speed estimation algorithm outputs an accurate signal with about the same delay as the direct differentiation of the position, but with considerably reduced noise. The remaining delay on the estimated speed signal is difficult to quantify, due to the absence of an accurate reference speed measurement.

In a second experiment, sinusoidal force chirp reference signals are used to excite the drive in open loop control. Offsets on the force reference signal are manually compensated for, and the used frequencies are chosen sufficiently high to avoid instability of the system. This test is performed to evaluate the accelerometer-enhanced speed estimation as well as the accelerometer gain identification algorithm on a wide range of different frequencies.

The observation time period is chosen to 5ms, i.e. 50 sampling intervals. According to Section 4.3.5, there results an edge frequency f_{edge} of the acceleration and position component of about 60Hz. Below this frequency, the accelerometer signal makes only a minor contribution to the resulting speed signal. Therefore, the chirp frequencies are chosen in the range between 50Hz and 500Hz. The amplitude of the sinusoidal reference force is set to 25N, i.e. a third of the drive's maximum force.

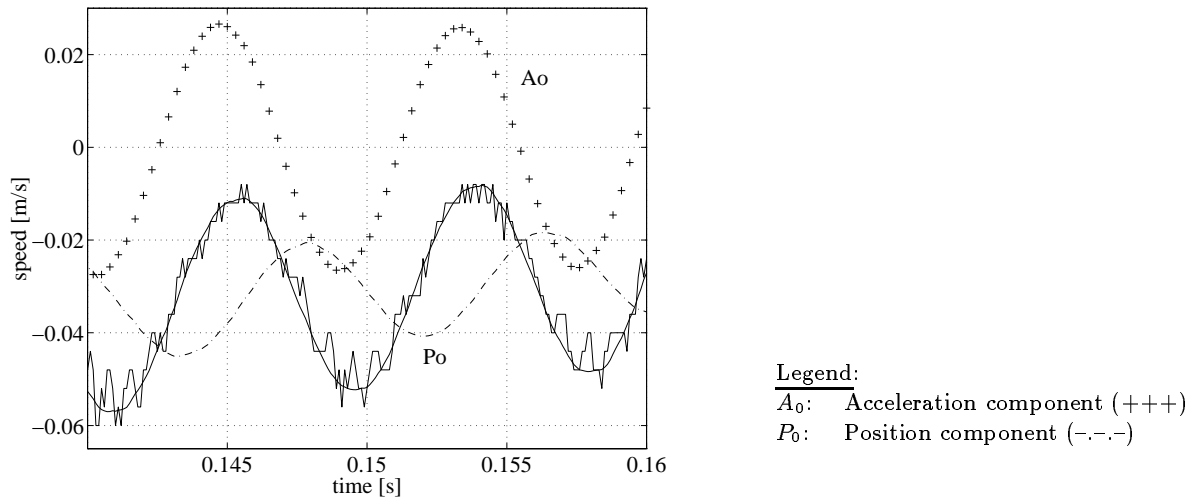


Figure 4.21: Speed signal at a frequency of about 110Hz.

The part of the resulting speed estimate with a frequency of about 110Hz is drawn in Figure 4.21. The accelerometer-enhanced speed estimation turns out to be accurate, over the whole tested frequency range. It seems even to have a bit less delay than the signal of the direct differentiation. Due to some minor non-idealities of the linear drive and the open loop setup of this experiment, there is some low frequency movement superposed to the principal one with sinusoidal form. The speed in the part shown in Figure 4.21 is always negative. Only the position component contains the DC component of the speed. The acceleration component has a zero

mean value. Hence, this example illustrates how the resulting speed estimation is composed of the low frequency band component P_0 and the high frequency band component A_0 . The observation period length of 5ms is clearly visible in Figure 4.21 as a delay of 2.5ms of the position component P_0 compared to the speed signal.

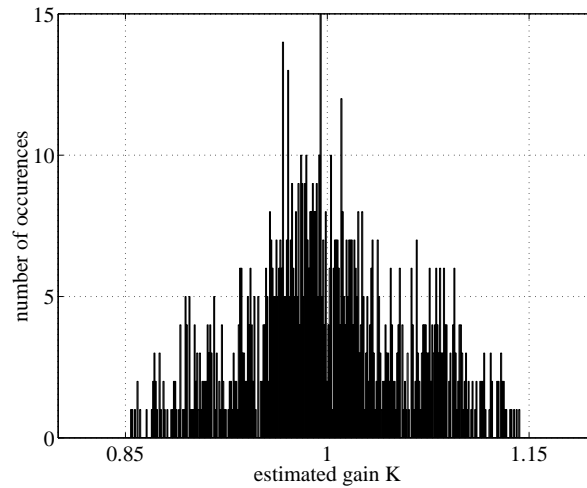


Figure 4.22: Distribution of normalised estimated accelerometer gain K .

Based on the same experiment, the accelerometer gain calibration algorithm is evaluated. In addition to the observation period of 5ms, a second one of 2.5ms is chosen for the parameter identification. Sufficient excitation is supervised according to Equation (4.16) on page 71. About 90% of the estimates of K_A are dropped due to this supervision. The distribution of the remaining estimates of K_A are shown in Figure 4.22. They are normalised (denoted K) with the nominal accelerometer gain. About 60% of them are within a range of 5% around the nominal value and none of them is outside a range of 15%. Low pass filtering with a long time constant adapted to the long time constants of possible drifts of K_A leads to an accurate estimate of K_A .

To sum up, the implementation of the accelerometer-enhanced speed estimation algorithm has shown its feasibility and accuracy for the one-accelerometer case, even when using low cost piezoresistive accelerometers. The delay on the resulting speed signal is equivalent to or even a bit lower than the one of the direct differentiation of the position. The noise on the speed signal is considerably reduced compared to the direct differentiation. The identification of the accelerometer gain is possible, assuming that there is sufficient excitation of the drive. Indeed, it is possible that the normal movements of machine-tool axis do not produce enough excitation for the gain calibration, and, therefore, special calibration movements have to be performed at machine startup.

4.3.7.2 The Two-Accelerometer Case

For the two-accelerometer case, a second series of experiments is made on the 2200N drive explained in Appendix C.1.2. Due to the high accelerations of the drive, a mass relation of about 1:8 between slider and base and the slider mass of about 100kg, the base is not completely fixed to the ground but placed on pieces of rubber to enable some movements of the base. Therefore, the base is mobile to some extent and slider as well as base acceleration have to be measured. The accelerometer-enhanced speed estimation algorithm is tested with an open loop chirp frequency

force reference signal, as before. The encoder resolution of this axis is $0.2\mu\text{m}$, i.e. half the value of before.

The axis is moved by a chirp force reference signal with an amplitude of 500N , about a quarter of the maximum force, and frequencies in the range from 100Hz to 500Hz . The frequency range is adapted to the limits of open loop control of this drive and hence slightly reduced. The observation time period again is set to 5ms . Two different parts of the resulting

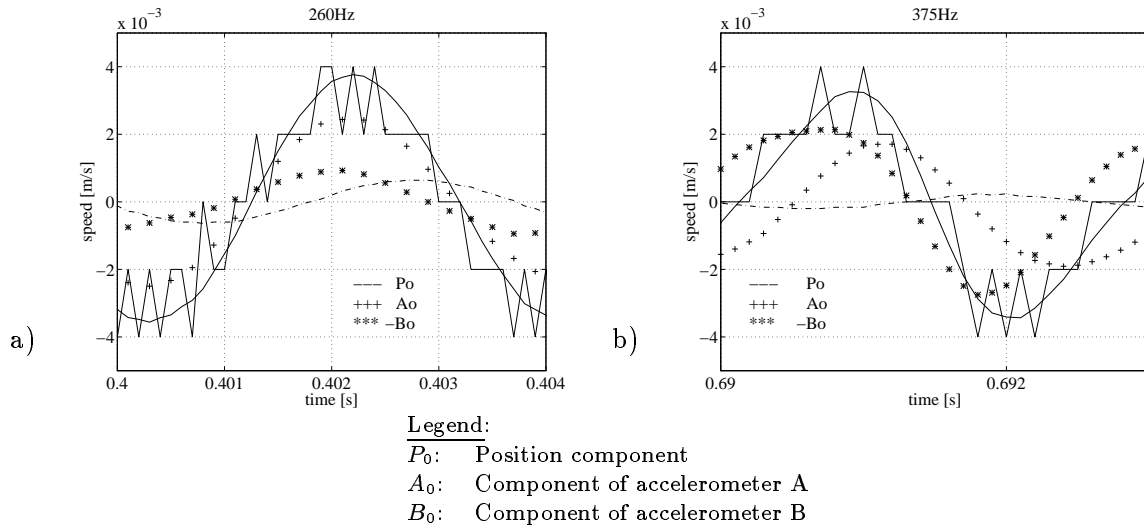


Figure 4.23: Speed estimation at (a) 260Hz and at (b) 375Hz.

speed signal are depicted in Figure 4.23, the first at the frequency of about 260Hz and the second at about 375Hz . Both examples show a slight delay of the accelerometer-enhanced speed estimation compared to the noisy direct differentiation. This delay can be explained by a decreased bandwidth of the here used accelerometers, compared to the one of the one-accelerometer case, and possibly by the additional shielding on the signal transmission cables. The quality of the obtained signal is in fact much better than the one of the direct differentiation, the noise effects are drastically reduced. The examples demonstrate that for this setup, it is indispensable to mount two accelerometers. For the 375Hz example on the right graph of Figure 4.23, the contribution of B_0 of the base accelerometer is even bigger than the one of A_0 of the slider accelerometer. This special situation is caused by a resonance of the base which is visibly excited at this frequency.

Based on the same setup with the same frequency range, the two accelerometer gains K_A and K_B are identified. The three observation periods are set at 25ms , 50ms , and 75ms , respectively. The resulting normalised distributions of gain K_A and K_B are shown in Figure 4.24. 90% of the samples for K_A and 94% of the samples for K_B are dropped by the supervision algorithm. As a result, about 55% of the estimates for K_A and 22% of the estimates for K_B are within a 5% error range. Nevertheless, the variation of the different gain estimates is in this case much higher. This can be explained by a certain correlation between the acceleration signals a_A and a_B , because the force of the drive acts between the two parts and leads to a movement of them in inverse directions. Therefore, the gain estimation algorithm cannot differentiate well between the influences of the two accelerations. This leads to an increased variance of the estimated gains. A good means to counteract this effect is to excite resonances of the base part, as it is the

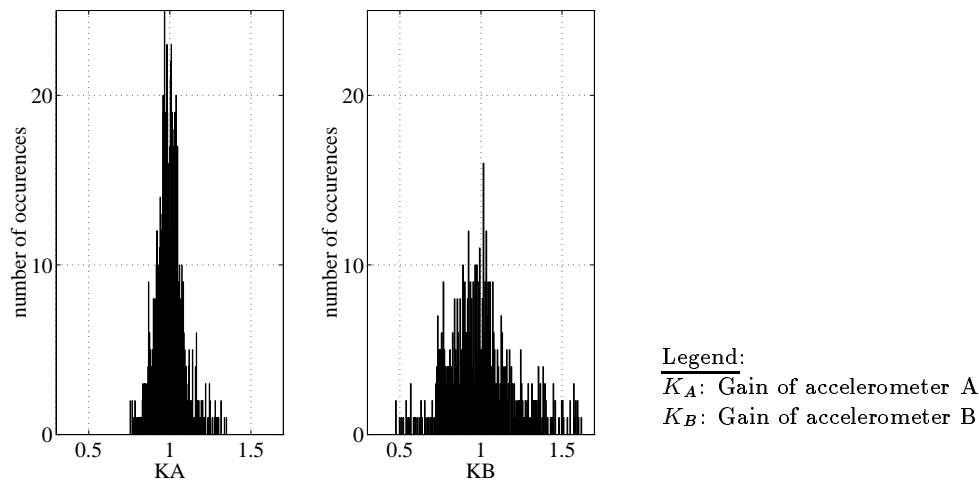


Figure 4.24: Distribution of estimated accelerometer gains.

case at about 375Hz shown in the right graph of Figure 4.23. Exciting resonances guarantees independent accelerations of the two parts of the axis and hence, an accurate identification of the two gains. The example in Figure 4.24 has been obtained based on a wide range of frequencies with and without base resonances. The result is an almost Gaussian distribution around the nominal value of the gains. By low pass filtering, accurate estimates of the gains are obtained. Possibly, drive excitation during normal operation is too small to calibrate the two gains, especially K_B . Hence, specialised identification movements have to be performed at system startup.

4.3.8 Concluding Remarks on Accelerometer-Enhanced Speed Estimation

A novel algorithm for accelerometer-enhanced speed estimation (AESE) has been proposed. In the following, its main characteristics are summarised, the experimental results briefly commented, and the proposed solution is compared to the complementary filter solution.

4.3.8.1 Characteristics of Proposed Algorithm

The algorithm observes position and additional acceleration measurement over a fixed past time period and calculates an accurate speed estimation. As a result, the influence of position quantisation and accelerometer noise on the output speed signal is reduced. The design of the method consists of the choice of one single parameter, namely the observation period length. This parameter determines the frequency at which the main contribution to the speed signal gradually moves from position to acceleration measurement. The same parameter fixes position measurement amplification and acceleration measurement attenuation. The design procedure consists of a trade-off between position quantisation noise and influence of accelerometer measurement errors, mainly accelerometer offsets. Methods for on-line identifying accelerometer gain and offset simplify the commissioning and maintenance of the system.

The algorithm is designed in view of practical problems arising when using measured acceleration and position. Accelerometer noise as well as position quantisation influence are considerably attenuated. The algorithm is robust against accelerometer offset in the sense that the resulting

speed contains an offset proportional to the not compensated accelerometer offset, but does not drift and become unstable. The recursive implementation of the algorithm reduces the necessary calculation power of the numerical controller.

Experiments on two direct-drive axes using low cost piezoresistive accelerometers show very accurate results for the accelerometer-enhanced speed estimation. The influence of accelerometer noise is sufficiently attenuated by the employed algorithm. Experiments have shown that low pass filters for the accelerometer inputs are only useful for filtering the influence of disturbances caused by the choppers of the power electronics. Because the bandwidth of the accelerometers in the employed setup is below the Shannon frequency of the sampled system and disturbances at these frequencies are only minimum, aliasing on the analog inputs is practically not present. As a result, it turns out to be more advantageous to accept the remaining aliasing effects than to add a time constant by adding an anti-aliasing filter. Different observation periods have been tested. As expected, for short periods the influence of the position quantisation is dominant and leads to a noisier speed signal. Longer observation periods lead to a smoother signal, but increase the influence of the accelerometer measurement inaccuracies. In practice, observation periods in the range from 40 to 150 sampling periods turn out to be optimal. The proposed gain estimation algorithm shows excellent results for the one-accelerometer case. For the two-accelerometer case, correlation of the two accelerometer signals deteriorates the quality of the obtained gain estimates. By using special movements to reduce this correlation, this problem is solved, and accurate gain estimates are obtained. Sensor offset identification is possible by simple mean value calculation and is implemented without problems. Mounting of the accelerometer turns out to be crucial. Mechanical resonances have to be avoided in order to obtain accurate signals.

4.3.8.2 Comparison with Complementary Filter Approach

The basic idea behind the fusion method of position and acceleration measurement proposed in this dissertation is close to the complementary filter method of Section 4.3.1.1. Both solutions extract high frequency speed information from the acceleration measurement and low frequency information from position measurement. The sum of the position and the acceleration component theoretically results in both cases in a unity gain transfer function with zero phase shift over the whole frequency range. However, the structure of the employed filters is different. In Figure 4.25, the acceleration-to-speed transfer functions of the two solutions are compared. The sampling frequency in this figure is normalised to 1s. For the AESE-method, an observation period of 20 sampling periods is selected. As an example, the complementary filter method in the figure is designed with a damping ratio of 0.7 ($k_1 = 0.1$; $k_2 = 0.005$). The acceleration-to-speed transfer function of the AESE-method is a limited bandwidth integration. The transfer function of the complementary filter method is a combination of a differentiator with a second order system.

$$\frac{\text{speed component}}{\text{measured acceleration}} = s \cdot \frac{1}{s^2 + k_1 s + k_2}$$

As it can be seen in Figure 4.25b, the transfer function has differentiation property for low frequencies and integration property for high frequencies. The frequency band of the differentiation part varies with different design parameters (k_1 , k_2), but it remains always a region with differentiation property. The differentiation of a measured value, also in a limited frequency

band, raises noise sensitivity. It can be concluded that the complementary filter solution is more sensitive to acceleration measurement noise than the solution proposed in this work.

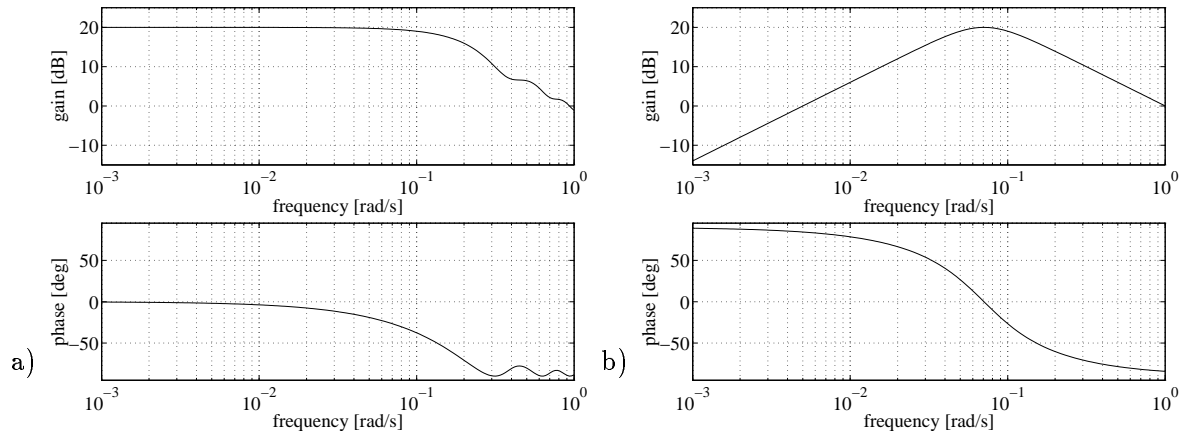


Figure 4.25: Transfer functions from acceleration to speed component: (a) proposed method; (b) complementary filter method.

In [SS90], an implementation of the complementary filter approach is presented. The filters are designed in the continuous time domain and discretised. The main problems consists in design and implementation of the filters. The AESE-method proposed in this dissertation simplifies this method in that this filter design is done implicitly, based on one single design parameter. The IIR filter structure chosen in [SS90] turns out to be very sensitive to quantisation of acceleration measurement. In contrast, the FIR structure, employed in this dissertation is not sensitive to input signal quantisation and its recursive form is easily implemented. Accelerometer offset identification is not necessary with the method of [SS90], because the DC part of the accelerometer signal is completely cut off by the used high pass filter, as opposed to our AESE-method, for which special accelerometer offset compensation is necessary.

The Kalman filter design approach of [Jag94] poses problems because the assumptions of Kalman design are not satisfied. Detuning of the obtained feedback parameters is necessary to obtain reasonable performance. Apparently, accelerometer noise problems also arise: first, according to Jager, proper anti-aliasing filtering (40Hz bandwidth) is important to obtain usable experimental results. Second, accelerometer noise problems limit the obtained performance of the combination of accelerometer-enhanced observer and direct acceleration feedback. Jager concludes that *“an accurate and clean acceleration signal is needed to be useful, so a high accuracy sensor is necessary and filter should be used to increase the signal-to-noise ratio, without adding too much phase shift”*. In contrast, no anti-aliasing filtering is necessary (see Section 4.3.7) for our proposed solution.

4.4 Conclusions

The aim of this chapter has been to collect different methods to obtain a “good” speed estimation of the linear movement of a machine-tool axis. “Good” means, on the one hand, a minimum of time delay on the obtained speed signal and, on the other hand, almost no noise on the signal due to measurement inaccuracies. As far as possible, all presented methods have been explained

in terms of these two characteristics in order to directly compare them. Figure 4.26 finally summarises the presented results.

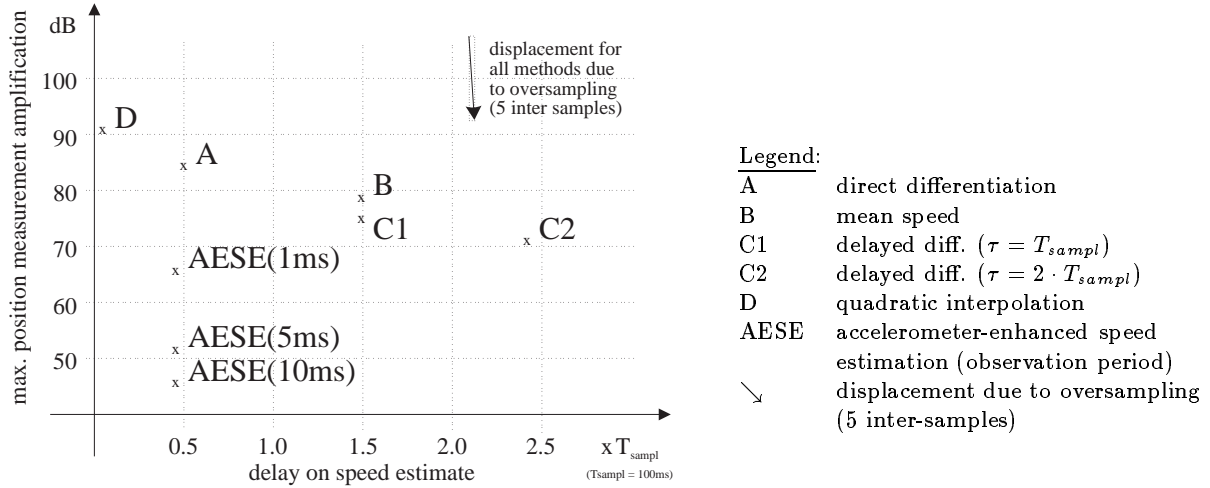


Figure 4.26: Delay/quantisation-noise characteristics of different speed estimation methods.

All examples in Figure 4.26 are based on a sampling period $T_{\text{sampl}} = 100\mu\text{s}$. The ordinate indicates the resulting delays on the speed estimate denoted as number of sampling periods. On the abscissa, the maximum position measurement amplification as a measure of quantisation noise amplification is indicated on a logarithmic scale. It is important to note that the indicated amplification values are maximum values over the whole frequency range up to Shannon frequency and, therefore, have to be considered as worst case values. The high amplifications may surprise, but they are the result of the division by the very short sampling period. The figure exemplifies the trade-off between noise and delay of the different position-only speed estimation algorithms. The solution which is the most sensitive to position quantisation among the presented ones is the quadratic interpolation (D). Higher order interpolation algorithms would be even more sensitive to quantisation because quantisation is not modelled in this approach. The most commonly used direct differentiation (A) has a delay of half a sampling period. The mean speed method (B) adds, as expected, one sampling period of delay. The estimation of the delay for the two examples of the delayed differentiation (C1, C2) is not completely exact, because their IIR structure does not fit well with the used scheme dealing with pure delays. However, for this figure, some approximative values have been estimated, based on comparison of their phase with the one of solution (B).

A delay around half a sampling period is indicated for the accelerometer-enhanced speed estimation (AESE) according to results of different experiments. This value depends on the acceleration measurement system, including sensor, signal transmission, and the analog filtering. The algorithm itself does not have any delay. For all discussed solutions, the method of position oversampling is possible. The example of 5 inter-samples using the burst method proposed in Section 4.2.4 is interesting in practice because it presents a good compromise between necessary calculation time and gain in accuracy. For this example, the result is a reduction of approximately 14dB in position quantisation sensitivity and an additional delay of about a twentieth of a sampling period, as visualised by an arrow in Figure 4.26. The accelerometer-enhanced speed estimation reduces the sensitivity to position quantisation by some order of magnitudes without adding any delay. The longer the selected observation period, the higher the attenua-

tion of position quantisation but the bigger the influence of the accelerometer inaccuracies. In practice, observation periods of 5ms to 20ms turn out to be advantageous. The exact choice of the observation period is not crucial, the results being very similar in this wide range of different values. By the use of an accelerometer and the AESE-method, the demands on the position resolution necessary for an accurate speed estimation are reduced. In comparison, to obtain the result of the AESE-method with an observation period of 10ms (100 times the sampling period) without using any accelerometer, the position encoder resolution would have to be increased by a factor of 100.

Purely position-based speed observers have not been discussed in detail. The drawback of conventional observers is that the trade-off between noise reduction and reaction speed on external disturbances does not lead to better results than the ones obtained by the discussed position based methods. Disturbance observers are composed of two dynamic loops. The first estimates external disturbances and the second estimates the speed based on the estimated disturbances. The resulting dynamics of these two cascaded loops is no longer very high.

To sum up, the use of additional acceleration measurement is an interesting alternative to highly accurate speed estimation. The proposed speed estimation algorithm lowers the demands on the position encoder resolution, is a low cost solution with an easy implementation, and includes automatic calibration of the used accelerometers. Experimental results prove the successful implementation and accuracy of the proposed solution. A crucial point of the proposed solution is the mounting of the accelerometers. Points of structural resonances of the axis have to be avoided, which is possible by a knowledge of the mechanical resonances of the axis or simply by heuristics.

References

- [ASvdS96] Pervez M. Aziz, Henrik V. Sorensen, and Jan van der Spiegel. An overview of sigma-delta converters. *IEEE signal processing magazine*, 13(1):61–84, January 1996.
- [BG90] Markus Barmettler and Peter Gruber. Erhöhung der Auflösung digital erfasster Daten (Teil 2). *Precision*, (9):33–37, 1990.
- [Bra94] Karl Brammer. *Kalman-Bucy-Filter: deterministische Beobachtung und stochastische Filterung*. Oldenbourg, München, 4th edition, 1994.
- [BSMM95] I.N. Bronstein, K.A. Semendjajew, G. Musiol, and H. Mühlig. *Taschenbuch der Mathematik*. Verlag Harri Deutsch, Frankfurt am Main, 2nd edition, 1995.
- [Büh83] Hansruedi Bühler. *Réglages échantillonnés*, volume 2. Presses polytechniques romandes, Lausanne, 1983.
- [CS92] S. Colombi and F. Saghatchi. Digital position and velocity determination in controlled drive systems. In *IFAC Workshop on Motion Control for Intelligent Automation*, Perugia, 1992.
- [Föll85] Otto Föllinger. *Regelungstechnik*. Hüthig Verlag, Heidelberg, 5th edition, 1985.
- [Gee96] Andrea Gees. On-line accelerometer gain and offset identification. In *Proceedings of the International Symposium on Measurement and Control in Robotics (ISMCR '96)*, Brussels, 1996.

- [Hor93] Yoichi Hori. Robust and adaptive control of a servomotor using low precision shaft encoder. In *Proceedings of the International Conference on Industrial Electronics, Control and Instrumentation (IECON)*, volume 1, pages 73–78, 1993.
- [Ise87a] Rolf Isermann. *Digitale Regelsysteme*, volume 1. Springer Verlag, Berlin, 2nd edition, 1987.
- [Ise87b] Rolf Isermann. *Digitale Regelsysteme*, volume 2. Springer Verlag, Berlin, 2nd edition, 1987.
- [Jag94] Bram de Jager. Acceleration assisted tracking control. *IEEE Control Systems*, pages 20–27, Oct. 1994.
- [Mat94] Math Works, Inc. *MATLAB High Performance Numeric Computation and Visualization Software*, 1994. User’s Guide.
- [Mer96] Shmuel Merhav. *Aerospace sensor systems and applications*. Springer-Verlag, New York, 1996.
- [OS92] Alan V. Oppenheim and Ronald Schaffer. *Zeitdiskrete Signalverarbeitung*. Oldenbourg, München, 1992.
- [Phi92] W. Philipp. *Regelung mechanisch steifer Direktantriebe für Werkzeugmaschinen*. Springer Verlag, Berlin, 1992.
- [SS90] F.R. Shaw and K. Srinivasan. Bandwidth enhancement of position measurements using measured acceleration. *Mechanical Systems and Signal Processing*, 4:23–38, Jan. 1990.
- [Zir96] Oliver Zirn. *Beitrag zum Entwurf von Vorschubantrieben für die Hochgeschwindigkeitsbearbeitung*. PhD thesis, ETH Zürich, 1996.

Chapter 5

Axis Control with Acceleration Measurement

The aim of this chapter is to discuss the benefits of the acceleration measurement for closed-loop control. The influence of the accelerometer-enhanced speed estimation on controller bandwidth and noise is analysed for the cascade controller structure in Section 5.1. Then, the use of the accelerometer signal for direct acceleration feedback is briefly reviewed in Section 5.2. Further, possible limits of the combined use of both approaches are outlined. The aspects of controller structures and optimal controllers for linear-drive machine-tool axes are not the topic of this dissertation. The reader should refer to the literature [Phi92, Alt94, Zir96].

5.1 Influence of Speed Estimation on Closed-Loop Control

In Chapter 4, the speed estimation methods are classified according to their delay and quantisation noise. Therefore, the influences of these two parameters on closed-loop control are analysed. In the following, the employed cascade controller structure is defined, a pseudo-continuous model of the controlled system is derived, and the design of the controller parameters is discussed. The achievable closed-loop bandwidth is estimated. Then, the influence of position quantisation on the reference input of the linear motor is analysed. Maximum error bounds and power dissipation due to quantisation are determined. They are analysed with the open control loop but taking into consideration feedback parameters of a stable feedback loop. Thereby, the influence of quantisation is well approximated without the need of exact controller modelling. The results provide a knowledge of the importance of the expected quantisation effects and the possible improvements with the AESE-method.

In general, the different characteristics of the selected speed estimation method have the following influences:

- *Delay on the estimated speed signal* limits the available closed-loop bandwidth. Therefore, to obtain a maximum bandwidth, a minimum delay is required.
- *Noise on the estimated position and speed signal* is amplified by the controller gain factors and acts on the reference force input of the drive. To reduce the influence of quantisation effects, the gain factors have to be reduced. This also limits the closed-loop bandwidth.

5.1.1 Cascade Controller Structure

The cascade controller structure composed of a speed and a position loop is chosen as basic control structure in this work. This controller setup has the advantage that the speed loop is commissioned independently of the outer position loop. It provides the basis to take limitations into consideration at the point in the loop where they occur. In contrast, for global feedback systems, the limitation of internal variables is more complicated.

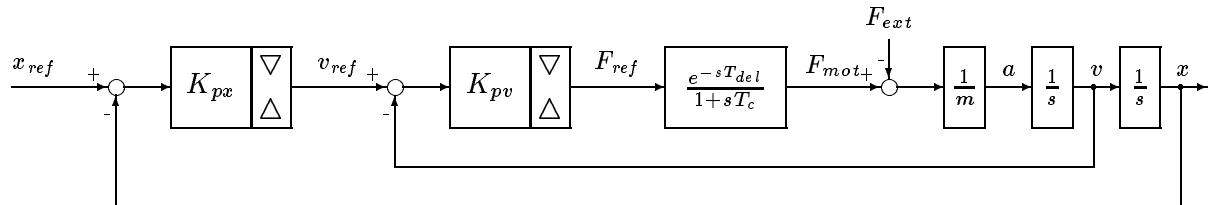


Figure 5.1: Cascade controller structure.

The structure with the used axis model is shown in Figure 5.1. The triangles in the controller blocks K_{px} and K_{pv} denote the limitations at the controller outputs. In the case of linear-drive machine-tool axes, such limitations are for instance the maximum speed due to the position-encoder electronics and the maximum force of the drive. In this chapter we are only interested in the position control loop with its underlying speed control loop. The current control loop with the power electronics is considered as a part of the basic drive, and its design is not further detailed here. According to Section 2.3.1 its transfer function is modelled as a constant factor, a pure time delay and a time constant. For the following discussion, the constant factor of the model is made a part of the controller factor K_{pv} and not present as an explicit factor anymore. It should be noted that the chosen cascade controller structure with proportional feedback gains is not optimal for axis control. It leads for instance to a stationary tracking error in case of a reference trajectory with a constant speed. In addition, PD-position- and PI-speed-feedback would result in a higher closed-loop bandwidth. However, proportional feedback provides good estimates of the influence of measurement inaccuracies on closed-loop control.

5.1.2 Control Loop and Parameters

The influence of speed-estimation delay on the achievable closed-loop bandwidth of a cascade controller is determined in this section. The analysis is made in continuous domain by approximating discrete sub-systems with pseudo-continuous elements. The basic concepts of continuous analysis of discrete systems are given, the axis model is completely converted into continuous domain and the equations of an example controller design are detailed.

5.1.2.1 Pseudo-Continuous Modelling

When a sufficiently low sampling period is used, a discrete control system can be modelled as a pseudo-continuous system and analysed with the tools of continuous control. In our case as in most control applications, the system is composed of continuous and discrete elements. The requirements for the use of pseudo-continuous modelling and the conversion of the system from discrete to continuous domain are given in [Büh94]. We briefly summarise the points that are

important for our design. The elements of the continuous motor with a discrete controller can be transformed into an approximative continuous systems by the following conversions:

- *Pure time delays* e^{-sT} are modelled as corresponding time constants: $\frac{1}{1+sT}$
- The *zero order hold element (ZOH)* of the digital controller is modelled as a time constant of half a sampling period: $\frac{1}{1+s\frac{T_{\text{sampl}}}{2}}$
- The *continuous motor model* is not affected by this transformation.

The model of a system with a sequence of time constants and delays results in a product of different time-constant terms ($\frac{1}{1+sT_i}$) after transformation into pseudo-continuous form. For simplifying the controller design, it is advisable to replace all these different time constants by a single time constant. The following simplification of time constants, which holds for not to high frequencies is usually employed [Föl85].

$$(1 + sT_1)(1 + sT_2) \dots (1 + sT_N) \approx 1 + s \sum_{i=1}^N T_i$$

It has been stated above that the sampling period T_{sampl} has to be sufficiently small in order to obtain a good approximation of a discrete system by a continuous model. Sufficiently small means that it must be lower than half the lowest dominant time constant of the system. In the absence of dominant time constants, it has to be chosen smaller than the sum of motor and measuring-device time constant [Büh94]. The correspondences have been derived by assuming a sampling period which tends towards zero. Therefore, the higher is the sampling period, the larger are the inaccuracies of the pseudo-continuous model. In practice, the sampling frequency is often selected a factor 10–20 higher than the closed-loop bandwidth.

5.1.2.2 Model of the Axis

The transfer function of a linear-drive axis from controller output $U(z)$ to the assumed measured speed input $V_m(z)$ is shown in Figure 5.2. It is composed of an D/A -converter, a delay T_{del} from power electronics, a time constant T_c from the current controller, a mass-factor m , an integration $\frac{1}{s}$, and an A/D -conversion. The control algorithm in the numerical controller causes

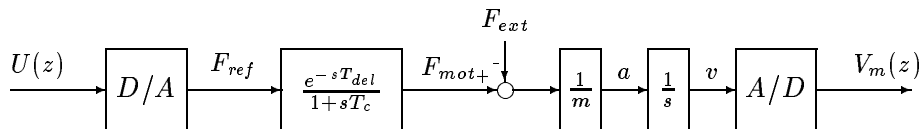


Figure 5.2: Motor transfer function for pseudo-continuous modelling.

an additional time delay which is modelled as a time constant T_{contr} (not shown in the figure). In this model, the speed is supposed to be directly measured, which is not the case for real axes. The fact that it is obtained by differentiation of the measured position is modelled by an additional delay. The length of this delay depends on the differentiation method. A factor N_{diff} is defined to indicate the number of sampling periods of this delay for the different methods. For

instance, the direct differentiation has a factor $N_{diff} = 0.5$. The delays of the different methods are discussed in Section 4.2.

The pseudo-continuous transfer function of the motor and controller are obtained by transforming all time delays into corresponding time constants and adding time constants for the ZOH, the differentiation, and controller delay:

$$\frac{V_m(s)}{U(s)} = \frac{1}{1 + sT_{del}} \cdot \frac{1}{1 + sT_c} \cdot \frac{1}{m} \cdot \frac{1}{s} \cdot \underbrace{\frac{1}{1 + s\frac{T_{sampl}}{2}}}_{\text{ZOH}} \cdot \underbrace{\frac{1}{1 + sN_{diff}T_{sampl}}}_{\text{differentiation}} \cdot \underbrace{\frac{1}{1 + sT_{contr}}}_{\text{controller}}$$

As explained above, the different time constants are now replaced by one single time constant T_v , which corresponds to the sum of all time constants.

$$T_v = T_{del} + T_c + \frac{T_{sampl}}{2} + N_{diff} \cdot T_{sampl} + T_{contr}$$

The resulting simplified pseudo-continuous transfer function of controller, drive, axis, and speed measurement is shown in Figure 5.3.

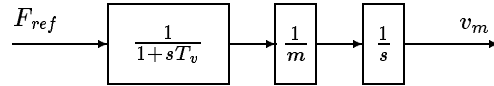


Figure 5.3: Pseudo-continuous model of controller and axis.

The influence of friction and limitations are not taken into consideration in this model. These simplifications are justified because we only want to establish the range of achievable bandwidths and realistic controller gains. Controller performance aspects, such as tracking error, are not the topic of this dissertation.

5.1.2.3 Controller Parameter Design

The aim of this section is to derive feedback parameters which are realistic in order to determine the order of magnitude of the bandwidth and to obtain realistic values of the controller gains. We are only interested in the order of magnitude of the parameters. The design of optimal controller structures and parameters for motion control systems is widely discussed in literature (e.g. [Stu81]).

The speed feedback loop is designed with the time constant T_v . In order to have a more general model, the mass factor $\frac{1}{m}$ is included in the feedback gain factor K_{pv} . The resulting speed control loop with speed reference v_{ref} as input and measured speed v_m as output is shown in Figure 5.4. This model is rather general and applies for different drive types, because the time constants are always in the same order of magnitude and because the mass, which significantly varies for different axes, is part of the factor K_{pv} . It is important to note that the output of this loop is the measured speed v_m and not the real speed v . The relationship $v = (1 + sN_{diff}T_{sampl})v_m$ will be neglected below and the two speeds v_m and v will be supposed to be identical. Our error estimations and simulations have shown that, for our purposes, it is admissible to neglect the small time constant $N_{diff}T_{sampl}$ without significantly affecting the

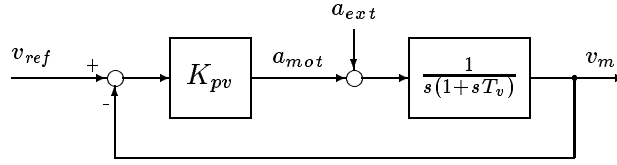


Figure 5.4: Model of simplified speed loop.

obtained results. The transfer function of the speed control loop with reference-speed input and real-speed output results as a second order system with damping D_v and bandwidth ω_v :

$$\frac{V(s)}{V_{ref}(s)} = \frac{\frac{K_{pv}}{s(1+sT_v)}}{1 + \frac{K_{pv}}{s(1+sT_v)}} = \frac{1}{1 + s\frac{1}{K_{pv}} + s^2\frac{T_v}{K_{pv}}} = \frac{1}{1 + s\left(\frac{2D_v}{\omega_v}\right) + s^2\left(\frac{1}{\omega_v^2}\right)}$$

Figure 5.5 shows the resulting position feedback loop with the position error feedback parameter K_{px} and an additional integrator in the system. The inner speed loop is represented as a second order system without the explicit feedback path. It should be noted that the external acceleration a_{ext} as a part of the speed feedback loop is not explicitly shown anymore in the following.

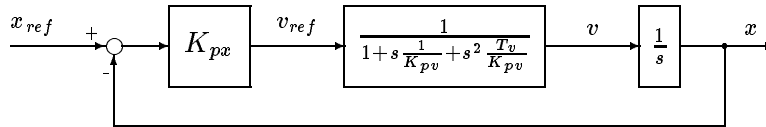


Figure 5.5: Model of position feedback loop.

The transfer function of the closed control loop with a position and a speed cascade results as:

$$\frac{X(s)}{X_{ref}(s)} = \frac{1}{1 + s\frac{1}{K_{px}} + s^2\frac{1}{K_{px}K_{pv}} + s^3\frac{T_v}{K_{px}K_{pv}}}$$

This closed-loop transfer function is of third order. We impose three poles at: $p_{1,2} = -\rho \pm j\rho$ and $p_3 = -\rho$. This pole placement guarantees a fast step response and practically no overshoot [Büh94]. By comparison of the coefficients, the formulae for the calculation of the feedback gains K_{px} and K_{pv} as well as the speed-loop bandwidth f_v are obtained. The closed-loop bandwidth f_x of the complete position control system is approximately proportional to the factor K_{px} [Stu81].

$$\begin{aligned} K_{px} &= \frac{1}{6T_v} & f_x &\approx \frac{K_{px}}{2\pi} = \frac{1}{12\pi T_v} \\ K_{pv} &= \frac{4}{9T_v} & f_v &= \frac{1}{3\pi T_v} \end{aligned}$$

The derived formulae will be employed for the calculation of an example feedback control loop. The aim is to have factors K_{pv} and K_{px} which have realistic values for implementation in order to evaluate the available closed-loop bandwidth and the influence of position quantisation and speed estimation method on realistic values.

5.1.3 Quantisation Effects

The influence of quantisation errors on the control loop are estimated based on open-loop considerations. The position quantisation errors influence the feedback path for position-error feedback as well as the one for speed-error feedback. The latter influence is due to the use of the position measurement for speed determination. The quantisation is analysed from its source, the position measurement, to its point of action, the reference acceleration variable. The two controller feedback gains also influence the result. Example values for our analysis are taken from the above-derived design example. This enables one to compare the influence of quantisation on the position and the speed feedback path.

This open-loop consideration is certainly a simplification of the real system. Noise on the actuator input also influences the system output, i.e. the measured position. This influence would have to be analysed by nonlinear control theory [SL91] employed to the closed-loop system. The absence of limit cycles caused by quantisation would have to be determined [Col87]. Such a nonlinear-system analysis depends on the selected controller structure. Different controller structures and parameter sets would have to be analysed in detail. This exceeds the scope of this dissertation. Nevertheless, the evaluation of the noise directly acting at the point of force generation gives a good estimation of the quantisation influences. The relative reduction of the quantisation effects by employing accelerometer-enhanced speed estimation leads to a general assessment of the benefits of this method. However, quantisation is a nonlinear effect. A reduction of quantisation does not necessarily lead to linear reduction of its effects.

Two different approaches for modelling the quantisation error are chosen. First, the maximum error bounds are determined. They denote the maximum disturbance peaks which possibly act on the input signal of the motor. Second, the variance of the error signal on the reference force is calculated, which indicates the mean power dissipation due to quantisation noise.

The analysis of quantisation effects is here restricted to the discussion of position quantisation influence which is dominant. Rounding errors of the numerical controller are practically absent when using floating-point processors. For the employed observation period lengths (some tenth of sampling periods) of the accelerometer-enhanced speed-estimation algorithm, the influence of measurement noise of acceleration measurement is low in comparison to the influence of position quantisation. Therefore, it will be neglected in the following analysis.

5.1.3.1 Maximum Error Bounds

The maximum absolute error on the reference acceleration signal as worst-case error is calculated by adding the maximum absolute quantisation errors of all elements with quantisation of a formula. The influence of position quantisation on the reference force value will now be derived for the direct differentiation for speed estimation. It is based on the cascade controller structure of Figure 5.1 on page 88. The reference acceleration a_{ref} as controller output is obtained from the reference position $x_{ref,k}$ and the position measurements $x_{m,k}$ and $x_{m,k-1}$ as follows:

$$a_{ref,k} = x_{ref,k} \cdot K_{px} \cdot K_{pv} - \left(K_{px} \cdot x_{m,k} + \frac{x_{m,k} - x_{m,k-1}}{T_{sampl}} \right) \cdot K_{pv} \quad (5.1)$$

By assuming that $x_{m,k}$ and $x_{m,k-1}$ have a maximum quantisation error of $\frac{q}{2}$, the maximum

absolute reference-acceleration error Δa_{ref} results as:

$$\max |\Delta a_{ref}| = \left(K_{px} \cdot \frac{q}{2} + \frac{q}{T_{sampl}} \right) \cdot K_{pv} \quad (5.2)$$

Equation (5.2) is now generalised for the other discussed differentiation methods. We define a factor n_{diff} which is the multiplicative factor of $\frac{q \cdot K_{pv}}{T_{sampl}}$ to obtain the maximum absolute quantisation error on the speed estimate.

$$\max |\Delta a_{ref}| = \left(K_{px} \cdot \frac{q}{2} + n_{diff} \cdot \frac{q}{T_{sampl}} \right) \cdot K_{pv}$$

In Table 5.1, the factors for n_{diff} are summarised. They are obtained exactly the same way as in the above example. The differentiation methods are defined in Section 4.2; the method for accelerometer-enhanced speed estimation is explained in Section 4.3.

Method	n_{diff}	Remarks
A: direct differentiation	1	
B: mean speed calculation	2/3	
C: delayed differentiation	1	independent of τ
D: quadratic interpolation	2	
AESE: accelerometer-enhanced speed estimation	1/N	observation period: $N \cdot T_{sampl}$

Table 5.1: Quantisation error factors n_{diff} of different speed estimation methods.

5.1.3.2 Power Dissipation due to Quantisation Noise

To estimate the heat-up of the drive due to position quantisation, we calculate the expected power dissipation. For a noise signal with zero mean value, the variance is equivalent to the quadratic mean value, which denotes the power dissipation. As an example, the variance for the use of the direct-differentiation method is derived. The calculations are based on Equation (5.1). The theory is found in Appendix A.1. Assumed that $x_{m,k}$ and $x_{m,k-1}$ contain an uncorrelated and uniformly-distributed quantisation noise, their total variance σ^2 results as:

$$\sigma^2 = \underbrace{\frac{q^2}{12} \left(K_{px} + \frac{1}{T_{sampl}} \right)^2 \cdot K_{pv}^2}_{\text{from } x_{m,k}} + \underbrace{\frac{q^2}{12} \cdot \frac{K_{pv}^2}{T_{sampl}^2}}_{\text{from } x_{m,k-1}} = K_{pv}^2 \cdot \frac{q^2}{12} \cdot \left(K_{px}^2 + \frac{2K_{px}}{T_{sampl}} + \frac{2}{T_{sampl}^2} \right)$$

The values of the other methods are obtained the same way as for the direct differentiation. The results are summarised in Table 5.2. The square root of the obtained variance σ is equivalent to the standard deviation. Its square, the variance σ^2 itself is equivalent to the mean power (as expressed in square of acceleration) due to quantisation. The relation with the maximum power, the square of the maximum acceleration indicates, what degree of the power dissipation is caused by quantisation.

Method	Variance σ^2
A: direct differentiation	$K_{pv}^2 \cdot \frac{q^2}{12} \left[K_{px}^2 + \frac{2K_{px}}{T_{sampl}} + \frac{2}{T_{sampl}^2} \right]$
B: mean speed calculation	$K_{pv}^2 \cdot \frac{q^2}{12} \left[K_{px}^2 + \frac{K_{px}}{3T_{sampl}} + \frac{5}{9T_{sampl}^2} \right]$
C: delayed differentiation	$K_{pv}^2 \cdot \frac{q^2}{12} \left[K_{px}^2 + \frac{2K_{px}}{\tau + T_{sampl}} + \frac{2}{(2\tau + T_{sampl})(\tau + T_{sampl})} \right]$
D: quadratic interpolation	$K_{pv}^2 \cdot \frac{q^2}{12} \left[K_{px}^2 + \frac{3K_{px}}{T_{sampl}} + \frac{6.5}{T_{sampl}^2} \right]$
AESE	$K_{pv}^2 \cdot \frac{q^2}{12} \left[K_{px}^2 + \frac{2K_{px}}{NT_{sampl}} + \frac{2}{N^2T_{sampl}^2} \right]$

Table 5.2: Variances on controller output for different speed estimation algorithms.

5.1.4 Design Example from Practice

The formulae and relationships will now be applied to real axis data in order to determine the order of magnitude of noise and delay influences. The different methods for position-only speed estimation will be compared with the accelerometer enhanced speed estimation (AESE) method. The description of the position-only methods is found in Section 4.2, the description of the AESE-method in Section 4.3.

5.1.4.1 Axis Data

The theoretical relationships which have been derived in the previous section are now applied to data from an existing system. We use the data from our linear-drive axis with 2200N maximum force, which is discussed in Appendix C.1.2. A summary of the important data in this context is given in Table 5.3.

Parameter	Symbol	Value
maximum acceleration	a_{max}	$22 \frac{m}{s^2}$
Current controller time constant	T_c	0.2ms
Power electronics time delay	T_{del}	0.1ms
Position resolution	q	$0.1 \mu m$

Table 5.3: Technical data of 2200N linear-drive axis.

The influence of the sampling period on closed-loop performance is shown in [Zir96]. It is stated there that sampling periods of less than $500 \mu s$ are desirable, because the controlled system performance decreases with higher sampling periods. Therefore we base our examples on sampling periods of $100 \mu s$ and $200 \mu s$. The delay T_{contr} due to the calculation time in the numerical controller is assumed to be $20 \mu s$. This value turns out to be appropriate for the implementation of a simple controller structure and the accelerometer-enhanced speed estimation method.

5.1.4.2 Bandwidth

The controller design is done according to the explanation given in Section 5.1.2. The resulting feedback gains K_{px} and K_{pv} as well as the bandwidths f_x and f_v are summarised in Table 5.4. The bandwidths are grouped in descending order. For the acceleration-enhanced speed estima-

	$T_{sampl} = 0.1ms$				$T_{sampl} = 0.2ms$			
	$K_{px} [\frac{1}{s}]$	$K_{pv} [\frac{1}{s}]$	$f_x [Hz]$	$f_v [Hz]$	$K_{px} [\frac{1}{s}]$	$K_{pv} [\frac{1}{s}]$	$f_x [Hz]$	$f_v [Hz]$
D	450	1200	72	290	400	1060	63	250
A, AESE	400	1060	63	250	320	860	51	200
B, C1	320	860	51	200	230	620	37	150
C2	280	740	44	180	190	510	30	120

Table 5.4: Effect of delay: feedback gains K_{px} , K_{pv} , and closed-loop bandwidths f_x and f_v .

tion (AESE) method, a delay of half a sampling period is assumed. According to our experiences, the delay is rather below this limit which thus denotes a worst-case bound.

The delay of the speed estimation algorithm has a significant influence on the closed-loop bandwidth. From the method D (quadratic interpolation without any delay) with a bandwidth of $f_x = 72Hz$ to the method C2 (delayed differentiation with $\tau = T_{sampl}$) with a bandwidth of $f_x = 44Hz$, it results a reduction of nearly 40% for a sampling period of 0.1ms. For the sampling time of 0.2ms, the reduction is even 50%.

It should be noted that the obtained bandwidths are maximum theoretical values. In practice, the achievable bandwidths are below these values because of modelling errors. Therefore, the given feedback gains are also maximum values.

5.1.4.3 Maximum Reference Acceleration Error due to Quantisation

The maximum reference acceleration error due to quantisation is now calculated for the different methods with the same feedback factor values. For the sampling time 0.1ms, the values are: $K_{px} = 280$, $K_{pv} = 740$, and $q = 0.1\mu m$. For the sampling time 0.2ms, the values $K_{px} = 190$, $K_{pv} = 510$, and $q = 0.1\mu m$ are chosen. For these parameters, the maximum reference-acceleration error results as:

$$\begin{aligned} \max |\Delta a_{ref}| &= 0.010 \frac{m}{s^2} + n_{diff} \cdot 0.74 \cdot \frac{m}{s^2} && \text{for } T_{sampl} = 0.1ms \\ \max |\Delta a_{ref}| &= 0.005 \frac{m}{s^2} + n_{diff} \cdot 0.26 \cdot \frac{m}{s^2} && \text{for } T_{sampl} = 0.2ms \end{aligned} \quad (5.3)$$

For the discussed position-only methods, the factor n_{diff} is in the range between 0.67 and 2 (see Table 5.1). It turns out that the speed-feedback term, denoted by the second term of Equation (5.3), has considerably more influence than the position-feedback term. In case of the accelerometer-enhanced speed-estimation method (example: $N = 50 \Rightarrow n_{diff} = 0.02$), both influences are better equalised. The concrete results are summarised in Table 5.5.

This fact that the speed estimation of the speed feedback loop makes greater demands on position resolution than the position feedback loop justifies the approach taken in this dissertation. By the AESE-method with an observation period of 50 sampling periods, the maximum error due to quantisation can be reduced by a factor of around 30 compared to direct differentiation

Method	$\max \Delta a_{ref} \quad [\frac{m}{s^2}]$	
	$T_{sampler} = 0.1ms$	$T_{sampler} = 0.2ms$
D	1.5	0.53
A, C	0.74	0.27
B	0.5	0.18
AESE ($N = 50$)	0.02	0.01

Table 5.5: Effect of position quantisation: worst case error on a_{ref} ($a_{max} = 22\frac{m}{s^2}$).

which causes the same delay on the estimated speed. The additional acceleration measurement provides the necessary dynamic information. Without the AESE-method, the need for a better position resolution for speed is the higher, the lower is the sampling period of the controller.

5.1.4.4 Power Dissipation

We restrict the comparison of the different methods to the comparison of direct differentiation with the accelerometer-enhanced speed estimation. The other position-only methods are easily obtained with the formulae from Table 5.2.

For the given data ($K_{px} = 280\frac{1}{s}$, $K_{pv} = 740\frac{1}{s}$, $T_{sampler} = 0.1ms$, $q = 0.1\mu m$) the variance due to quantisation results as $0.09\frac{m^2}{s^4}$ ($\sigma = 0.3\frac{m}{s^2}$) for the direct differentiation and $0.0001\frac{m^2}{s^4}$ ($\sigma = 0.01\frac{m}{s^2}$) for the AESE-method (with $N = 50$). By the use of the accelerometer enhanced speed estimation, the variance is reduced by a factor 900, the standard deviation by a factor 30.

Even in the case of direct differentiation, the total power dissipation due to quantisation is less than $\frac{1}{5000}$ of the maximum drive power ($(22\frac{m}{s^2})^2$). Therefore, the heat-up of the drive due to quantisation is less important than aspects of limit cycles, audible noise, and exciting of structural resonances.

5.2 Acceleration Feedback

The feedback of the acceleration to increase the stiffness is often discussed in the literature. Its a commonly employed method for control system design. Therefore, we do not discuss it in detail here. The aim of this section is to provide the basic notions of the acceleration-feedback scheme, to describe its main characteristics, and to point out possible problems which may be encountered when using feedback of the measured acceleration.

An overview of the basic acceleration feedback scheme is given in [BF91]. The block diagram of the acceleration-feedback subsystem which is adapted to our control system is shown in Figure 5.6. It illustrates the transfer function from the reference acceleration a_{ref} to the real acceleration a . External disturbance forces F_{ext} are directly detected by the measured or estimated acceleration and compensated in this acceleration feedback loop.

An excellent survey of the principles and implementation of acceleration feedback is found in [SL92]. Acceleration-feedback is shown there on the example of rotary servo drives. However, the results can be directly translated to linear-drive axes. The authors summarise the main characteristics of acceleration-feedback as follows. Acceleration feedback improves the performance

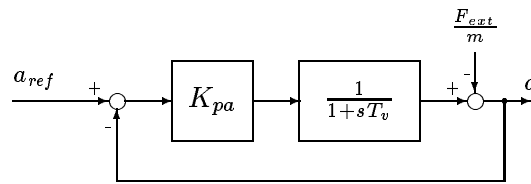


Figure 5.6: Subsystem with acceleration feedback.

and thus the stiffness of the servo-drives without the need of increasing the bandwidth. Without acceleration feedback, the bandwidth is automatically increased when position and speed feedback gains have to be raised to increase stiffness. Sometimes, such an increased bandwidth is not possible due to system limitations such as the maximum sampling frequency.

In other publications, the usefulness of acceleration feedback is also demonstrated. In [BF91], the robustness of the controlled systems towards mass variation is increased and the trajectory errors are lowered by proportional acceleration feedback. Experimental results in [CPS93] with a robot manipulator and a reconstructed acceleration signal show that the PI-acceleration feedback gives a better disturbance rejection than a PID-controller without acceleration feedback. Similar results are found in [Alt94] where force feedback instead of acceleration feedback is employed. By force feedback, the dynamic stiffness could be increased by 70–100%. In [Jag94], the use of measured acceleration feedback is compared to accelerometer-enhanced speed estimation (Kalman filter approach). The main results are:

- In experiments, both approaches improve the controller performance by about the same degree. There is only a small gain in robustness for both solutions, possibly due to the limited quality of the used acceleration measurement. A combination of both approaches (acceleration feedback and accelerometer-enhanced speed estimation) does not give better results than the use of only one of the two solutions.
- The main limitations of acceleration measurement are identified as disturbances on the measured acceleration, phase lag due to filtering, and non collocated position and acceleration sensors.

In most of the cases in the literature, the acceleration is not explicitly measured. It is estimated with observers based on position measurement. We expect that for our application, this is not feasible, as the encountered delays and quantisation problems for speed estimation are too important when estimating the acceleration based on position measurement. Therefore, the measured acceleration has to be used for feedback.

5.3 Conclusion

The accelerometer-enhanced speed estimation (AESE) considerably reduces the effects of position quantisation. When considering the worst case error bounds with $T_{s\text{ampl}} = 0.1\text{ms}$, this bound is reduced from around 3.5% of the maximum drive acceleration to around 0.1%. As a result from the AESE-method, the noise on the actuator input from the position feedback path is in the same range as the one from the speed feedback path. The speed-estimation problems caused by higher sampling frequencies are thus compensated for.

The application of acceleration-feedback for linear-drive axes is limited by the accelerometer noise. The accelerometer output signal is very noisy. Our algorithm for an accelerometer-enhanced speed estimation (AESE) filters the noise out of the signal to a high degree. For direct feedback, the signal would be directly used and the measurement noise directly fed back to the actuator input. To limit the noise influence, second-order filters have to be employed. This considerably limits the acceleration loop bandwidth. Therefore, we do not expect that a combined solution with acceleration feedback and accelerometer-enhanced speed estimation leads to better control performance. Further research will be necessary to determine the usefulness of a combined approach for different applications.

A practical implementation of acceleration feedback seems to be more difficult than the implementation of the AESE-method. The acceleration feedback loop has the highest bandwidth in the control system. Accelerometer noise is directly visible on the actuator input signal. Therefore, a proper design of accelerometer input filters and proper feedback gain design is of major importance. In contrast, the implementation of the AESE-method turns out to be simple. Accelerometer noise is considerably reduced by this method. The method is not sensitive towards design issues such as choice of the input filter of the accelerometer signal. Without acceleration feedback, the bandwidth has to be increased to raise the stiffness of the axis. This does not constitute a general problem, because with the AESE-method a high-bandwidth speed signal is available and the used numerical controllers provide the necessary high sampling rates.

References

- [Alt94] D.M. Alter. *Control of Linear Motors for Machine Tool Feed Drives*. PhD thesis, University of Illinois at Urbana-Champaign, 1994.
- [BF91] Frank Berlin and Paul M. Frank. Optimale Beschleunigungsrückführung in Roboterregelkreisen. *Automatisierungstechnik (at)*, 39:121–128, April 1991.
- [Büh94] Hansruedi Bühler. *Theorie du réglage de systèmes d'électronique de puissance*. Cours d'électronique industrielle, EPF Lausanne, October 1994.
- [Col87] Silvio Colombi. *Influence de la quantification et de non-linéarités sur la conception et la simulation de réglages digitaux*. PhD thesis, EPF Lausanne, 1987.
- [CPS93] Pasquale Chiacchio, François Pierrot, and Bruno Siciliano. Experimenting acceleration feedback loop for robot control. In *Proceedings of the second European Control Conference ECC'93*, volume 2, pages 565–569, 1993.
- [Föll85] Otto Föllinger. *Regelungstechnik*. Hüthig Verlag, Heidelberg, 5th edition, 1985.
- [Jag94] Bram de Jager. Acceleration assisted tracking control. *IEEE Control Systems*, pages 20–27, Oct. 1994.
- [Phi92] W. Philipp. *Regelung mechanisch steifer Direktantriebe für Werkzeugmaschinen*. Springer Verlag, Berlin, 1992.
- [SL91] Jean-Jacques E. Slotine and Weiping Li. *Applied Nonlinear Control*. Prentice Hall, Englewood Cliffs, N.J., 1991.

- [SL92] Peter B. Schmidt and Robert D. Lorenz. Design principles and implementation of acceleration feedback to improve performance of DC drives. *IEEE Transactions on Industry Applications*, 28(3):594–599, May/June 1992.
- [Stu81] G. Stute. *Regelung an Werkzeugmaschinen*, volume 5. Carl Hanser Verlag, München, 1981.
- [Zir96] Oliver Zirn. *Beitrag zum Entwurf von Vorschubantrieben für die Hochgeschwindigkeitsbearbeitung*. PhD thesis, ETH Zürich, 1996.

Chapter 6

Conclusions

6.1 Contributions

Motivated by the increased achievable control bandwidth of linear-drive machine-tool axes, the problem of speed estimation is analysed. The limitations of purely position-based velocity-estimation methods to deal with low resolutions are determined. The need for a higher position resolution for speed estimation than for position estimation in the case of high sampling frequencies is demonstrated, and the problems of increasing encoder resolution are discussed.

An adapted oversampling method to overcome the problem of a low position resolution is proposed and analysed. With a practical oversampling ratio around five, this solution reduces the position measurement noise and thus the noise on the speed signal to a certain degree.

A novel method of an accelerometer-enhanced speed estimation (AESE) is proposed as the main contribution of this dissertation. The method observes position and acceleration measurement over a fixed time period in the past and calculates the actual speed. Quantisation noise on the speed estimate is considerably reduced. Typically, a reduction of the influence of position quantisation by a factor of 10–100 is achieved. As a result, the influences of quantisation noise on the position and the speed feedback path of the control loop are equalised. Therefore, the controller gains have not to be reduced due to quantisation noise on the speed estimate and the bandwidth is maintained. Aspects of a simple practical implementation in an industrial environment are of major concern for the development of the proposed solution:

- Guidelines for a simple design are developed. In addition, the low sensitivity of the algorithm's performance on the single design parameter further simplifies the design.
- Simple algorithms for the implementation of the proposed solution on a numerical controller are developed. Due to the proposed recursive implementation of the method, the requirements on the calculation power of the numerical controller are not very high.
- Novel algorithms are proposed for the on-line identification of the gain and offset parameters of the employed accelerometers. As a result, the commissioning of the accelerometer-enhanced speed estimation is considerably simplified.
- The price of the proposed accelerometer solution is low compared to an increase in position resolution, which is avoided. Since the proposed method is not sensitive to acceleration measurement noise, low-cost accelerometers (< \$100) can be employed to obtain a high-accuracy speed estimation.

Experimental results demonstrate that acceleration measurement can be employed on linear machine-tool axes. Accelerometers provide the controller with important dynamic information on the axis. Measurement noise is not dominant. The experiments further show that the proposed AESE-algorithms for speed estimation and parameter identification can be implemented on real axes and that they give the expected results. Compared to direct position differentiation, quantisation noise on the speed is considerably reduced without adding any delay and thus limiting the closed-loop bandwidth.

Altogether, the proposed speed estimation algorithm can be recommended for an industrial application, as it lowers the demands on the position encoder resolution. In addition, it is a low-cost solution which is easily implemented and which includes automatic calibration of the used accelerometers. Experimental results demonstrate the feasibility, the accuracy, and the low noise sensitivity of the proposed solution.

6.2 Future Research Topics

During the research project that lead to this dissertation, the following aspects and directions turned out to be of interest for further investigation.

- One main direction of future work is the general assessment of the benefits for the closed-loop control due to the proposed high-quality speed estimation. In this context, it would be interesting to determine whether a combined use of the AESE-method with acceleration feedback poses the same problems as the combined use of the Kalman filters for speed estimation with acceleration feedback.
- In our experiments, acceleration and position measurement have always been collocated near the bearings of the axis. By placing the light-weight accelerometer somewhere near the tool, movements of the mechanical structure could also be estimated and resonances actively compensated for. It should be possible, in this setup, to use the low-frequency information of the position measurement at its original place near the bearings. In this case, the algorithm would have to be extended in order to also estimate the exact tool position.
- The usefulness of position oversampling for the measured axis position has been demonstrated in this work. Oversampling has a promising potential to considerably reduce position measurement noise. Research towards more sophisticated downsampling and filtering techniques is necessary to show how far the linear-axis position measurement can be improved by oversampling.

To sum up, a novel method of speed estimation which is based on additional acceleration measurement has been proposed and successfully implemented. From the obtained experimental results, it can be concluded that the method provides a high-quality speed estimation which can contribute to an improved control of the highly dynamic, linear-drive machine-tool axes in an industrial environment.

Appendix A

Mathematical Derivations

This appendix contains some mathematical explanations and derivations. The theory of stochastic signals is briefly reviewed in Section A.1. The derivations of the variances of the different position-only speed estimation methods are given in Section A.2.

A.1 Summary of Stochastic Signals

The theory of stochastic signals is applied in cases where a precise description of a process generating a signal to be analysed is extremely difficult, not desired, or not possible at all. Rounding and quantisation errors are often modelled as random noise. Stochastic theory is employed for their analysis.

As for the analysis of different problems in this dissertation the notion of stochastic signal theory is used, we summarise in the following its basics. This appendix is based on the discussion of time-discrete random variables in [OS92].

A.1.1 Basic Definitions

The basic elements of the theory of stochastic signals are *random variables* which describe stochastic processes. In the time discrete case, such a variable is a sequence of time discrete stochastic values. At each point in time an amplitude distribution for a certain stochastic variable can be defined. In our case these distributions are time invariant, because the stochastic processes behind are stationary, i.e. their stochastic characteristics does not vary in time. The *amplitude distribution* $f_x(\xi)$ denotes the probability of the random variable x to have exactly the value ξ . Random variables are characterised by different values based on the amplitude distribution:

- The *mean value* \bar{x} of a random variable $f_x(\xi)$ is also known as the expected value $\mathcal{E}(x)$ in the literature and defined as:

$$\bar{x} = \mathcal{E}(x) = \int_{-\infty}^{\infty} \xi f_x(\xi) d\xi$$

- The *variance* σ^2 indicates the expected value of the square of the variation of the random variable from the mean value:

$$\sigma^2 = \mathcal{E}(|x - \bar{x}|^2) = \int_{-\infty}^{\infty} (\xi - \bar{x})^2 f_x(\xi) d\xi$$

- The *mean square* $\overline{x^2}$ of a random variable $f_x(\xi)$ denotes the expected value of the square of the variable:

$$\overline{x^2} = \mathcal{E}(|x|^2) = \int_{-\infty}^{\infty} \xi^2 f_x(\xi) d\xi$$

Between these three values, there exists the following relationship:

$$\overline{x^2} = \sigma^2 + (\bar{x})^2$$

Mean value, variance, and mean-square value all belong to the class of *moments* which are calculated for a random variable. These moments have the property that *the moment of a sum is the sum of the moments*.

A.1.2 Quantisation-Noise Modelling and Analysis

As we work with a 32-bit floating point processor, quantisation and rounding errors of the signal processing are not modelled and neglected in this dissertation. However, the quantisation of the position measurement is modelled the same way as the quantisation of an A/D -converter. The position encoder provides an integer value which is equivalent to the quantised position. The error due to the *quantisation step-size* q is modelled as a uniformly distributed random variable in the range $\pm \frac{q}{2}$, because the measurement electronics rounds the real value to the nearest integer. The resulting uncertainty of $\pm \frac{q}{2}$ is called *quantisation noise*. As long as the quantisation step-size q is small compared to position variation between two samples, it is permissible to model the quantisation error by a random variable with uniform distribution. This uniform distribution has zero mean value and a variance of:

$$\sigma^2 = \frac{q^2}{12}$$

Based on the sum property of moments, the sum of different uncorrelated random variables x_i with mean value \bar{x}_i and variance σ_i^2 leads to an output signal with the following mean value and variance:

$$\bar{x} = \sum_i \bar{x}_i \qquad \sigma^2 = \sum_i \sigma_i^2$$

This result can be also adapted to the case of a digital filter with an input signal of variance σ_{in}^2 and mean value \bar{x}_{in} , as illustrated in Figure A.1. Output variance σ_{out}^2 and mean value \bar{x}_{out} are easily obtained based on the impulse response $h[n]$ of the discrete filter transfer function $H(z)$:

$$\bar{x}_{out} = \bar{x}_{in} \cdot \sum_{n=-\infty}^{\infty} h[n] \qquad \sigma_{out}^2 = \sigma_{in}^2 \cdot \sum_{n=-\infty}^{\infty} |h[n]|^2$$

The calculations of the variances of the different speed-estimation methods in Chapter 4 and Chapter 5 are based on these above-mentioned relationships.

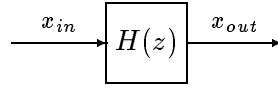


Figure A.1: Digital filter model.

A.2 Variances of Position-Only Speed-Estimation Algorithms

The variances of the position-only speed-estimation methods of Section 4.2.2 are derived in the following. The results are summarised in Table 4.1.

Direct Differentiation

$$v_k = \frac{x_k - x_{k-1}}{T_{\text{sampl}}}$$

$$\sigma^2 = \frac{q^2}{12} \cdot \frac{1}{T_{\text{sampl}}^2} \cdot [1^2 + 1^2] = \frac{q^2}{6 \cdot T_{\text{sampl}}^2} \approx 0.17 \cdot \frac{q^2}{T_{\text{sampl}}^2}$$

Mean Speed

$$v_k = \frac{x_k + 3x_{k-1} - 3x_{k-2} - x_{k-3}}{6T_{\text{sampl}}}$$

$$\sigma^2 = \frac{q^2}{12} \cdot \frac{1}{(6 \cdot T_{\text{sampl}})^2} \cdot [1^2 + 3^2 + 3^2 + 1^2] = \frac{q^2 \cdot 20}{432 \cdot T_{\text{sampl}}^2} \approx 0.05 \cdot \frac{q^2}{T_{\text{sampl}}^2}$$

Delayed Differentiation

$$v_k = \frac{x_k - x_{k-1} + \tau v_{k-1}}{T_{\text{sampl}} + \tau} = \frac{x_k}{T_{\text{sampl}} + \tau} - \sum_{i=0}^{\infty} \left[\left(\frac{\tau}{T_{\text{sampl}} + \tau} \right)^i \cdot \left(\frac{T_{\text{sampl}}}{(T_{\text{sampl}} + \tau)^2} \right) x_{k-1-i} \right]$$

$$\sigma^2 = \frac{q^2}{12} \cdot \frac{1}{(T_{\text{sampl}} + \tau)^2} + \frac{q^2}{12} \cdot \frac{T_{\text{sampl}}^2}{(T_{\text{sampl}} + \tau)^4} \cdot \sum_{i=0}^{\infty} \left(\frac{\tau}{T_{\text{sampl}} + \tau} \right)^{2i}$$

By employing the substitution $\tau = c \cdot T_{\text{sampl}}$, the variance results as:

$$\begin{aligned}
\sigma^2 &= \frac{q^2}{12T_{\text{sampl}}^2} \left[\frac{1}{(c+1)^2} + \frac{1}{(c+1)^4} \cdot \sum_{i=0}^{\infty} \left(\frac{c}{c+1} \right)^{2i} \right] \\
&= \frac{q^2}{12T_{\text{sampl}}^2} \left[\frac{1}{(c+1)^2} + \frac{1}{1 - \frac{c^2}{(c+1)^2}} \cdot \frac{1}{(c+1)^4} \right] \\
&= \frac{q^2}{12T_{\text{sampl}}^2} \left[\frac{1}{(c+1)^2} + \frac{(c+1)^2}{(c+1)^2 - c^2} \cdot \frac{1}{(c+1)^4} \right] \\
&= \frac{q^2}{12T_{\text{sampl}}^2} \left[\frac{1}{(c+1)^2} \left(1 + \frac{1}{(c+1)^2 - c^2} \right) \right] = \frac{q^2}{12T_{\text{sampl}}^2} \cdot \frac{2}{(c+1)(2c+1)} \\
&= \frac{q^2}{12} \cdot \frac{2}{(\tau + T_{\text{sampl}})(2\tau + T_{\text{sampl}})}
\end{aligned}$$

Quadratic Interpolation

$$\begin{aligned}
v_k &= \frac{3x_k - 4x_{k-1} + x_{k-2}}{2T_{\text{sampl}}} \\
\sigma^2 &= \frac{q^2}{12} \cdot \frac{1}{(2 \cdot T_{\text{sampl}})^2} \cdot [3^2 + 4^2 + 1^2] = \frac{q^2 \cdot 26}{48 \cdot T_{\text{sampl}}^2} \approx 0.54 \cdot \frac{q^2}{T_{\text{sampl}}^2}
\end{aligned}$$

References

- [OS92] Alan V. Oppenheim and Ronald Schaffer. *Zeitdiskrete Signalverarbeitung*. Oldenbourg, München, 1992.

Appendix B

Sensor Data Specification

In this appendix, technical data from commercially available sensors of the types discussed in Chapter 3 are summarised. The aim is to give an idea of resolutions and accuracy of these devices as well as their cost.

B.1 Interpolation of Optical Position Encoders

Resolution and accuracy of magnetic and optical *encoders* are discussed in Section 3.3.1. As an example, the list price of an encapsulated HEIDENHAIN optical encoder of $1m$ length with a resolution of $10\mu m$ is around \$2'000. The OEM-version is available for about half this price.

The company HEIDENHAIN sells interpolation boxes under the name EXE-box. These boxes are placed separately between the encoder and the numerical controller and have analog input signals and digital 90 degree phase shifted incremental output signals.

Type	Interpolation factor	Max. input frequency	Output frequency	Output mode
EXE 660	100	22kHz	10MHz	burst mode
	50	43kHz	10MHz	
	25	43kHz	5MHz	
EXE 650B	50	50kHz	10MHz	equally spaced

Table B.1: Specification of HEIDENHAIN interpolation boxes.

In Table B.1, the technical specifications of two examples of EXE-boxes [Hei92, Hei94], both used for our experiments, are summarised. Both boxes work with an internal cycle time of $2\mu s$. The EXE 660 outputs the incremental signals in burst mode for input frequencies exceeding $1.25kHz$ (with interpolation factor 100). HEIDENHAIN specifies that this burst mode can also appear as a result of vibrations even when encoders are stationary and not only at high velocities. The EXE 650B does not have burst mode. It distributes the increments regularly over one interpolation cycle. Both EXE-boxes poll the measured values at the beginning of a cycle. The corresponding output is only produced at the subsequent cycle. The total signal transmission time from the EXE-input to the EXE-output is indicated to be around $5\mu s$. HEIDENHAIN specifies an additional uncertainty of ± 2 cycle time, when using the EXE-box together with a

numerical controller. The reason of this uncertainty is not further detailed, partially it is due to the missing possibility of synchronisation between the two sampled devices. The list prize of these EXE-boxes is a bit less than \$1'000.

B.2 Laser Interferometer

As an example, we compile in Table B.2 the technical specification data, representing the state-of-the-art in 1995, of one specific linear motion interferometry device, the type HC250 from CSO. It is a device in the lower price segment, and is therefore most likely to be used for machine-tool applications. Other commercially available interferometry devices are more expensive than this type.

Resolution	10nm	with interpolation
Maximum position range	1m	
Guaranteed accuracy	1ppm	of measured distance
Output		analog (sin/cos) or digital (interpolation)
Weight	< 1g	of mobile part
Laser	class I	no danger for eyes (visible and invisible light available)
Size of device	very small	no supplementary space necessary
Maximum speed	$0.2 \frac{m}{s}$	
Prize	\$20.000	special versions for industrial applications: one third of this prize

Table B.2: Technical data of CSO HC250 interferometer.

This interferometry device has laser and photo detectors integrated on one chip. On the mobile part of the measured distance, only a small mirror is mounted. Therefore, there is absolute no contact between the base and the mobile part.

These sensors are measurement systems. They are calibrated and have temperature compensation. Therefore, their prize is rather high, compared to optical position encoders.

B.3 Accelerometers

Accelerometers are available in the prize range from \$10 up to \$1'000 or even more for very accurate sensors. For our purposes, only accelerometer in the lower prize segment are interesting, because it is the aim of the proposed solution to reduce the demands on position resolution with *low cost acceleration measurement*.

ICSensors OEM Low Cost Piezoresistive Accelerometers

The ICSensors low cost piezoresistive accelerometers consist of a micro-machined silicon mass suspended by multiple beams from a silicon frame. Piezoresistors located in the beams change their resistance as the motion of the suspended mass changes the strain in the beams. Silicon caps on the top and the bottom of the device are added to provide over-range stops, high shock

resistance, and durability. These accelerometers have a very low profile, built-in damping, low mass. They are batch fabricated at a low cost.

Parameter	ICS3028-010	ICS 3026-100-S	Units
Sensitivity	5.84	0.449	mV/g
Bridge resistance	3.11	4.17	k Ω
Resonant frequency	1.22	> 5	kHz
$\pm 5\%$ -frequency	0–400	0–960	Hz
Damping ratio	0.45	<i>n.a.</i> ^a	kHz
TCO (offset)	–0.2	–3.5	%FS/100°C
TCS (sensitivity)	–17.1	–20.0	%/100°C
TCR (resistance)	25.9	23.8	%/100°C
Linearity	0.2 (2) ^b	0.2 (1)	%FS
Transverse sensitivity	1 (3)	1 (3)	%FS
Acceleration limits (any directions)	20×		
Operating temperature	–40 to 125		°C
Weight	< 8		g

^an.a. — not available

^btypical value (maximum value)

Table B.3: Performance specifications for ICSensors piezoresistive accelerometers.

The specifications for a 10g and a 100g model [Pew94, Pew95], which are used in this dissertation, are listed in Table B.3. A detailed calibration sheet which provides measured test and calibration data for the sensor is included with each unit. Values for calibration and temperature compensation resistors are given on this calibration sheet. Standard ranges for this type of accelerometers are ± 2 , 5, 10, 20, 50, 100, 200, 500g. The price is around \$100 for small quantities. The output is of Wheatstone resistance bridge type. The sensor is easily mounted directly to the mechanical structures with screws.

Analog Devices Capacitive Accelerometers with Signal Conditioning

Analog Devices provides low cost capacitive accelerometers with integrated signal conditioning unit, e.g. the model ADXL05 [Ana95]. The full scale range of this type is user selectable and goes from 1g to 5g, and these sensors measure AC as well as DC signals. The output is of voltage type. A self-test with electrostatic deflection of the sensor beam is integrated and accessible with a TTL signal.

The usable output frequency range goes from 0Hz to 1kHz. The price for small quantities is less than \$30. The non-linearity lies typically around 0.2% of the full scale. These devices have to be mounted by soldering them on a printed circuit board. No holes for mounting with screws are present.

References

[Ana95] Analog Devices. *Capacitive accelerometer model ADXL05*, 1995. datasheet.

- [Hei92] Heidenhain. *EXE660 Interpolation and Digitising Electronics, operating instructions*, March 1992.
- [Hei94] Heidenhain. *EXE650B Interpolation and Digitising Electronics, operating instructions*, April 1994.
- [Pew94] Pewartron AG, Wallisellen (Switzerland). *ICSensors OEM piezoresistive, low cost accelerometer: models 3021 and 3026*, 1994. datasheet.
- [Pew95] Pewartron AG, Wallisellen (Switzerland). *ICSensors OEM piezoresistive, low cost accelerometer: models 3022 and 3028*, 1995. preliminary datasheet.

Appendix C

Experimental Environment

This appendix describes the experimental environment which has been used for the validation of the methods proposed in this dissertation. The experiments have been performed on two different linear-drive axes with 75N and 2200N maximum force. The technical data of the two drives are given in Section C.1. The numerical controller environment is explained in Section C.2.

C.1 Brushless Linear Drives

The two drives which are employed in this dissertation are bi-phase permanent-magnet synchronous drives. Due to their electronic commutation they are also called brushless DC motors. The drives which we describe in the following consist of the motor itself, the current control loop with the power electronics, and the position measurement system. For the trajectory generation, control and recording of real-time data, a numerical controller based on a digital signal processor (DSP) is employed.

C.1.1 Air-Cushion 75N Drive Axis

The employed 75N linear-drive is a prototype model from the company ETEL¹. It has almost friction-less air-cushion bearings, a low time constant of the current controller, and a low mass. Due to the low slider mass, its maximum acceleration is about 5g.

Total slider mass	m	1.6kg
Maximum force	F_{max}	75N
Current controller:	delay	T_{del} 0.1ms
	time constant	T_c 0.1ms
Position resolution	q	$0.4\mu m$

Table C.1: Technical data of 75N prototype linear-drive axis.

¹ETEL SA, Rue de la Gare 13, CH-2112 Môtiers, Switzerland

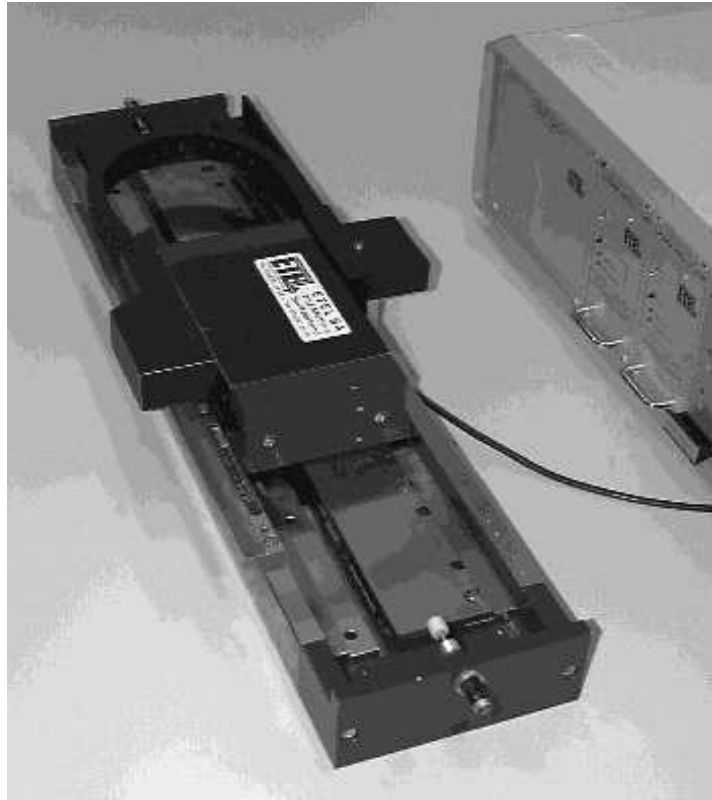


Figure C.1: 75N prototype linear-drive axis.

C.1.2 2200N Machine-Tool Drive Axis

The 2200N linear-drive axis is used for a machine tool for milling and engraving of small and precise workpieces. Due to its roller bearings it has considerable friction in the range of 6% of the maximum drive force. The technical data of the ETEL motor and the HEIDENHAIN encoder are summarised in Table C.2.

Total slider mass	m	100kg
Maximum force	F_{max}	2200N
Current controller:	delay	T_{del} 0.1ms
	time constant	T_c 0.2ms
Position resolution	q	$0.1\mu m$
Stiction		$120\pm 3N$
Friction		$135\pm 5N$

Table C.2: Technical data of 2200N linear-drive axis.

C.2 DSP-Based Numerical Controller Environment

For the trajectory generation, control and recording of real-time data, a numerical controller environment [Gee95] based on a digital signal processor (DSP) has been developed at the Microcomputing Laboratory (LAMI). The environment is based on a TMS320C40 [Tex91b] digital signal processor. The processor board [Mar92] has also been developed at the LAMI. This section provides complementary information to the basic description which is given in Section 2.5.

C.2.1 Schematic and Elements of the Environment

The developed numerical controller environment provides the interfaces for the control of two machine-tool axes. Its block diagram is illustrated in Figure C.2.

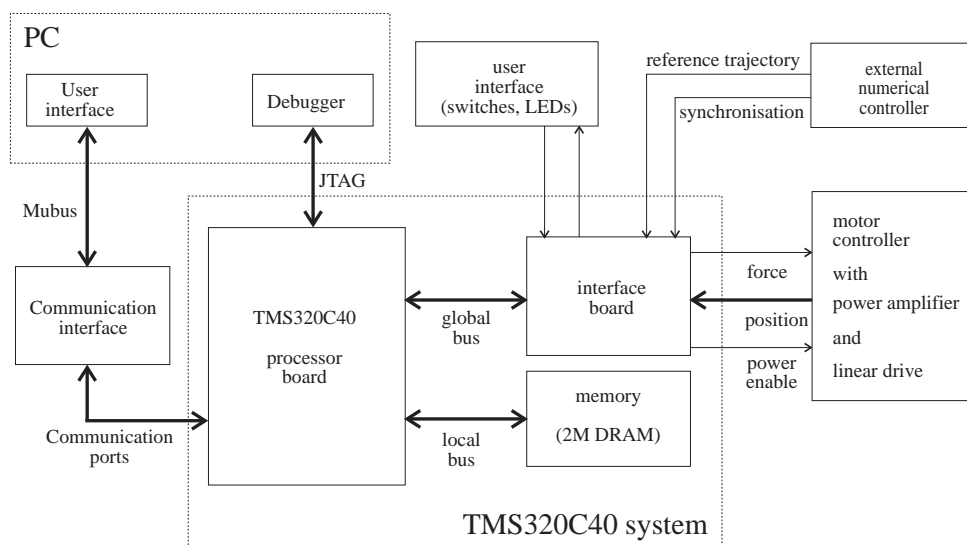


Figure C.2: Block diagram of the numerical controller environment.

The signal-processor system consists of the processor board, an external memory board, and an interface board. The *processor board* contains one TMS320C40 32-bit floating-point digital signal processor from Texas Instruments, the basic memory, the interfaces for six high-speed communication channels, and two independent system buses (global and local) for external boards. The *memory board* has a capacity of 2M words of 32 bits. The *interface board* provides the following interfaces for linear-axis control:

- 4 analog outputs for 2 phase current reference values per axis (range: $\pm 10V$).
- 2 quadrature-decoder inputs and counters for Heidenhain EXE-box encoder signals (24 bit counters with an input sampling frequency of 20MHz).
- 8 configurable analog inputs with analog and switched capacitor filters (input range: $\pm 10V$).
- Several binary inputs and outputs.
- One input for the synchronisation with an external numerical controller.

The dedicated outputs for motor control are two analog phase-current reference signals per axis and one power-enable signal which performs an emergency stop of the axis if it is deactivated. A watchdog on the interface board supervises that every three milliseconds a new value is written on the outputs of the phase-current reference values. If this writing operation is missing, the power-enable signal is deactivated and the axis performs an emergency stop. The axis position is transmitted from the position interpolation unit to the interface board via two differential, incremental signals (RS-422).

A signal for the synchronisation of the DSP controller with an external numerical controller which generates the desired trajectories is provided. The DSP works thus synchronised with the external controller at a multiple of the sampling frequency of this controller.

C.2.2 Programming and User-Interface

An optimising C-compiler [Tex91a] and a debugger [Tex92] from Texas instruments is available for the programming of the DSP. These tools are supported on PC and workstation platforms and access the processor board via a JTAG interface. With this JTAG connection, download, start, execution and step-by-step execution of the program with a comfortable source debugging tool is performed.

The optimising C compiler generates optimised assembler code (optimised for minimum execution time or minimum memory usage). Complex control applications are completely programmed in C language. The generated machine-code is fast. Therefore, high sampling frequencies (>10kHz) are easily achieved while the advantage of a high-level programming language are retained.

The developed environment provides two different user interfaces are provided. First, a simple switch box enables one to start and stop control and data-recording. Second, an interface, which is based on a terminal window on the PC, provides additional functions, such as the adjustment of controller parameters, the choice of reference trajectories and controller structures.

References

- [Gee95] Andrea Gees. Environment for digital control of two machine-tool axes based on a TMS320C40 digital signal processor. Technical report, Laboratoire de microinformatique, EPF Lausanne, 1995.
- [Mar92] Christophe Marguerat. Développement avec le TMS320C40. Technical report, Laboratoire de microinformatique, EPF Lausanne, 1992.
- [Tex91a] Texas instruments. *TMS320 Floating-Point DSP Optimizing C Compiler*, 1991.
- [Tex91b] Texas instruments. *TMS320C40 User's Guide*, 1991.
- [Tex92] Texas instruments. *TMS320C4x C Source Debugger, User's Guide*, 1992.

List of symbols

a_{ext}	acceleration caused by external forces
a_m	measured acceleration
\bar{a}_m	mean value of measured acceleration
a_{max}	maximal acceleration of drive
a_{mot}	acceleration due to drive force
a_{ref}	acceleration reference value
a_0	accelerometer offset
A	system dynamics matrix
A_i	component of accelerometer A (speed estimation algorithm)
B	system input matrix
B_i	component accelerometer B (speed estimation algorithm)
C^T	system output matrix
D_v	damping of closed speed control loop
$\Delta\epsilon_k$	estimation error of observer
ΔP_{min}	constant for excitation supervision (speed estimation algorithm)
Δt	observation period duration
Δt_{burst}	oversampling burst period duration
Δx	position difference of speed estimation algorithm
ΔX_a	double integration of acceleration (speed estimation algorithm)
ΔX_{max}	maximum position deviation during oversampling burst
$E(z)$	controller error
ϵ	accelerometer gain calibration error
$\mathcal{E}(x)$	expected value of a random variable x
f_{edge}	transition frequency between position and acceleration contribution
f_{sampl}	controller sampling frequency
f_v	closed-loop bandwidth of speed control loop
f_x	closed-loop bandwidth of position control loop
$f_x(\xi)$	amplitude distribution of a random variable x
F_{ext}	external disturbance force
F_{mot}	motor force
F_{ref}	reference force
φ	phase shift between motor windings and permanent magnets
$G(s)$	continuous system transfer function
$G(z)$	discrete system transfer function
$h[n]$	impulse response (discrete system)
H	state observer feedback matrix
$H(z)$	sampled system transfer function
i	index for distinction of different observation period durations
\underline{I}_{phase}	phase current vector of linear motor
k_{gain}	position measurement amplification / acceleration measurement attenuation
K_A	gain factor of accelerometer A
K_B	gain factor of accelerometer B
K_{mot}	constant gain factor of power electronics and motor
K_{pa}	acceleration-error feedback gain
K_{pv}	speed-error feedback gain

K_{px}	position-error feedback gain
$K(z)$	discrete controller transfer function
\mathcal{L}	Laplace transform operator
M_i	measured acceleration A before scaling
n_{diff}	noise of differentiation method expressed in $\frac{q}{T_{sampl}}$
N	number of samples within one observation period
N_{diff}	delay of differentiation method expressed in $\frac{T_{sampl}}{2}$
N_i	measured acceleration B before scaling
P	instantaneous power
P_i	position component (speed estimation algorithm)
q	(position) quantisation stepsize
$q(t)$	(position) quantisation error
σ^2	variance of a random variable
T_{acc}	time constant modelling acceleration measurement
T_c	time constant of current controller
T_{contr}	time constant modelling controller delay
T_{del}	time delay of power electronics chopper
$T_{encoder}$	position-encoder interpolation sampling time
T_{os}	oversampling period
T_{sampl}	sampling period
T_{switch}	switching period of power electronics
T_v	time constant modelling speed control loop
τ	delay parameter of delayed differentiation
$u(k)$	sampled controller output and system input
$U(z)$	controller output and system input
\underline{U}_{ind}	permanent-magnet-induced voltage of linear drive
\underline{U}_{phase}	phase voltage of linear motor
$v(t)$	axis speed at time t
v_k	axis speed at sampling step k
v_{max}	maximum absolute speed of axis
v_{real}	real axis speed
v_{ref}	reference speed
$V(s)$	system speed output
$V_m(s)$	measured speed output
$V_m(z)$	measured speed output (discrete)
$V_{ref}(s)$	reference speed input
$W(s)$	external disturbance input
ω_{edge}	transition frequency between position and acceleration contribution (in $\frac{rad}{s}$)
ω_v	closed-loop bandwidth of speed control loop
\bar{x}	mean value of stochastic variable x
$\overline{x^2}$	mean square value of stochastic variable x
$x(t)$	axis position at time t
x_k	axis position at sampling step k
$\hat{\mathbf{x}}_k$	estimated state vector
$\hat{\mathbf{x}}_{k-1}$	previous estimated state vector
x_{max}	maximum absolute position of axis
x_m	measured position

$x_m(t)$	measured axis position at time t
x_m	measured axis position
$x_{os}(t)$	oversampled axis position at time t
x_{ref}	reference axis position
$X(s)$	axis position
$X_{encoder}$	position encoder resolution (without interpolation)
$X_{ref}(s)$	reference axis position
y_k	sampled system output
\hat{y}_k	estimated system output
$Y(z)$	system output
$Y_{ref}(z)$	reference input
z	operand of z-transform (discrete systems)
\mathcal{Z}	z-transform operator

Abbreviations

AC	alternating current
A/D	analog to digital converter
AESE	accelerometer-enhanced speed estimation
CMOS	complementary metal-oxide semiconductor
D/A	digital to analog converter
DC	direct current
DSP	digital signal processor
GPS	global positioning system
LVT	linear-velocity transducer
OEM	original equipment manufacturer
ppm	parts per million
RAM	random access memory
TCO	temperature coefficient of offset (piezoresistive accelerometers)
TCR	temperature coefficient of resistance (piezoresistive accelerometers)
TCS	temperature coefficient of sensitivity (piezoresistive accelerometers)
ZOH	zero order hold block

Curriculum Vitae

Andrea Gees was born on 19th March 1966 in Baden, Switzerland. He is Swiss citizen, married and has one child.

Education:

- 1995-1996 Postgraduate course in computer science “*Reseaux de communication*” at École polytechnique fédérale de Lausanne.
- 1994 Postgraduate education “*Traitement de signaux et images*” at École polytechnique fédérale de Lausanne.
- 1987–1993 *Diploma in Electrical Engineering*
from Swiss Federal Institute of Technology in Zürich
Specialisation: control systems, power electronics, and real time systems.
Thesis: Self-learning neural controller for inverted pendulum balancing (at ABB corporate research, Baden-Dättwil).
- 1979–1986 *Matura C* from Bündner Kantonsschule (Chur).

Professional experience:

- Oct. 1993– *École polytechnique fédérale de Lausanne, Microcomputing Laboratory (LAMI):* research assistant.
- Apr. 1993–June 1993 *ABB corporate research, Baden:* investigations on learning and stability of self-learning neural controller.
- Mai 1991–June 1991 *ABB corporate research, Baden:* implementation of a transputer based neural controller.
- Jan. 1991–Feb. 1991 *BSG Schaltungstechnik, Balingen (Germany):* design of a car battery controller prototype.
- Aug. 1990–Dec. 1990 *ABB Verkehrssysteme AG, Turgi:* development of hardware for a simulation model for locomotives.

